Faculty of Engineering

Department of Electrical and Computer Engineering

Titre En Français:

Nanotechnologie des Semi-conducteurs Quantiques III-V pour la Détection de *Legionella pneumophila* en Milieu Aqueux

English Title:

Nanotechnology of III-V Quantum Semiconductors for Detection of *Legionella pneumophila* in Aqueous Environment

A Thesis

Submitted in Partial Fulfilment of the Requirements for the Degree of

Doctor of Philosophy in Electrical Engineering

By

Mohammad Reza Aziziyan

Sherbrooke, Quebec, Canada January 2019

Doctoral Committee

Prof. Jan J. Dubowski (Supervisor)

Department of Electrical and Computer Engineering

Faculty of Engineering

Université de Sherbrooke

Prof. Denis Morris

Department of Physics

Faculty of Sciences

Université de Sherbrooke

Prof. Eric H. Frost

Department of Microbiology and Infectiology

Faculty of Medicine and Health Sciences

Université de Sherbrooke

Prof. Zbigniew Wasilewski

Department of Electrical and Computer Engineering

Faculty of Engineering

University of Waterloo

Résumé

Il a été avéré que le GaAs et l'AlGaAs peuvent être décomposés dans des environnements aqueux et que s'ils sont irradiés avec des photons d'énergie dépassant la bande interdite de ces matériaux, leur décomposition s'accélère grâce à un processus de photocorrosion bien connu. La sensibilité de la photoluminescence (PL) des semi-conducteurs à la présence d'états de surface a fait l'objet des études approfondies pendant de nombreuses années. Cependant, ce n'était que récemment qu'il a été démontré que les mesures de PL étaient sensibles à la photocorrosion *in situ* avec une précision de sous-monocouche. Une conséquence importante de ces caractéristiques est la forte sensibilité de PL à la perturbation d'un champ électrique proche de la surface et au transfert de la charge électrique. Ceci a rendu la photocorrosion des nano-hétérostructures de GaAs/AlGaAs attrayante, en tant que transducteur propice, pour détecter les perturbations de la charge électrique proche de surface induite par les bactéries chargées négativement.

Dans cette thèse, les mécanismes de dissolution des semi-conducteurs III-V photo-induits ont été étudiés en réalisant une spectrométrie de masse à plasma à couplage inductif (ICP-MS) de produits aqueux de photocorrosion. Les expériences réalisées pour la photocorrosion de nano-hétérostructures GaAs/$Al_{0.35}Ga_{0.65}As$ dans des milieux DI H_2O et NH_4OH ont confirmé que la photocorrosion digitale (DIP) de ces nano-hétérostructures pouvait être contrôlée avec une précision inférieure à la monocouche. Les conditions conduisant à une décomposition congruente, définie par un taux de photocorrosion constant, ont été étudiées avec des mesures ICP-MS et un ensemble de méthodes de caractérisation de surface/interface utilisant FTIR, XPS et AFM. Cela a permis de démontrer que, contrairement à l'environnement DI H_2O, l'environnement NH_4OH conduit à la formation des surfaces stœchiométriques des nano-hétérostructures étudiées, d'au moins 100 nm. Le taux de photocorrosion constant a également été observé *in situ* en analysant les positions temporelles des interfaces révélées par PL entre les couches de GaAs et d'AlGaAs. Ces résultats démontrent la faisabilité d'un procédé simple et relativement peu coûteux pour le diagnostic *in situ* de la gravure par couche atomique de semi-conducteurs composés qui pourrait conduire à la formation de surfaces stœchiométriques de tels matériaux.

L'étude de la photocorrosion digitale a été étendue à l'étude de ce processus pour la détection sensible de *Legionella pneumophila* chargée électriquement en milieu aqueux. L'immobilisation efficace de ces bactéries sur la surface du biocapteur a été confirmée avec une

biopuce GaAs/AlGaAs polarisée électriquement. Ainsi, l'hypothèse principale proposée est que la décoration de *L. pneumophila* avec des biomolécules chargées négativement devrait mener à une détection à base de la photocorrosion digitale avec une limite de détection améliorée. En concordance avec les mesures du potentiel zêta, la bactérie *L. pneumophila* décoré avec du dodécylsulfate de sodium (SDS) a montré une interaction beaucoup plus forte avec les biopuces GaAs/AlGaAs photo-corrodées, ce qui a permis de détecter ces bactéries dans une solution saline tamponnée au phosphate (PBS) à 10^3 UFC/ml (unités formant colonies).

Les résultats de cette recherche permettent de mieux comprendre la capacité du processus DIP à identifier les conditions conduisant à la formation de surfaces stœchiométriques de semi-conducteurs gravés. De plus, cette thèse contribue au développement d'une méthode innovante de détection de molécules chargées électriquement dans des environnements liquides.

Mots clés: semi-conducteur quantique III-V, nano-hétérostructure GaAs/AlGaAs, photoluminescence, photocorrosion, gravure sur couche photo-atomique, gravure digitale, biocapteur, théorie DLVO, longueur de Debye, *Legionella pneumophila*, Limite de détection améliorée, potentiel zêta bactérien

Abstract

It has been known that GaAs and AlGaAs could be decomposed in aqueous environments and, if irradiated with photons of energy exceeding bandgap of these materials, their decomposition accelerates through a well-known photocorrosion process. The sensitivity of photoluminescence (PL) of semiconductors to the presence of surface states has been investigated quite extensively for many years, however it was not until recently that the measurements of PL were proven to be sensitive to monitor *in situ* photocorrosion with a sub-monolayer precision. One important consequence of this characteristics is a strong sensitivity of PL to the perturbation of a near surface electric field and transfer of the electric charge. This made photocorrosion of GaAs/AlGaAs nanoheterostructures appealing, as a propitious transducer, for sensing the near surface electric charge perturbations induced by the negatively charged bacteria.

In this thesis, the mechanisms of photo-induced III-V semiconductor dissolution have been investigated by conducting inductively coupled plasma mass spectrometry (ICP-MS) of aqueous photocorrosion products. The experiments carried out for GaAs/$Al_{0.35}Ga_{0.65}As$ nanoheterostructures photocorroding in DI H_2O and NH_4OH milieus confirmed that the digital photocorrosion (DIP) of these nanoheterostructure could be controlled with a sub-monolayer precision. The conditions leading to a congruent decomposition, defined by a constant photocorrosion rate, were investigated with ICP-MS measurements and a set of surface/interface characterization methods employing FTIR, XPS and AFM. This allowed demonstrating that, in contrast to the DI H_2O supporting photocorrosion, the NH_4OH environment leads to formation of stoichiometric surfaces of the investigated nanoheterostructures photocorroding by at least 100 nm. The constant photocorrosion rate was also observed *in situ* by monitoring temporal positions of PL revealed interfaces between GaAs and AlGaAs layers. These results demonstrate the feasibility of a simple and relatively inexpensive process for *in situ* diagnostics of atomic layer etching of compound semiconductors that could lead to formation of stoichiometric surfaces of such materials.

The study of digital photocorrosion were expanded on investigation of this process for sensitive detection of electrically charged *Legionella pneumophila* in an aqueous environment. The enhanced immobilization of these bacteria on the biosensor surface was confirmed with

electrically biased GaAs/AlGaAs biochip. Thus, a central hypothesis was that decorating naturally found *L. pneumophila* with negatively charged biomolecules should lead to a digital photocorrosion based detection with a much-enhanced limit of detection (LOD). In agreement with the zeta potential measurements, the sodium dodecyl sulfate (SDS) decorated *L. pneumophila* interacted much stronger with the photocorroding GaAs/AlGaAs biochips. This allowed detecting these bacteria in a diluted phosphate buffered saline (PBS) solution at 10^3 colony forming units (CFU) per ml.

The results of this research give a deeper insight into the capability of DIP process for tracking down the conditions leading to formation of stoichiometric surfaces of etched compound semiconductors. Furthermore, this thesis contributes towards development of an innovative method of detecting electrically charged molecules in liquid environments.

Key Words: III-V quantum semiconductor, GaAs/AlGaAs nanoheterostructure, Photoluminescence, Photocorrosion, Photo-atomic layer etching, Digital etching, Biosensor, DLVO theory, Debye length, *Legionella pneumophila*, Enhanced limit of detection, Bacterial zeta potential

Dedicated to my kind parents

& my lovely wife!

Acknowledgment

First, I would like to thank my adviser, Prof. Jan J. Dubowski, for his vast contribution to my thesis and for his patience, motivation and enthusiasm throughout my PhD. He provided me with ideas and guidance that allowed me to better understand my research. I would like to express my sincere gratitude to Prof. Eric H. Frost, who shared his enthusiasm and knowledge with me. I certainly enjoyed and learned a lot from the fruitful discussions I had with him during my research. I would like to thank my thesis committee for taking time to read my thesis and giving me their encouragement and insightful comments. I also thank Prof. Maxime Darnon who chaired my defense committee.

I am deeply grateful for being part of QSPB group. I wish to thank Dr. Khalid Moumanis and Dr. Walid M. Hassen and I greatly value and appreciate the time and effort they put for the group members, especially myself. I spent many memorable moments with current and former group members, Srivatsa, Hemant, Lilian, Vivien, Neng, Elnaz, Romain, Dominic, Juliana, Aman, Rene, Hakim, Amirul, Lucas and Daniela. I thank all of them for being part of my professional and personal life.

Furthermore, I would like to thank Prof. Nasim Annabi for providing an opportunity for me to visit her laboratory at the Northeastern University, USA. I especially thank her availability during my stay in Boston and even afterward. I had a great time inside and outside the lab with Ehsan, Brian, Roberto, Dev, Iman, Andrew and Jon. Thanks to all of them for kindly and warmly hosting me in Boston.

Last but not least, I would like to thank my parents who have been supporting me, unconditionally, throughout my life. I am also thankful to my best friend Narjes, who is also my wife, for always being there for me.

Table of Contents

List of Figures

List of Tables

List of Acronyms

AFM	Atomic force microscopy
Bio-PEG	Biotinylated polyethylene glycol
BSA	Bovine serum albumin
CFU	Colony forming unit
DC	Duty cycle
DI H_2O	Deionized water
DIP	Digital photocorrosion
EDC	1-ethyl-3-(3-dimethylaminopropyl)-carbodiimide
FET	Field effect transistor
FTIR	Fourier transform infrared spectroscopy
HDT	1-hexadecanethiol
HI-PLM	Hyperspectral imaging PL mapper
ICP-MS	Inductively coupled plasma mass spectrometry
ISFET	Ion-sensitive FET
LED	Light-emitting diode
LOD	Limit of detection
PBS	Phosphate buffered saline solution
PLM	PL mapper
XPS	X-ray photoelectron spectroscopy

CHAPTER 1. Introduction

1.1. Context and Issue

Detection of micro-organisms in foods and fluids, such as water, is an essential part of any health-related control and human safety plan, in order to prevent outbreaks of pathogens. Many conventional methods were used for detecting foodborne and waterborne pathogenic bacteria, however they were regularly time-consuming because of the need for growth of bacteria in culture media [1]. Often, some other steps such as isolation, biochemical and/or serological identification and sometimes sub-specific characterization, e.g. antibiotic sensitivity measurements, should be done in addition to these conventional methods to produce accurate results [1, 2]. There are other approaches, which are faster than culture-based methods, but they require the use of sophisticated apparatus, expensive facilities and highly qualified personnel [2]. Furthermore, these qualitative evaluations usually do not have sufficient sensitivity with direct testing and some growth in an enrichment medium is still required before attempting an analysis. Therefore, developing more convenient solutions than those established with traditional assay-based methods necessitates progress in technology and new trends in biosensing, particularly once fast and quantitative data are required to prevent outbreaks of hazardous pathogens.

Currently, one of the ongoing challenges is finding low levels of bacteria in aqueous environment, especially in water sources, which are one of the most important vital resources associated with every day of human life and almost each and every living creature. Instability of these resources by any means not only endangers human health but also disturbs the environment. Currently a considerable number of people around the world do not have access to clean water and it will be more complicated when the population increases [3]. Although quality of water is important, at this point of time the main challenge is water purification, which is an involute issue especially in the theme of finding traces of pathogenic bacteria in water by means of a low cost, untroublesome and rapid technique [4]. Another important issue concerns the industrial water such as those used in cooling towers and evaporative condensers, since they can become the source of bacterial growth and propagation. Pathogenic *Escherichia coli* and *Legionella pneumophila* were the leading sources of contamination existing in water as they can infect and endanger human health with their related disease [5]. *E. coli* is a gram negative and rod-shaped bacterium of the

genus *Escherichia* that is commonly found in the lower intestine of warm-blooded organisms. Although most strains of *E. coli* do not cause illness, some strains were found to be the reason of cramps and diarrhea in humans and a particular strain (O157:H7) caused severe illness by producing a powerful toxin [6]. *Legionella* is also a gram negative, cylindrical or rod-shaped bacterium, which can cause Legionnaires' disease or Pontiac fever. Since its identification in 1976 in Philadelphia, USA, it has been recognized as a pathogenic bacterium. Given conditions make our modern-day plumbing systems and cooling towers a good habitat for the *Legionella*. Inhalation of aerosols from contaminated water sources or contamination of waters from cooling towers with *Legionella* led to *Legionella* infections [7]. Outbreaks of this bacteria resulted in large numbers of fatalities, including the unfortunate event during the summer of 2012 in Quebec City where 182 cases were declared among which 13 people died. In that case contamination was started from a cooling tower [8]. Such outbreaks demonstrated that regular monitoring systems were not efficient and, for that reason, frequent *Legionella* testing should be essentially conducted to make sure that bacterial concentration in the water system is under control.

Today, control of *Legionella* is included in the legislation of many countries throughout the world, as well as Canada. The number of bacteria in water should not be more than some specified standards, which are normally described by health and safety organizations for each different type of bacteria, including *Legionella* [9]. This created an obligation for numerous water control tests, requiring a real-time monitoring of domestic and/or industrial water aimed at sensing the presence of pathogenic bacteria at early stages. Consequently, rigorous monitoring of industrial and recreational water for the presence of *Legionella* is required. Unfortunately, conventional methods have failed many times to prevent the spread of *Legionella*, because growth of *Legionella* takes 10-14 days [10]. In addition, other state of the art techniques were either expensive, complicated or unreliable owing to producing too many false positive results [11]. Then, a great deal of effort has been directed toward designing remote biosensing platforms for providing fast and reliable response at a reasonable cost, with capability of being automated and regenerated [12]. Even though there are many outstanding progresses, thus far, to our knowledge, none of them were satisfactory. For instance, Surface Plasmon Resonance (SPR) [13], Surface Acoustic Wave (SAW) [14], and Electrochemical Impedance Spectroscopy (EIS) [15] have been used to detect *Legionella* and *E. coli*, but they suffered from more or less major problems for instance high cost of chemical

materials and employed systems, large variability in results, being impossible or difficult to automate the system, lack of possibility for reusing the biosensor and need for bulky equipment.

Meanwhile, semiconductors' optoelectronic properties made them one of the most promising approaches for biosensing transducers. They could be miniaturized to an extremely small size and could provide rapid response to environmental changes as well they were capable of achieving remarkable sensitivity perhaps down to the molecular-level counting. For example, specific binding of a single molecule using silicon-based nano-wires [16, 17] and carbon nanotubes [18] have been recently reported. Some other semiconductor-based sensors were also developed for liquid-phase sensing for example ion-sensitive field effect transistors (ISFETs) [19]. Liquid-phase sensors based on silicon [20], gallium nitride [21, 22], diamond [23, 24] and lately gallium arsenide (GaAs) [25] were also investigated.

GaAs is a high electron mobility compound semiconductor that allowed fabrication of advanced devices, operating at high frequencies. Since the GaAs and AlGaAs have nearly identical lattice constants, the band-gap of their heterostructure could be flexibly engineered to create the two-dimensional electron gas (2DEG) devices [26, 27]. Above all, optically confined GaAs/AlGaAs epitaxial heterostructure exhibited strong PL in near-infrared window, where the biological samples have minimal absorption (700 nm to 1300 nm) [28]. This made GaAs/AlGaAs heterostructures an attractive choice for photonic biosensing applications chiefly for monitoring biological activities and detection of pathogenic bacteria. Then, the quantum semiconductor photonic biosensing (QSPB) technology for monitoring the presence of biomolecules in aqueous environments and monitoring inter-molecular reactions in the vicinity of the semiconductor surface was proposed [29]. Initially, PL emission intensity of specially designed quantum semiconductor nanoheterostructures allowed detection of *E. coli* at 10^4 Colony Forming Unit (CFU)/ml in less than 2 hours, which was a relatively short time compared to most available techniques [25]. Temporal PL characteristics of GaAs/AlGaAs nanoheterostructures were later investigated for *in situ* detection of *E. coli* bacteria down to 10^3 CFU/ml [30]. Thus, the QSPB technology offered an attractive sensitivity with a fast response time. Not surprisingly, cost of biosensor-based diagnostic has been considered an important issue [31], and PL technique has shown some promise in this respect. Accordingly, the QSPB technology was found potentially a very good candidate to improve the process of bacterial detection in bio-recognition based

applications, exclusively whenever frequent, fast and cost-effective tests were the main prerequisites.

1.2. Research Question

Although the results obtained with the QSPB technology were favorable, more rigorous research was necessarily required to establish an enhanced biosensing system based on the photocorrosion phenomena that could be offered as an alternative for frequent testing of industrial water for detecting *L. pneumophila*. At the top of the list, there was understanding of the mechanism of photo-induced oxidation and dissolution of GaAs/AlGaAs nanoheterostructures, whether this technique could be incorporated into nano-scale etching of compound semiconductors, and what advantages would it bring in for such an application?

Concurrently, what were the fundamental mechanisms, playing a crucial role in defining the sensitivity of this system for bacteria detection? Would it be possible to implement this system in detection of *L. pneumophila* with comparable outcomes to that of previously published results for *E. coli*? Most importantly, regarding the latter question, could it be possible to enhance the limit of detection (LOD) of this biosensor, using uncomplicated, and low-cost techniques? Ultimately, what would be the LOD of this system, employing the proposed enhanced techniques, for finding traces of *L. pneumophila* in water?

1.3. Objectives and Hypothesises of the Research Project

In consideration of the aforementioned discussions, the present thesis deals with investigation of the photocorrosion effect for biosensing in aqueous solutions. The work covers the underlying mechanism of photo-atomic layer etching (photo-ALE) of GaAs/AlGaAs nanoheterostructures with implication for stoichiometric and nanoscale etching of III-V materials. The PL intensity oscillations due to atomic-layer etching of semiconductor nanoheterostructures have been used as the principle strategy for detection of bacteria immobilized on the surface of biofunctionalized GaAs/AlGaAs nanoheterostructures. Hence, the central goal is investigation of advanced techniques for improving the LOD of this biosensing platform for enhanced detection of *L. pneumophila* in water. To this end, the main objectives of the present research are classified as follows:

First, elucidating the fundamental aspects of photo-induced material removal and formation of stoichiometric III-V surfaces. Here, the hypothesis was that photocorrosion of GaAs/AlGaAs nanoheterostructures could be controlled down to sub-monolayer resolution, while the stoichiometry of the etched surface was preserved. This is of importance to the advancement of digital photocorrosion (DIP) for photo-ALE processing of GaAs/AlGaAs and other III-V nanoheterostructures. To address this, inductively-coupled plasma mass spectrometry (ICP-MS) was employed for a systematic analysis of aqueous environments, in which the photo-ALE of GaAs/$Al_{0.35}Ga_{0.65}As$ nanoheterostructures was carried out. Furthermore, the low temperature (20 °K) and room temperature PL characteristics of GaAs/AlGaAs were investigated. Lastly, using state of the art characterization techniques, such as AFM, FTIR, and XPS, the surface of processed samples was studied.

Second, demonstrating detection of *L. pneumophila* as the main and the most important target of the research conducted thus far, using photonic response of GaAs/AlGaAs nanoheterostructures. The assumption was that by selecting an appropriate bioreceptor for selectively immobilizing *L. pneumophila* on the surface of a biosensor, these bacteria could be detected using photocorrosion technique. Moreover, it was hypothesized that the Debye length could be altered to further intensify the charge effect of bacteria. In spite of the recent publications on this relatively new approach for detection of *E. coli*, an extensive evaluation was required, especially in the context of biophysical properties of different bacteria and potentially their different surface electric charge and immobilization efficiency. To address these concerns, surface electric charge effect of various bacteria was determined using zeta potential measurements and the binding efficiency was evaluated by fluorescence and optical microscopy. Hence, the potential problems and obstacles concerning the LOD of QSPB technology for detection of *L. pneumophila* were explored.

Third, improving bacterial adhesion to the surface of biosensor for enhancing LOD. The presumption included reducing the surface repulsion effect to facilitate bacterial immobilization at the surface of bio functionalized semiconductors. The bacterial adhesion process was studied based on the previously developed models of the DLVO theory and semiconductor band energy structure in an electrolytic environment. For that purpose, a microfluidic setup for electrically

biasing biochips was designed and implemented. Then, the electrochemical impedance spectroscopy system was applied for providing precise control over electrical bias measurements.

Fourth, enhancing the LOD of photocorrosion based biosensors by modifying the bacterial electric charge. The hypothesis was that the surface electric charge of bacteria could be modified in a way that bacterial negative charge increases, leading to an enhanced LOD. For such an idea, conjugation of synthetic molecules that carry multiple negative charges to the surface of bacteria, mechanisms of interaction of bacteria with these organic moieties and other critical aspects of decorating bacteria were studied.

1.4. Original Contributions and Thesis Layout:

The chapters of this thesis are ordered in a way to, at first, provide a clear definition of the photocorrosion process and its implication for atomic layer etching of GaAs/AlGaAs nanoheterostructures. Then, the biosensing application for detection of *L. pneumophila* as well as the nature of bacteria detection with a photocorrosion biosensor is explained. Finally, the enhanced methods that were employed for improving the sensitivity of such a platform are discussed along with the related details. Details of the original contributions for each chapter are explained in the following paragraphs.

The present chapter introduces the research project and defines the research objectives. It also highlights the original contributions of this research.

Chapter 2 reviews conventional approaches as well as development of biosensors for detection of bacteria in aqueous environment along with their related critical aspects, such as technological pros and cons, dynamic range of their performance, LOD, etc. This chapter exposes the picture of the presented research objectives in more depth. Besides, biosensing based on electric charge of bacteria and photonic behaviour of quantum semiconductors is elaborated in this chapter.

Chapter 3 presents a comprehensive study of GaAs/AlGaAs nanoheterostructure photocorrosion, putting forward a viable technique for sequential (digital) atomic layer etching of GaAs/AlGaAs nanoheterostructures while potentially maintaining the stoichiometry of the

photoetched surfaces. The essence of this chapter includes establishing, with ICP-MS, the conditions of achieving congruent decomposition, which is required for producing a stoichiometric surface. Notably, it is argued and proved that the surface stoichiometry can be examined *in situ*, instead of using ICP-MS, by measuring the temporal position of PL-revealed interfaces of GaAs-electrolyte, AlGaAs-electrolyte and GaAs-AlGaAs. Using ICP-MS data, it is confirmed that the proposed technique resulted in homogenous digital photoetching of GaAs/$Al_{0.35}Ga_{0.65}As$ nanoheterostructures in NH_4OH, for etch depths approaching 100 nm. It is also shown that the DIP process of GaAs/AlGaAs nanoheterostructures allowed an atomic layer precision of material removal without the need of changing the hardware that, normally, is required by the conventional digital etching methods. Finally, the feasibility of a simple and relatively inexpensive process for fabrication of compound semiconductor nanodevices, with stoichiometric surfaces extending deep into etched nanoheterostructures is discussed in this chapter. This chapter is in preparation for a journal publication.

In Chapter 4, detection of *L. pneumophila* using a photocorrosion based biosensor is demonstrated. The main biophysics differences of *L. pneumophila* compared to *E.coli K12* are exposed, and the role of ionic strength of phosphate buffered saline solution is extensively discussed. Cooperation of these findings led to experimentally establishing a LOD of 10^4 CFU/ml for *L. pneumophila*. This chapter reveals the importance of the Debye screening length, which relates to the zeta potential of bacteria, and eventually the LOD of the biosensor. Prior to this research, a hyperspectral imaging PL mapper was employed for detection of *E. coli* K12 using GaAs/AlGaAs nanoheterostructures [25, 30]. Conversely, in this chapter, design and application of a portable and miniaturized device for optical reading of the quantum semiconductor biosensor, referred to as quantum semiconductor photonic biosensor reader (QSPB Reader) is demonstrated. It is shown that QSPB Reader provides the conditions to obtain excellent temporal PL characteristics. This chapter provides also the proof of heterostructure layer removal with the DIP process, using low temperature optical spectroscopy carried out at the Department of Physics of Université de Sherbrooke. This chapter has been published in the *Biointerphases* journal.

Chapter 5 discusses an approach in which the electrically biased biochip was proposed for attracting more bacteria to the surface of a biosensor, aiming at improving the transfer of the bacteria to the surface of the biosensor and eventually enhancing LOD. Applying electrical bias to

biochips increased the number of immobilized bacteria, however the oxidation/dissolution of the surface due to the electrochemical reaction of GaAs imposed some limitations. The required conditions and the challenge with engaging the electrical bias method on the semiconductor-based biosensor are discussed. This chapter is published in *Synthesis and Photonics of Nanoscale Materials XIII* (Proceeding of SPIE).

Chapter 6 addresses the problem of a biosensor detecting electrically charged biomolecules. It presents an innovative technique of nanoengineering the functional groups of bacterial surfaces for improving their negative charge, which leads to an enhanced LOD of a biosensor. It is shown that decorating the surface of bacteria with negatively charged molecules of different moieties can increase the net negative charge of bacteria, however the efficiency of interaction of molecule with the surface of bacteria and the magnitude of the electric charge enhancement strongly depends on the interaction type, e.g. electrostatic interaction, covalent binding or hydrophobic interaction. This chapter focuses on hydrophobic interaction of sodium dodecyl sulphate with bacteria and its effect on viability and binding ability of bacteria. We successfully demonstrated detection of heat inactivated *L. pneumophila* with a reproducible LOD at 10^3 CFU/ml, which represents one order of magnitude improvement compared to our previously published data. This chapter has been submitted for the *Biosensors and Bioelectronics* journal.

Chapter 7 offers a brief summary and overview of the entire thesis. The perspective and suggestions for future work are explained in this chapter.

CHAPTER 2. State of the Art

Design and implementation of a biosensing system that can satisfy the specified requirements for a particular environment, such as water, requires information about the available techniques and their advantages/limitations, so a plausible method of interest could be proposed and developed. Hence, the present chapter starts with describing biosensor and providing analysis of the modern techniques that were technologically advanced over the past years for detection of some biomolecules. Subsequently, the photoluminescence (PL) transducer, as the core of this study, is introduced and in the light of recent progresses that were made, the main drawbacks of PL based biosensing, to be addressed, are exposed. For further clarification of the objective of the thesis as well as justification of the proposed solution with respect to the hypothesis presented in chapter 1, critical aspects for enhanced detection of bacteria, such as semiconductor electrolyte interface, nature of bacterial electric charge effect and bacteria adhesion mechanism are also described here. This chapter ends with comparing the performance of PL technique in with other common biosensing methods, employed for detection of *E. coli* and *L. pneumophila* in water.

2.1. Biosensors

Biosensors are analytical devices that can provide quantitative or qualitative information about presence of an analyte in the environment of interest. In general, they consist of a bio-receptor to recognize the interrogating molecule (analyte), a transducer to convert the bio-

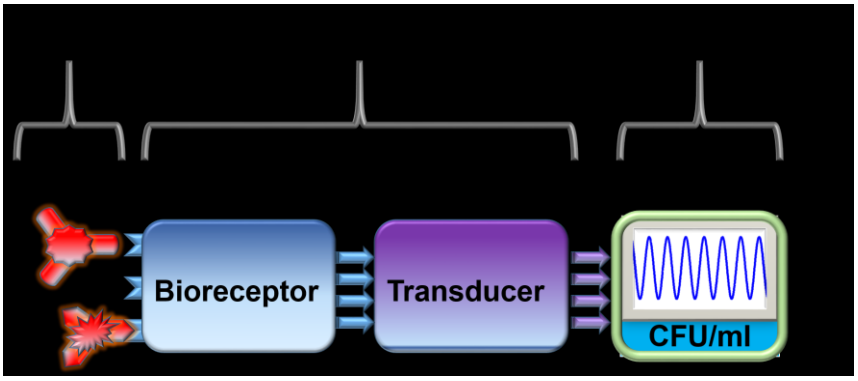

Figure 2-1. Schematic view of a biosensing system for detection of bacteria.

recognition event into a properly measurable signal and a biosensor reader, which presents the signal produced by the transducer in a user-friendly way. **Figure 2-1** shows a schematic representation of a typical biosensing system.

Biosensors could be classified according to the type of employed bioreceptor or the mode of signal transduction or even the combination of both aspects. In these systems, bioreceptor determines the degree of selectivity or specificity of the biosensor and they are divided as biocatalytic, bioaffinity and hybrid receptors. Biocatalytic receptors are generally based on the detection of organic compounds assimilated by the microorganisms or monitoring changes occurring in respiration activity during metabolism. The interaction of biological material and the target analyte could modify the analyte into the new chemical molecules. They mostly contain enzyme, whole cells and plant or animal tissue slices. Sensors based on biocatalytic receptors are usually slow and they show low selectivity [32]. Bioaffinity receptors, on the other hand, work based on binding of the analyte to the biomolecule on the biosensor. These are mainly composed of antibodies, nucleic acids etc. They selectively interact with a given analyte and form a thermodynamically stable complex [33]. Depending on the availability of this type of receptor, the affinity biosensors delivered an excellent degree of specificity and selectivity in the case of immunosensors, in spite of the fact that sensitivity of the method also strongly depends on the engaged detection method. Remarkable specificity of antibodies toward antigens offered powerful antibody-based biosensing systems [34]. Lastly, hybrid receptors such as DNA and RNA are based on detection of a unique sequence of nucleic acid bases through hybridization. They take advantage of base-pairing property for sensing duplex formation of a single strand, which recognizes its

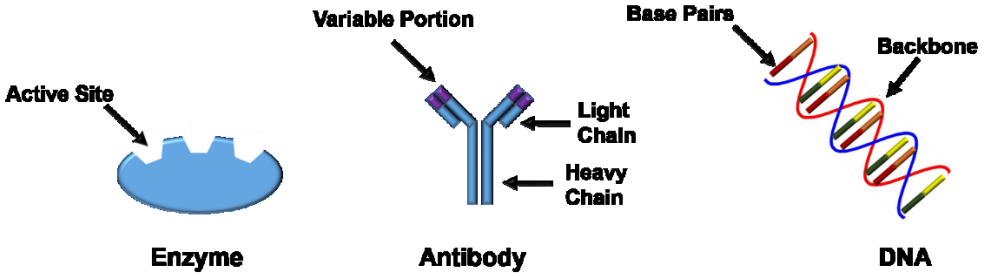

Figure 2-2. Different type of bio-receptors enabling us to specifically recognize analyte of interest.

complementary strand [35]. **Figure 2-2** shows some of these receptors used for specific recognition of the analyte.

The biological analyte can introduce different types of variation resulting in mechanical, electrical and optical characteristic variations. Using an appropriate transducer, each of these alterations is recognizable, thus biosensors could also be categorized regarding the type of produced and/or detection signal [33]. Nonetheless, the nature of selected phenomena, viz. type of the transducer, for analysis of a specific analyte has direct impact on the achievable outcomes. In the field of biosensing, transducers receive the biggest research interest, because not only they determine the overall quality of the system, but also they contribute to define the detection limit and the sensitivity of a biosensing platform. For the most part, bioreceptors control the amount of analyte delivered to the transducer and it directly affects the limit of detection (LOD), besides selection of a bioreceptor depends on availability of a specific biocomponent. In due course, the sensitivity of a biosensor is determined by the minimum-required quantity of analyte for creating a measurable detection signal. In other words, sensitivity of a biosensing system predominantly depends on the intrinsic characteristics of the transducer, but LOD depends on the efficiency of bringing the analyte of interest to the activity scope of transducer.

2.2. Transducers

The type of a transducer defines the detection signal and ultimately the form of a biosensor reader that subsequently regulates the cost of the biosensing platform. Consequently, in the design of a biosensing platform, the transduction element is the major part of its building block. Different types of bio-transducers based on electrochemical, gravimetric, electronic, and optical signals have been used for conversion of a physical phenomenon to a measurable signal. Here, each of these systems is briefly described and whenever available, examples of bacteria biosensing for each class of transducers are discussed. At the end of this section, a comparison of the principle, advantages and problems for each class of transducer is provided and their typical sensitivity (dynamic range) and limit of detection are also indicated.

2.2.1. Gravimetric Transducers

Gravimetric transducers generally produce a response to the mass changes and, in the most common form, they employ mechanical acoustic waves for biosensing. These transducers were developed based on piezoelectric quartz crystals, either as quartz crystal microbalance (QCM), or as surface acoustic wave (SAW) devices. In QCM, classified as bulk acoustic wave device, the acoustic wave propagates through the bulk, whereas in SAW the acoustic wave propagates through the surface and this made them more suitable for performing in liquid environments, since in the liquid the propagated wave could be attenuated [36]. Furthermore, SAW operates at higher frequencies (GHz rather than MHz) that brings about higher sensitivity by reducing the acoustic wave penetration depth into the adjacent medium [37]. **Figure 2-3** depicts the schematic view of a QCM setup and a SAW system. The QCM uses a quartz crystal resonator, which has been sandwiched between two electrodes (often gold) and it measures a mass per unit area by measuring the changes in frequency of quartz crystal resonator. The gold electrodes are used to induce an oscillating field and any disturbance to the surface of crystal immediately affects the oscillation frequency [38]. The performance of this biosensing systems was described by Sauerbrey equation, as follows:

$$\Delta m = \frac{-\Delta f \; A \sqrt{p_q \mu_q}}{2 f_0^2} \qquad (2\text{-}1)$$

where Δm is the adsorbed mass per unit area, Δf is the frequency change, A is the area of the gold, f_0 is the fundamental mode resonant frequency of the crystal (for an AT-cut crystal the usual

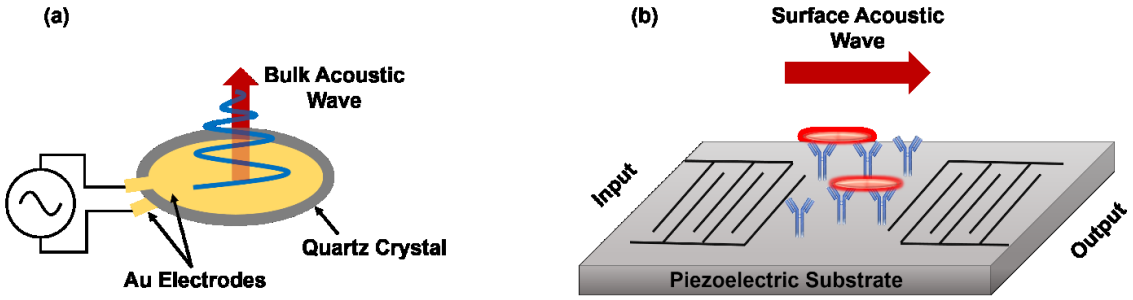

Figure 2-3. Quartz Crystal Microbalance (QCM) setup (a), Surface Acoustic Wave setup consist of piezoelectric crystal with two interdigital transducers on its sides (b). Adopted from (Fogel *et al.* 2016).

frequency range is ~ 10 MHz), p_q is the density of quartz and μ_q is the shear modulus of quartz [39].

The SAW based biosensor generates and detects acoustic waves typically using interdigital transducers (IDT), which are fabricated on the surface of a piezoelectric (ST-cut crystal) thin film, deposited on a substrate (e.g. silicon-based). In the path of the traveling wave between the two interdigital transducers, whenever bacteria bind to antibody the mass of the bio-layer will be altered. Hence, loading of mass perturbs the surface boundary conditions and consequently shifts the frequency of the traveling SAW [37]. It is also possible to measure the delay of acoustic wave travel between the two IDTs [38]. For detection of bacteria in water, the acoustic piezoelectric sensors usually employ shear waves rather than longitudinal waves, since they have lower attenuation values when operating in aqueous solution [40]. Using SAW biosensor, Howe and Harding reported detection of *E.coli* and *Legionella* at concentrations of 10^5 and 10^6 CFU/ml, respectively, in about 3 hours [14].

In a more advanced setup, Micro- and nano-electromechanical systems (MEMS and NEMS) allowed engaging a cantilever structure in mass sensing mode by taking advantage of a piezo-resistor element. In this system, the bio-recognition event occurs on the biofunctionalized side of the cantilever, then a change in surface mass results in a measurable variation in vibrating frequency of the cantilever. This could be measured using a piezo-resistor incorporated at the fixed

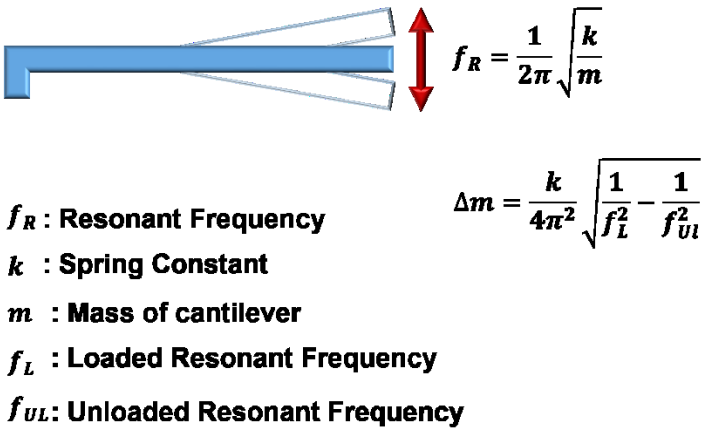

Figure 2-4. Schematic view of a cantilever structure used in mass sensing, along with the descriptive formulation of device performance. Adopted from (Bashir *et al.* 2004).

edge of the cantilever [41]. Bio-MEMS/NEMS are attention-grabbing due to their dimensional scales as well, because they can deliver very sensitive measurements when incorporated with optical monitoring of vibrations [42]. For the purpose of bacteria detection in a water environment, Bio-MEMS and Bio-NEMS, in addition to the acoustic wave based biosensors, faced some limitations due to fluid damping as well the complication in electrical interfacing in liquid [38]. **Figure 2-4** graphically illustrates the principle and formulation of the cantilever structure in a simple view. The Δm could be calculated by measuring the resonant frequency at loaded and unloaded situations [41].

2.2.2. Electrochemical Transducers

Electrochemical transducers provide specific, quantitative or semi-quantitative analytical information based on the study of redox reactions taking place at the interface of an electrode coated with a bio-sensitive receptor. These reactions take into account the exchange of electric-charges/ionic-species between the biofunctionalized electrode and the electrolyte [43]. As a result, there are variety of measurable changes such as change in the electrical current associated with the electrons of redox processes (amperometric), change in electrode potential because of charge accumulations (potentiometric) and change in conductance (conductometric) or impedance (impedimetric) of the ionic medium between the electrodes [44]. In general, this method uses a three-electrode setup consist of a working electrode, a reference electrode (commonly Ag/AgCl) and a counter electrode (mostly platinum, gold, carbon), as shown in **Figure 2-5**. Reference electrode enables precise measurements by providing a well-defined and a stable potential.

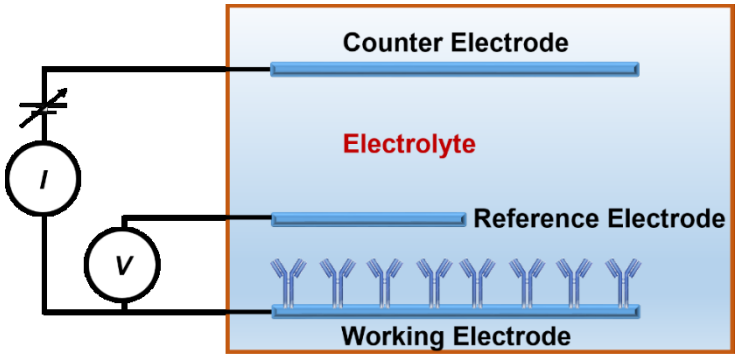

Figure 2-5. Schematic view of a three-electrode electrochemical setup. The working electrode is biofunctionalized with antibodies to capture bacteria. Adopted from (Mello *et al.* 2002).

Amperometry identifies the variations in the electrical current, at a constant applied potential, due to the ions originating from the oxidation/reduction reactions in a solution, and its response is a linear function of (directly proportional to) the concentration of the analyte. However, the sensitivity of these devices is only governed by the redox potential of the presented electro-active species, consequently the current that is measured by the instrument can include the contributions of several chemical species [45]. Furthermore, this sensor is not universally applicable, since all analytes are not capable of serving as redox partners in the electrochemical reactions [44]. By means of standard immunoassay amperometry technique, Zeynep *et al.* reported detection of *E. coli* with LOD of 1.99×10^4 CFU/ml, which was later significantly improved using nanomaterial amplified immunoassay [46].

Conductometric/Impedimetric technique senses the changes in the conductive properties of medium between the electrodes and in this case the sensitivity of the system depends on the ability of the medium to conduct electrical current [44]. Normally, conductometric transducers are considered as a subset of impedimetric transducers, which measures both resistance and capacitance variations due to a bio-recognition event. In this approach a sinusoidal electrical potential is applied between the electrodes and the electrical current is measured. Then, by varying the excitation frequency of the applied potential the impedance components could be determined. This technique combines the analysis of both real and imaginary components of impedance (electrical resistance and reactance) as shown below:

$$Z(j\omega) = \frac{U(j\omega)}{I(j\omega)} = Z_r(j\omega) - jZ_i(j\omega); \quad \omega = 2\pi f \qquad (2\text{-}2)$$

where Z is the complex impedance, U is the applied potential, I is the current response and f is the excitation frequency [44]. The conductivity of the solution depends on the number and type of ions, temperature and the viscosity. This implies that the main problems of this type of sensors are their sensitivity to the environmental temperature changes, the fluctuations in amounts of dissolved gases as well the degradation of culture medium during bacterial incubation [43].

Potentiometric technique discerns the surface charge accumulations at the working electrode, thus it is a sensitive method for detecting electrically charged species. Using a high impedance voltmeter, the potential of the working electrode, also called ion selective electrode

(ISE), versus a reference electrode is measured, while the current flow is negligible. Then, the relation between the potential variations and logarithm of the analyte concentration could be described by the Nernst equation, as follows [47]:

$$E_{cell} = E^{o}{}_{cell} - \frac{RT}{nF} \ln Q \qquad (2\text{-}3)$$

where $E^{o}{}_{cell}$ is standard electrode potential, R is the universal gas constant, T is the absolute temperature in Kelvin, n is the charge number of the electrode reaction, F is the Faraday constant and Q is the ratio of ion concentration at the anode to ion concentration at the cathode. These devices are mainly used as a *p*H sensor.

2.2.3. Electronic Transducers

In this approach the electronic properties of a semiconducting material, such as electron transport, is tuned or affected by the presence of an analyte. For such a purpose, field effect transistors have been widely designed for converting molecular properties to electronic signal [27]. Electronic transducers, typically in form of an ISFET (Ion-Sensitive Field-Effect Transistor), are in fact another version of electrochemical transducers that employ the channel of a transistor to measure the current variations due to the potentiometric effect at a Gate terminal surface [43, 44]. As the main advantage, these types of sensors can be conveniently integrated into the

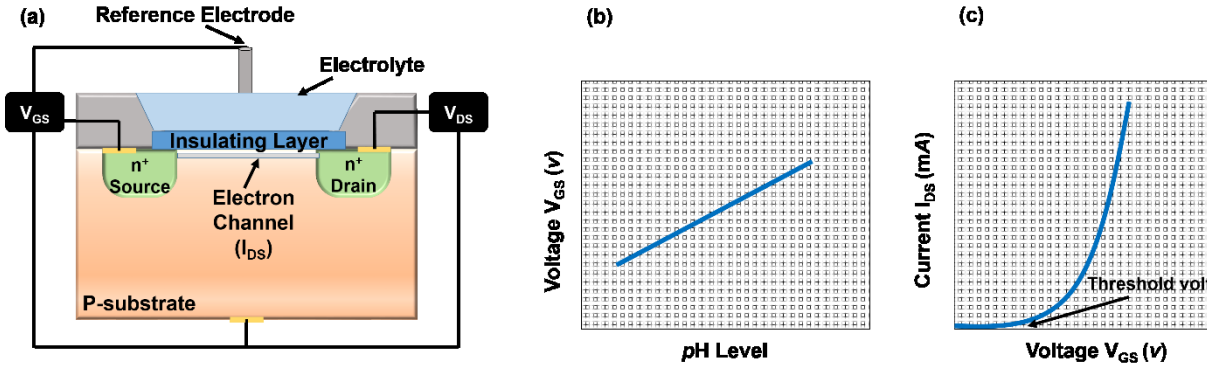

Figure 2-6. An ion sensitive system based on based on field effect transistors (a), the pH response of device according to V_{GS} (b), and the I-V characteristics of the transistor, showing the threshold voltage for starting the electron channel formation (c). Adopted from (Pohanka *et al.* 2017).

microelectronic systems with a high throughput [48]. **Figure 2-6** shows an ISFET structure, which has been usually used as a *p*H sensor [49]. Depending on the doping type of the semiconducting material, the presence of sufficient charged biomolecules at the Gate terminal would either attract charge carriers (e.g. electrons) or repel charge carriers in the conducting channel between the Source and the Drain terminals of transistor. This would hence alter the conductance between them, namely slope of I-V curve, which can be associated to the analyte concentration (or *p*H) at the Gate terminal.

2.2.4. Optical Transducers

With the developments of optical systems as well as laser technology, optical transducers have been more frequently considered in biosensing application. Optical bio-transducers transform the bio-recognition event into an optical signal [43]. These transducers use photons in order to collect information about the analyte that makes them highly sensitive, specific, and most importantly they can be effectively miniaturized. Interaction of the bioreceptor with the target analyte can change the photonic properties such as fluorescence/phosphorescence, reflectance, scattering and refractive index that are all distinguishable by optical biosensors.

2.2.4.1. Surface Plasmon Resonance (SPR):

In the context of optical transducers, SPR received considerable attention. This system collects data based on refractive index variations at the interface of two materials with opposite sign permittivity [50]. **Figure 2-7** shows the schematic view of a SPR system, along with the type of produced signal. Typically, a gold/silver coated glass slide is incorporated as one of the walls of a thin flow-cell. The metallic part is covered with the bioreceptor and then the target analyte is flowed through the flow-cell. Beams of visible or near infrared light excites the interface of metal/glass to provide the plasmon resonance condition. The energy carried by photons will be coupled or transferred to electrons of the metal and results in the creation of a plasmon, which is a group of excited electrons on the surface of the metal [51]. Immobilization of the target analyte can affect the plasmon resonance, which is monitored by following the change in the angle of reflection, shown in **Figure 2-7 (b)**, or shift in the wavelength of absorbed light, shown in **Figure 2-7 (c)**. Therefore, SPR can provide information about the density of the analyte in the vicinity of the gold/glass interface, typically with distance of less than 200 nm [52]. However, most of bacteria

are relatively large objects, for instance *E. coli* is ~ 0.5 µm in width and ~ 2µm in length [53]. This can significantly affect the detection limit of SPR [54]. Notwithstanding, Usachev1 *et al.* reported LOD of 1.5×10^3 CFU/ml for detection of *E. coli* using a SPR system [54].

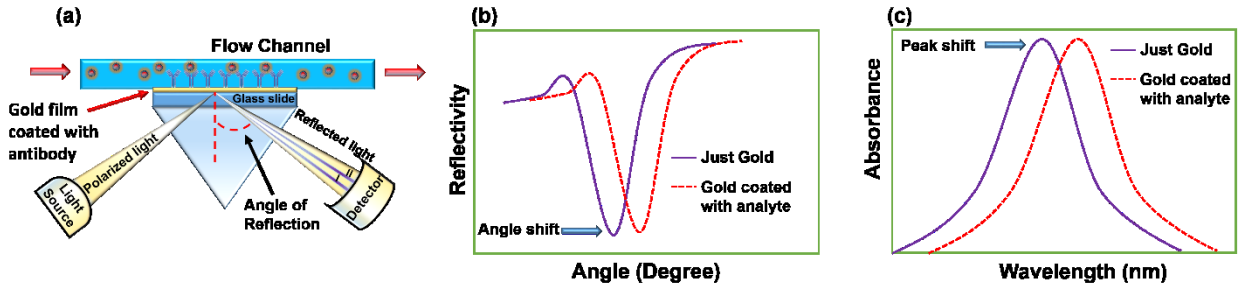

Figure 2-7. Schematic view of a typical SPR system (a), monitoring the angle at which the reflection is minimum (b), monitoring the wavelength at which the absorption of reflected light is maximum (c). Adopted from (Mello *et al.* 2002).

2.2.4.2. PL Transducers: Latest Trend for Analyzing Bio-Molecular Interactions

In the study of surfaces and interfaces, the PL characterization method is a popular technique, because it is flexible and can be used to assess a surface in almost any environment, as well it is one of the approaches available for measuring fast optical transitions in materials, especially semiconductors [55]. Chemisorption of some species can induce surface states possessing energy within the bandgap of the semiconductor. In that respect, modification of the GaAs surface has been considered as one of the most efficient techniques to control its surface electronic, for instance using organic molecules [56]. As one of the latest applications, PL based study of surfaces' perturbation induced by electrically charged biomolecule was reported, showing promising results for detection of *E. coli* [25, 30]. The PL of a semiconductor is very sensitive to its surface potential, and the bacterial cell surface carries a net charge (mostly negative under normal physiological conditions) [53]. Once bacteria are close enough to the surface of a semiconductor, they can affect the surface potential of the semiconductor and change the PL characteristics. This makes PL transducer an attractive approach for *in situ* monitoring the presence of charged particles such as bacteria in water. Bacteria can impact the PL emission intensity by changing the surface recombination velocity (SRV) [57], at the same time they can change the temporal PL kinetics by changing photochemical reactions, taking place at the semiconductor/electrolyte interface. In such a case, heterostructures are very important, as they

can provide some efficient and specific characteristics, such as current density oscillations [58] or PL intensity extremums [30]. **Figure 2-8** compares the PL profiles of an n-type bulk GaAs and a GaAs/AlGaAs nanoheterostructure both exposed to DI-water. Absorption of light creates photo-excited carriers in a semiconductor. For an n-type semiconductor in an electrolytic environment, holes come up to the semiconductor/electrolyte interface and the electron moves toward the bottom of the sample, owing to the interface electric field. This could lead to photonically induced corrosion, known as photocorrosion, of the semiconductor and some modification of its surface morphology, consequently an increment of the semiconductor PL-intensity could be observed [59, 60]. For the GaAs/AlGaAs nanoheterostructure, depending on the designed structure, this leads to appearance of some explicit temporal PL extremums. The mechanism of such a temporal PL behavior is broadly explained in chapter 3. Nevertheless, even though the initial photochemical reaction is similar for both samples in **Figure 2-8**, the temporal PL of a GaAs/AlGaAs nanoheterostructure provided more pronounced PL intensity increment compared to an n-type bulk GaAs. Hence, one can monitor the position of PL maximum intensity versus time, in order to obtain information about the involved surface chemistry. The principle of detecting bacteria using semiconductor photocorrosion is explained in detail in the next section of this chapter.

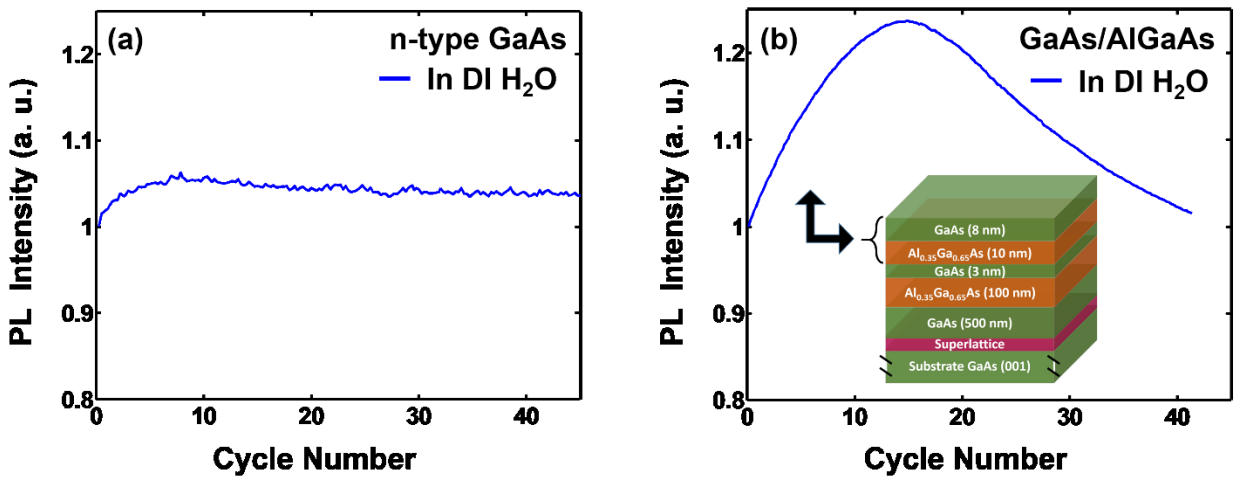

Figure 2-8. Comparison of temporal PL-intensity variations from an n-type bulk GaAs (a) and a GaAs/AlGaAs nanoheterostructure (b), both carried out in DI H_2O with duty cycle of 6/60 and power density of 40 mW/cm^2.

Figure 2-9 shows the results for detection of *E. coli* obtained using a PL transducer. By only monitoring the PL intensity increment, Duplan *et al.* demonstrated detection of *E. coli* in

phosphate-buffered saline (PBS) solution with LOD down to 10^4 CFU/ml [25]. They showed that the increased PL intensity of GaAs based biochips could be correlated to the concentration of negatively charged *E. coli* in PBS, as presented in **Figure 2-9 (a)**. Alternatively, Nazemi *et al.* monitored temporal PL intensity maxima of GaAs/AlGaAs nanoheterostructures for *E. coli* detection, shown in **Figure 2-9 (b)**. It was presumed that immobilization of negatively charged bacteria slowed down the photochemical processes at the interface of the semiconductor/electrolyte, leading to the delayed PL maximum-intensity appearance, compared to the PL profile of a well-defined reference sample (a sample that has not been exposed to bacteria).

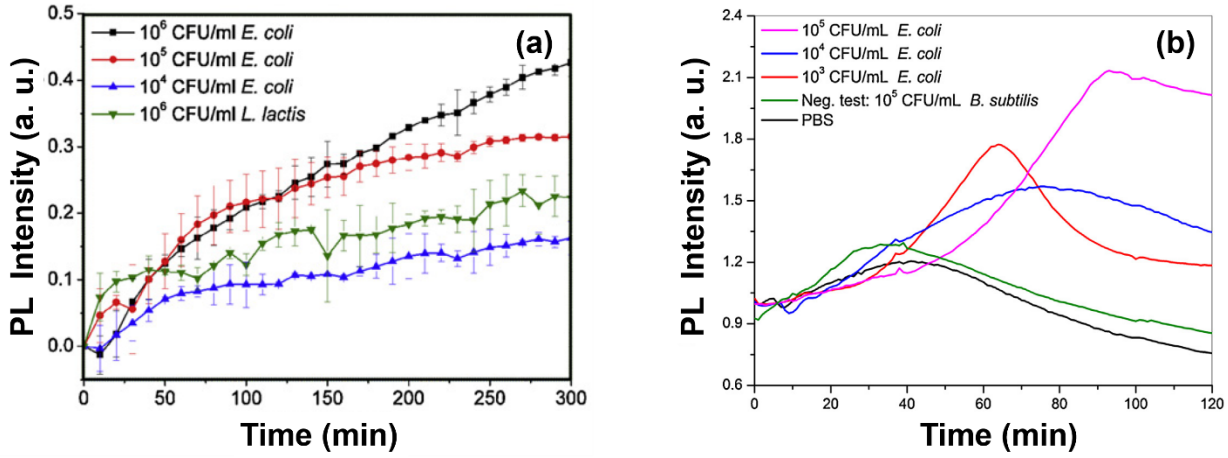

Figure 2-9. PL intensity of GaAs based biochips versus *E. coli* concentrations (a), temporal PL-intensity profile of GaAs/AlGaAs nanoheterostructure for different concentration of *E. coli* (b). Figures (a) and (b) were adopted from (Duplan et al. 2011) and (Nazemi et al. 2015), respectively.

2.3. Principles of PL Based Detection of Bacteria Detection in Water

Interpreting and modeling the performance of a PL based biosensor is a complicated challenging subject, since it is a highly interdisciplinary field of research, comprising of physics, biochemistry and microbiology. Nonetheless, the most important aspects related to the semiconductor-PL based biosensors could be categorized as i) formation of a double layer at the interface of semiconductor/electrolyte, ii) nature of the photocorrosion process and iii) effect of the bacterial surface charge on the photocorrosion process due to the interaction of double layers. These features are systematically discussed in the following 3 sections.

2.3.1. Semiconductor in Electrolyte and Double Layer Formation

Figure 2-10 displays the schematic view of a double layer formed on an n-type semiconductor. When we bring a semiconductor in contact with an electrolyte, the difference between the work function of the two side materials imposes a transient charge transfer, which will tend to zero after reaching the thermodynamic equilibrium condition. Therefore, the Fermi levels of both components will adopt an equal value at their interface and will force redistribution of the charge carriers. At the surface of the semiconductor, this causes formation of a region depleted of majority carriers called space charge region or depletion region, leading to surface band bending that is upward for n-type or downward for p-type semiconductors [61]. Besides, the electric field associated with the depletion region at the surface dissociates the electron-hole pairs at the semiconductor/electrolyte interface, which results in the reduced PL intensity for GaAs [62]. Furthermore, the electric field of the depleted region extends to the electrolyte and adsorbs ions on the surface of the semiconductor to create the Stern layer (see **Figure 2-10**), that is strongly adsorbed to the semiconductor surface. To satisfy the charge neutrality, a second layer named diffuse layer is created that is loosely bonded to the Stern layer ions. The Stern and diffuse layers (also called double layer) generate some extrinsic surface states that are mainly governed by the type of electrolyte. In this condition, not only the accumulated holes (for n-type semiconductor) cannot participate in the PL signal formation but also, they adsorb an electron from the electrolyte and participate in the current (if there is an electrically closed loop) [63].

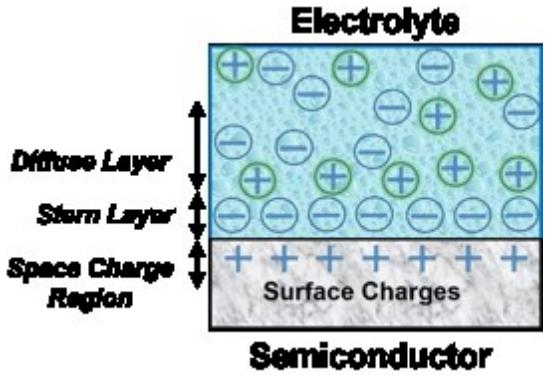

Figure 2-10. Schematic view of semiconductor/electrolyte interface, representing Stern and diffuse layers. Adopted from (van de Krol et al. 2012).

2.3.2. Photocorrosion: Photo-Electrochemical Reactions Influencing PL Profile

At the GaAs/electrolyte interface, the semiconductor material can undergo an oxidation process (oxide development) depending on many parameters including *p*H, ionic strength of electrolyte and the presence of an excitation energy that could be provided by photons possessing energy larger than the semiconductor band gap. Semiconductors are capable of absorbing light with energy higher than their band gap and consequently creating photo-excited carriers. In the case of n-type semiconductor, the electric field created at the surface will push the holes toward the semiconductor/electrolyte interface, whereas electrons will travel toward the bulk region [64]. Therefore, these holes induce the oxidation process, which experimentally proved to affect the spectral and temporal PL characteristics of bulk-GaAs [65]. **Figure 2-11** shows a graphical view of how photo-excited carriers are driven to/from the surface due to the surface band bending, as well the generally accepted photochemical reaction for GaAs [30]. Therefore, the rate of this process can be regulated by the number of hole-carriers from GaAs or the number of electrons from electrolyte reaction species. As generally accepted, for the III-V semiconductors the holes are responsible for initiating the oxidation of semiconductor surface. Hence, the degree of the surface modification process is a function of the band bending condition, as well as the concentration of reduced ions. Therefore, if some charged particles, such as bacteria, approach the semiconductor surface and change its band bending, this will affect the oxidation (surface modification) rate, thus changes the PL kinetics. By monitoring the temporal PL of a semiconductor nanoheterostructure, this rate variation can be determined and correlated to the presence of charged particles. This has been previously employed for detection of *E. coli* [30] and initially studied by Aithal *et al.* [108]. However, a more systematic approach was required towards the analysis of photocorroding GaAs/AlGaAs nanoheterostructures and providing a semi-quantitative description of the process.

- *Hence, in the present thesis, PL spectroscopy at low temperature was employed to investigate the photocorrosion process of GaAs/AlGaAs nanoheterostructures in an aqueous solution for providing concrete evidence for capability of a PL based system to precisely support nanometer scale optically driven etching of semiconductor layers. Furthermore, to investigate the dynamics of photon induced semiconductor dissolution, inductively coupled plasma mass spectrometry was conducted on the residual product of GaAs/$Al_{0.35}Ga_{0.65}As$ nanoheterostructures photocorroding in*

deionized water or ammonium hydroxide. The surface characteristics of photoetched samples were further analyzed with X-ray photoelectron spectroscopy, Fourier transform infrared absorption spectroscopy and atomic force microscopy.

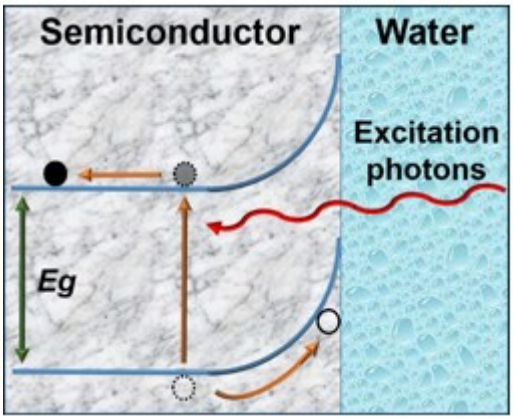

$$GaAs + 2H_2O + 6h^+ \rightarrow Ga^{3+} + HAsO_2 + 3H^+$$

h^+ : hole-carriers

Figure 2-11. Photo-carrier generation and reaction at the interface of n- type GaAs and water.

2.3.3. Bacteria Characteristics: Double Layer and Zeta Potential

Almost all particles suspended in an electrolyte have a surface charge, which affects the distribution of counter ions in the solution and gather them around the particle, creating a double layer region over which the influence of surface charge is extended. Once again, electrical double layer consists of a Stern layer, the first layer of counter ions that are tightly attracted to the particle surface, and the diffuse layer, where ions are loosely bound and they screen the charges of the Stern layer. When the particles move, the ions in closer distance to their surface, up to a certain extent, will also move with particles. The surface of hydrodynamic shear or slipping plan is defined as the boundary beyond which the ions do not move with the particle movement and the electro kinetic potential or zeta potential is defined as the potential of this point (distance) [66]. **Figure 2-12** displays a particle with the boundary of double layer and slipping plane, where the zeta potential is basically defined.

In the case of bacteria, protonation and dissociation of functional groups at their surface create an electrically charged surface. In fact, at physiological *p*H values, i.e. between 5 and 7 the surfaces of almost all bacteria (except a few of them) are negatively charged owing to the presence

of proteins and other wall and cell membrane components containing phosphate, carboxyl and other acidic groups [53]. Bacteria could be captured near the semiconductor surface covered with antibodies targeting specific bacteria. After the molecular interactions between bacteria and antibodies become dominant, for n-type semiconductor, the negative charge of bacteria repels the negative ions (responsible for dragging hole from semiconductor) at the surface of GaAs and leads to lowering of band bending and thinning of the depletion region. Hence, lower amounts of holes of valance band can reach the surface and the rate of photocorrosion decreases (see chemical reaction in **Figure 2-11**). For that reason, the photocorrosion of GaAs/AlGaAs is expected to be decelerated in the presence of bacteria. In that context, Miller and Richmond experimentally demonstrated that, for n-type GaAs, the rate of photocorrosion is faster for upward band bending condition (wider space charge) in comparison with n-type GaAs biased at flat band condition (thinner space charge) [60].

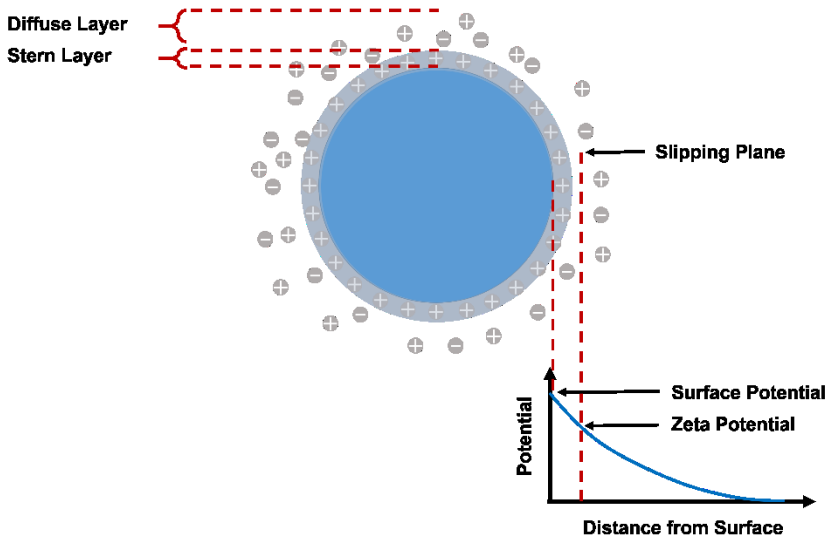

Figure 2-12. Schematic representation of double layer and slipping plan around particle, suspended in an electrolytic solution. Zeta potential is defined as the potential at a distance equal to the slipping plan. Adopted from (Kaszuba *et al.* 2010).

Zeta potential measurements allow us to investigate the electric charge effect of bacteria. **Figure 2-13** shows a typical setup for the laser Doppler micro electrophoresis, through which the mobility of bacteria in the solution can be obtained. Then, the Helmholtz-Von Smoluchowski equation can relate the bacterial mobility to their zeta potential in the surrounding solution. For

that purpose, a very thin layer of bacterial solution (in a capillary cell) is exposed to a known electrical field, while a laser beam interferes at a stationary point inside the capillary cell. The signal from this point is collected and compared to the reference signal (without scattering). Movement of bacteria due to applied bias causes a scattering of the laser light and results in frequency shift, which can directly indicate the bacteria velocity and ultimately their mobility [53, 66, 67].

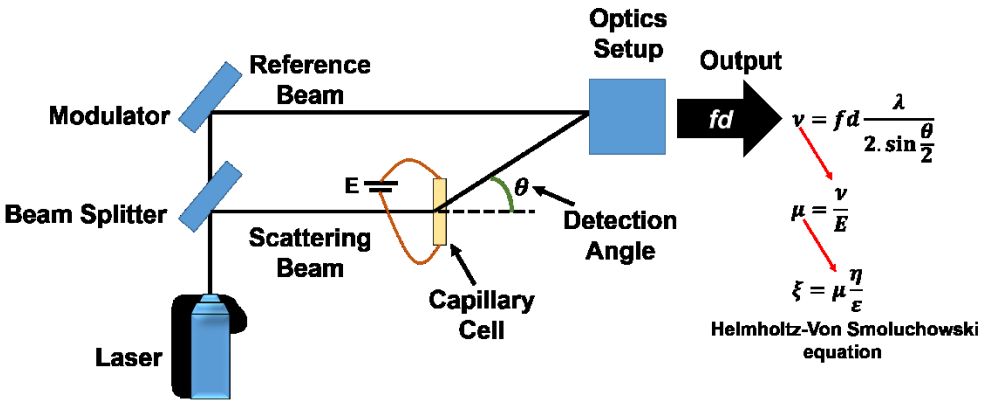

Figure 2-13. Schematic of a typical configuration for laser Doppler electrophoresis measurements. Adopted from (Kaszuba *et al.* 2010). In the equations, ζ is the bacterial zeta potential, μ is the electrophoretic mobility, ε and η are, respectively, the dielectric permittivity and the bulk viscosity of the suspending solution, v is the bacterial velocity, E is the applied electric field, θ is the detection angle, λ is the wavelength of laser and fd represents the frequency (phase) shift.

2.4. Enhanced Bacterial Detection Using PL Transducer Based on GaAs/AlGaAs

2.4.1. Ionic Screening Effect (Debye Length)

In a PL based biosensor, binding of a charged biomolecule changes the electrostatic condition of the semiconductor band structure at the semiconductor/electrolyte interface via altering the charge carrier density of the transducer surface. However, the detection performance for the case of biological aqueous environments is limited by ionic screening effects arising from formation of double layer that is related to the force of the depletion region's electric field [68-70]. The charges of the semiconductor depletion region attract counter ions from the electrolyte and

result in formation of an electrical double layer, which in turn effectively screens off the charge effects near the GaAs surface. Similarly, the same phenomenon happens for the bacteria. At a certain distance characterized by the Debye length, the charge of both GaAs and bacteria surfaces will be compensated by counter ions and their surface potentials reach almost to zero value. Since the bacteria are kept away from the GaAs surface at a certain distance, depending on the length of employed bioreceptor, the charge of bacteria might affect the semiconductor band bending to a different degree.

- *For these reasons, one important problem in charge (bio)sensing is the double layer screening effect that should be minimized in order to increase influence of the immobilized bacteria with as low as possible concentration of bacteria. As a general solution, the properties of the surrounding aqueous milieu such as ionic strength could be modified to achieve better results, but to engineer a method to be used in relatively high ionic strength environments, the decoration of bacteria with negatively charged molecules is proposed and investigated here.*

2.4.2. Bacteria Immobilization: Brief Review of DLVO Theory

Only a few types of bacteria and microbes have a free-roaming lifestyle, while the rest prefer to stick to a surface. Before having stable adhesion through intermolecular interactions, bacteria experience an electrostatic interaction, which is an important factor influencing the bacterial adhesion process. Since bacteria could be modelled with colloidal particles, researchers used the DLVO theory, developed by **D**eryagin, **L**andau, **V**erway and **O**verbeek, to describe the forces acting on bacteria. Conceptually, the DLVO theory considers two governing forces to predict the attachment of bacteria to the first phase (reversible physical phase), which occurs before intermolecular interaction with antibody (irreversible molecular phase) [71]. These forces are i) the van der Waals forces that are the result of induced dipole interactions, and they are generally attractive forces, ii) the double layer forces arising from counter ions, and they are repulsive [72]. Study of these forces may provide a conceptual framework to understand bacterial attachment.

Since the two surfaces (semiconductor and bacteria) have the same charge they will repel each other. The calculations are very difficult and numerous factors must be considered, however a simplified picture points out that the repelling force of the two charged surfaces is inversely

proportional to the distance between them. On the other hand, the van der Waals force is caused by the interactions between oscillating dipoles on the surface of molecules and it relatively unaffected by the ionic strength [73]. The van der Waals force is very strong, but it is efficient only at small distances. The DLVO theory in its simplest form considers only these two main forces and gives a picture of how surfaces interact electrostatically.

Based on the DLVO theory the van der Waal attraction is a short-range force and the double layer repulsion is a long-distance force, so it repels the bacteria before Van der Waals attraction can capture them. Then, there would be a lower probability for charged particles to overcome this barrier and reach the bioreceptor and initiate intermolecular attachment. This reduces the number of immobilized bacteria; however, the double layer repulsion is strongly related to the width of GaAs space charge or, to be precise, to the depletion region's electric field [74].

- *Accordingly, another significant research questions that remains unanswered is how to modify the band bending of the semiconductor region in order to reduce the depletion region's electric field and create a condition, where more bacteria can approach the surface of GaAs, while still providing enough sensitivity for bacteria detection. The proposed strategy to overcome this problem is applying an electric bias to the GaAs/AlGaAs nanoheterostructure, which would reduce the surface band bending, hence immobilize more bacteria at the surface of the transducer.*

2.5. PL Transducer vs Other Techniques

To put PL based transducer performance in perspective, sensitivity, dynamic range and major pros and cons of common biosensing techniques has been compared. Table 2-1 provides a detailed comparison of the main features and characteristics related to the biosensor that were employed for detection of bacteria, chiefly *E. coli* and *L. pneumophila* in an aqueous environment.

Table 2-1. Comparison of different transducers employed for detection of *E. coli* and *L. pneumophila* in water.

Transducer	Electrochemical	Optical (SPR)	Optical (PL)	Electronic	Gravimetric
Principle	Electrical variations	Photonic variations	Photonic variations	Electronic variations	Mass variations
Advantages	- Low cost - Variety of methods	- Sensitive - Fast	- Low cost - Fast - Easy integration for remote sensing - Miniaturized	- Low cost - Mass Production - Easy integration for Lab-on-a-Chip systems	- Fast - Sensitive
Problems	- Interpretation of data is difficult - Large variability - Hard to reuse electrodes	- Relatively complicated - Relatively expensive - Not appropriate for large objects such as bacteria	- Moderate sensitivity - Only applicable to specific materials	- Low sensitivity - Temperature sensitive - Large variability	- Low sensitivity in liquid
Typical Sensitivities	10^2-10^5 CFU/ml	10^4-10^8 CFU/ml	10^4-10^6 CFU/ml	10^6-10^9 CFU/ml	10^6-10^8 CFU/ml
LOD *E. coli*	70 CFU/ml [75]	10^3 CFU/ml [54]	10^3 CFU/ml [30]	10^5 CFU/ml [76]	10^6 CFU/ml [77]
LOD *L. pneumophila*	10^4 CFU/ml [78]	10^4 CFU/ml [79] 10^3 CFU/ml [13]	10^3 CFU/ml [This Work]	10^5 CFU/ml [80]	Not found

CHAPTER 3. Photo Atomic Layer Etching of GaAs/AlGaAs Nanoheterostructures

3.1. AVANT-PROPOS

Auteurs et affiliation:

- Mohammad Reza Aziziyan : Étudiant au doctorat, Université de Sherbrooke, Faculté de génie, Département de génie électrique et informatique.
- Hemant Sharma : Stagiaire postdoctoral, Université de Sherbrooke, Faculté de génie, Département de génie électrique et informatique.
- Jan J. Dubowski : Professeur titulaire, Université de Sherbrooke, Faculté de génie, Département de génie électrique et informatique.

Titre français : Photo-gravure de couche atomique des nanoheterostructures GaAs/AlGaAs

Contribution au document : Ce chapitre présente certains aspects fondamentaux de l'élimination de matière photo-induite et de la formation de surfaces stœchiométriques III-V. Ici, la photocorrosion des nanohétérostructures GaAs/AlGaAs est systématiquement étudiée par spectrométrie de masse à plasma à couplage inductif (ICP-MS). Il a été montré que la photocorrosion des nanohétérostructures GaAs/AlGaAs pourrait être contrôlée avec une résolution d'une sous-monocouche. De plus, les conditions de formation de la surface stœchiométrique et du processus de gravure congruente sont discutées. Il a été démontré que le PL de semi-conducteur pourrait être utilisé pour évaluer les propriétés de surface. Cela est important pour l'avancement du processus de gravure de couche photo-atomique des nanohétérostructures GaAs/AlGaAs, ainsi que pour la performance de transduction de ces nanohétérostructures.

Résumé français : La gravure de couche photo-atomique (Photo-ALE) de semi-conducteurs de GaAs et d'AlGaAs a été étudiée dans de l'eau désionisée et dans une solution aqueuse de NH_4OH. Le procédé est basé sur une photo-excitation séquentielle ($P \approx 16\text{-}20$ mW/cm^2) de trous porteurs présents à la surface des matériaux traités permettant leur conversion en oxydes et autres composés devenant solubles dans les solutions environnantes. Une analyse par spectroscopie de masse à

plasma à couplage inductif (ICP-MS) des produits de photogravure a révélé une gravure stœchiométrique du GaAs dans une solution aqueuse de NH_4OH linéairement corrélé avec le nombre de cycles de réaction, typiquement à des vitesses inférieures à ~ 0.35 nm/cycle. Un taux de photo-ALE inférieur à ~ 0.1 nm/cycle, fraction d'une monocouche de GaAs, a été mis en évidence dans le DI H_2O, mais un déficit significatif en Ga dans les produits de photogravure a été détecté avec ICP-MS, ce qui démontre une difficulté à produire des surfaces stœchiométriques et lisses de GaAs ou d'AlGaAs dans un tel environnement. Les mesures en microscopie à force atomique ont montré une rugosité moyenne ($\sigma_{RMS} \approx 0.9$ nm) légèrement augmentée des nanohétérostructures GaAs/AlGaAs photogravées dans NH_4OH, ce qui était lié au rendement relativement bas de dissolution des composés Al accumulés en surface dans cet environnement. En accord avec les données ICP-MS et les emplacements d'interface connus dans les nanohétérostructures étudiées, le suivi de la vitesse de photogravure constante a été démontrée *in situ* avec les mesures de photoluminescence dans NH_4OH. Ainsi, la décomposition congruente, associée à la possibilité d'une simple commutation entre les environnements de gravure, ouvre la possibilité d'une nanostructuration contrôlée des matériaux III-V avec des surfaces à composition stœchiométriques ou proches de la stœchiométrie.

Note : Ce chapitre constitue le matériel en préparation pour publication dans une revue scientifique. Par conséquent, après la publication, le contenu de ce chapitre peut différer de celui publié.

3.2. Abstract

Photo atomic layer etching (Photo-ALE) of GaAs and AlGaAs semiconductors was investigated in deionized H_2O and aqueous solution of NH_4OH. The process is based on sequential photo-excitation ($P \approx 16\text{-}20$ mW/cm^2) of hole carriers at the surface of processed materials that allows their conversion to the oxides and other compounds with a desirable dissolvability in the surrounding solutions. An inductively-coupled plasma mass spectroscopy (ICP-MS) of the photoetching products revealed stoichiometric etching of GaAs in an aqueous solution of NH_4OH proceeding linearly with the number of reaction cycles, typically at rates less than ~ 0.35 nm/cycle. A photo-ALE rate of less than ~ 0.1 nm/cycle, fraction of a GaAs monolayer, was demonstrated in DI H_2O, however a significant deficit of Ga in the photoetching products was detected with ICP-MS, consistent with a difficulty in producing stoichiometric and smooth surfaces of GaAs or AlGaAs in such an environment. Atomic force microscopy measurements showed the slightly increased root-mean-square roughness ($\sigma_{RMS} \approx 0.9$ nm) of GaAs/AlGaAs nanoheterostructures photoetched in NH_4OH, which was related to the relatively poor efficiency of this environment in dissolving the surface accumulating Al-compounds. In agreement with the ICP-MS data and the known interface locations in the investigated nanoheterostructures, the constant photoetching rates monitoring were demonstrated *in situ* with the photoluminescence measurements in NH_4OH. Thus, the congruent decomposition, along with the ability of a simple switching between etching environments, opened the possibility of a controlled nanostructuring of III-V materials with stoichiometric, or near stoichiometric surfaces.

3.3. Introduction

Unique electronic and optoelectronic properties of GaAs made it attractive for fabrication of high electron mobility transistors, metal-semiconductor field-effect transistors and a variety of quantum effect devices [81-83]. The nearly identical lattice constants of GaAs and $Al_{0.35}Ga_{0.65}As$ allowed fabrication of flexibly engineered heterostructures with modulated bandgaps, and the two-dimensional electron gas at the interface of such materials was investigated, e.g., for tunable plasmonic bandgap structure devices [84]. The fabrication of damage free and stoichiometric surfaces of materials with an atomic depth resolution is of high importance to the nanofabrication techniques delivering advanced III-V low dimensional nanostructures [85, 86]. However, the

ability to fabricate stoichiometric surfaces of etched GaAs, AlGaAs and other III-V semiconductors represents a significant challenge. For instance, it has been demonstrated that ion beam assisted etching consumes at least 10 nm of wet-etched GaAs to produce a stoichiometric surface [87], rendering this approach unsuitable for fabrication of devices with atomic depth resolution. Reactive ion beam etching was used for dry etching of GaAs and AlGaAs and despite fabricating relatively smooth surfaces [88], ion-induced surface damage appeared unavoidable [89]. To address this problem, GaAs chlorine radical etching without ion bombardment was proposed, although etching rates between 3 nm/min and 10 μm/min were possible only when samples were heated in the range of 300-400 °C [90]. In an electron beam excited plasma system, the surface of GaAs was bombarded sequentially using Ar ions in the presence of Cl_2 or Cl. However, it was reported that accumulation of Cl on GaAs could have passivated the surface and suppressed the etch rate for the Cl_2 feed time over ~ 0.9 sec [91]. Maki *et al.* proposed bilayer etching of GaAs using a low-pressure Cl_2 chamber to induce a chemical reaction and a 193 nm laser radiation to remove the products of reaction [92]. Although this technique is in principle similar to the Cl_2 etching of GaAs by means of an ion beam, it has been argued that it was the application of low-fluence laser photons that allowed producing high-quality surfaces [92, 93]. In that context, etching with near monolayer depth resolution, also known as digital etching or atomic layer etching (ALE) of semiconductors, has been studied for almost three decades now [94], with some recent works reporting on thermal-ALE of aluminium oxide [95], titanium nitride [96] and silicon [97], all aiming at replacing the continuous etching processes that inevitably produce low quality surfaces.

DeSalvo *et al.* carried out a two-phase wet chemical digital etching of GaAs surfaces based on the application of a self-limited oxidation reaction [98]. Light assisted etching of III-V semiconductors has been investigated by Ruberto *et al.* who reported microscale photoetching of GaAs and InP using an argon ion laser delivering a 257 nm radiation of power density ranging from 10 mW/cm^2 to 10kW/cm^2 [99]. The etch rates achieved with this technique, ranging between 0.5 mm/min ([99]) and 2.8 μm/min ([100]), were obtained by controlling the potential of a sample immersed in an electrolyte and/or employing a secondary light beam [101]. Fink *et al.* used this approach for photoetching of GaAs/AlGaAs heterostructures illuminated by a halogen lamp delivering up to 250 mW/cm^2 of optical power density [58]. By measuring current density variation, these authors reported etch rates of ~ 0.5 μm/min for GaAs and ~ 0.4 μm/min for

AlGaAs. To monitor the process, they took advantage of current density oscillations during etching of GaAs/AlGaAs interfaces and demonstrated resolving a GaAs/AlGaAs interface. Although attaching an ohmic side contact to the sample enhanced the sensitivity of this technique, the demonstration of a layer-by-layer etching was not possible. The foregoing discussion underlines that contrary to deposition techniques, advanced methods capable of a comparable controllability and providing accuracy of III-V materials removal have not been developed, primarily due to the lack of the universal process as well as diagnostics for *in situ* monitoring of digital etching processes [98],[102, 103].

We have recently demonstrated that so-called **di**gital **p**hotocorrosion (DIP) of GaAs/AlGaAs nanoheterostructures could be monitored with photoluminescence (PL) emitted by such nanoheterostructures [104, 105]. Sensitivity of DIP to the external perturbations induced by electrically charged molecules allowed detecting the presence of negatively charged bacteria immobilized in the vicinity of the GaAs/AlGaAs nanoheterostructure surfaces [104, 106], as well as monitoring bacterial response to antibiotics in H_2O environment [107]. This concept has also been investigated for post-growth diagnostics of interface locations in PL emitting quantum wells [108] with the possibility of extending it to nanoheterostructures with no PL emission by measuring open circuit potential of the photocorroding semiconductor surface [109]. Along with the progress of research in this newly discovered area, it is compelling to understand the mechanisms of photo-induced material removal and formation of stoichiometric surfaces at atomic level that would be of a particular importance to the development of ALE of III-V materials and fabrication of advanced nanoheterostructure devices.

In this paper, inductively coupled plasma mass spectrometry (ICP-MS) was employed for a systematic analysis of aqueous environments employed for supporting photo-ALE of $GaAs/Al_{0.35}Ga_{0.65}As$ nanoheterostructures. The ICP-MS technique is capable of providing highly precise and quantitative determination of elements owing to the invention of chromatographic detectors [110]. A dilution of analyzed liquid samples in HNO_3 and deionized (DI) water allows for separation of matrix elements, which is important in view of high volatilities of both Ga and As chlorides [111]. A comparison between the ICP-MS detected ions and those released by the photoetching nanoheterostructure of a well-defined thickness allowed investigating the conditions for formation of stoichiometric surfaces. A correlation between ICP-MS and PL data concerning

constant photoetching rates indicated the feasibility of this approach for the attractive *in situ* monitoring of the formation of stoichiometric, or near-stoichiometric surfaces of interest to the nanostructuring and *in situ* passivation of III-V semiconductor nanodevices.

3.4. Experimental Section

3.4.1. GaAs/AlGaAs nanoheterostructures

The GaAs/$Al_{0.35}Ga_{0.65}As$ wafer J0152 was grown by molecular beam epitaxy (CPFC, National Research Council of Canada, Ottawa) on a semi-insulating GaAs (001) substrate. It consists of a 20-pair AlAs/GaAs (2.4 nm/2.4 nm) superlattice applied as a barrier against propagation of defects and a 500 nm thick GaAs PL emitter. A 100-nm thick $Al_{0.35}Ga_{0.65}As$ layer, 3 nm thick GaAs and 10 nm thick $Al_{0.35}Ga_{0.65}As$ layers were grown on the top of the GaAs emitter. The nanoheterostructure was capped with an 8 nm thick GaAs layer. The D3422 wafer was grown by metal organic chemical vapor deposition (CPFC, National Research Council of Canada, Ottawa) also on a semi-insulating GaAs (001) substrate. It consists of a 20-pair AlAs/GaAs (2.4 nm/2.4 nm) superlattice and a 500 nm GaAs layer followed by a 100 nm thick $Al_{0.35}Ga_{0.65}As$ layer. However, in this case, 6 pairs of 12 nm thick GaAs and 10 nm thick $Al_{0.35}Ga_{0.65}As$ were grown and capped with a 12 nm thick GaAs layer.

Figure 3-1 shows cross-section of GaAs/AlGaAs nanoheterostructures employed in this work, along with their room temperature PL spectra obtained with a commercial Philips PL mapper (PLM-150). The nanoheterostructures were excited with a second harmonic of Nd:YAG laser source (λ_{ex} = 532 nm) and the emitted PL signal was collected with InGaAs photodiode detector array. The PL mapping spatial and spectral resolutions were 20 μm and 0.6 nm, respectively. Both wafers, shown in **Figure 3-1,** emitted PL peaks at $\lambda \approx 870$ nm originating from 500 nm thick GaAs epitaxial layers. No PL emission was observed at room temperature from other GaAs layers sandwiched between AlGaAs barriers or from the AlAs/GaAs superlattice. At 20 K, a quantum confined PL peak at 724 nm was observed from the 3 nm thick GaAs layer of the J0152 wafer. The intensity of that peak was found at ~ 6 times weaker than that of the bulk GaAs at 821 nm (see **Figure 3-10**).

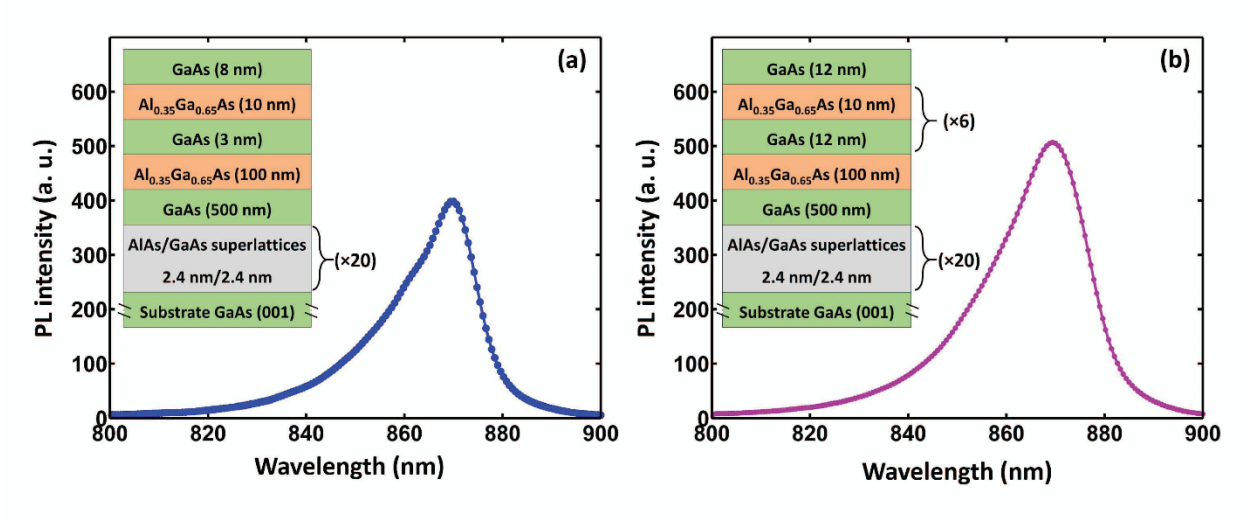

Figure 3-1. Room-temperature PL spectra of GaAs/$Al_{0.35}Ga_{0.65}As$ nanoheterostructures taken from J0152 wafer (a) and D3422 wafer (b). Samples were excited with a 532 nm laser beam of the Philips PL mapper (PLM-150). In both cases the PL emission originated from 500 nm thick GaAs layers shown in cross-section of the investigated samples.

3.4.2. Photo-ALE process of GaAs/AlGaAs nanoheterostructures

Individual samples were mounted in a Teflon holder capped with an optically transparent window and irradiated intermittently for 3 s in each 60 sec cycle (DC = 3/60) or for 3 sec in each 25 sec cycle (DC = 3/25). This made it possible to observe the photoetching at relatively low rates. **Figure 3-2** displays a schematic view of the photo-ALE setup employed for photo-ALE of GaAs/AlGaAs nanoheterostructures. The measurements of PL emission were carried out with a custom made QSPB (quantum semiconductor photonic biosensing) reader described elsewhere [104]. Briefly, a homogenized beam of a 660 nm light-emitting diode (LED) allowed for a simultaneous excitation of the surface of a sample, while spatially resolvable PL emission intensity maps were collected with a CCD camera. A calibrated Si photodiode (S130C, Thorlabs, NJ, USA) was employed to monitor the LED power (P) during photo-ALE experiments. The cycled irradiation of samples, with a non-irradiation period designed to give enough time for the photoetching products to dissipate into the etching environment (DI H_2O or NH_4OH), allowed observing etch rates below 2.82 Å/cycle, corresponding to the thickness of a monolayer of GaAs.

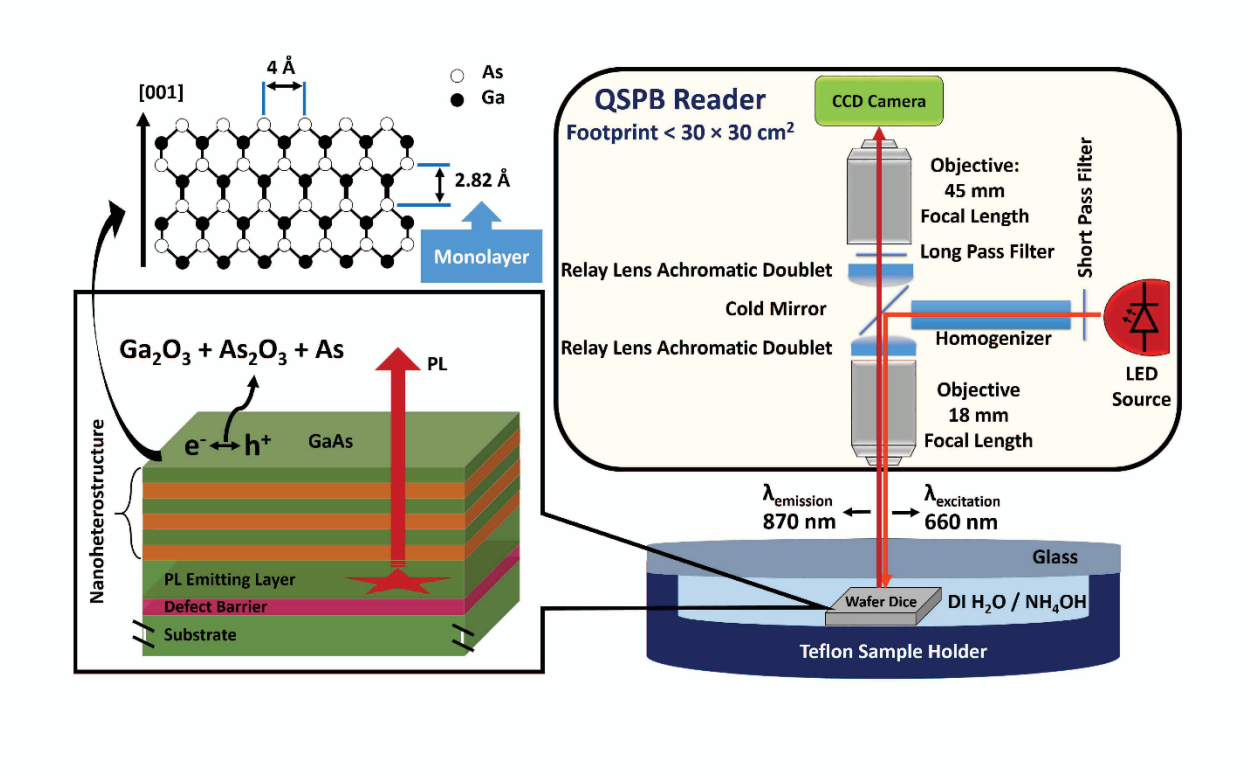

Figure 3-2. Schematic view of the setup employed for demonstrating photo-ALE of GaAs/$Al_{0.35}Ga_{0.65}As$ nanoheterostructures. Samples were irradiated with λ = 660 nm of LED. Emitted PL of GaAs/$Al_{0.35}Ga_{0.65}As$ nanoheterostructures was filtered in the range of 840–1650 nm (long pass filter, Edmunds 86–070) and PL data, dominated by λ ≈ 870 nm emission from the 500 nm thick GaAs layer, were recorded using a CCD camera.

3.4.3. Sample Preparation

Samples of 2 mm by 2 mm dimensions were cut out from photoresist (S1813, Shipley) coated wafers. Following the exposure to acetone for 5 min and ultrasonication (designed to remove the photoresist), the samples were degreased in an ultrasonic bath of OptiClear, acetone and isopropyl alcohol, each for 5 min. Samples were dried with high purity nitrogen 4.8 HP (99.998%). Then, they were exposed to an aqueous solution of ammonium hydroxide (NH_4OH at 28 %) for 2 min and rinsed with DI H_2O.

3.4.4. Chemicals

Chemicals were purchased from the following sources: OptiClear from National Diagnostics (Mississauga, Canada), acetone from ACP (Montréal, Canada), isopropyl alcohol

(IPA) from Fisher Scientific (Ottawa, Canada), ammonium hydroxide 28% (NH_4OH) from Anachemia (Richmond, Canada) and high purity nitrogen 4.8 HP (99.998%) from Praxair Canada Inc. (Mississauga, Canada). The 18.2 MΩ DI H_2O, used in these experiments was produced by means of a Millipore purification customized system assembled by Culligan (Quebec, Canada).

3.4.5. Inductively Coupled Plasma Mass Spectrometry

The solutions containing photo-ALE products were collected for the ICP-MS analysis at the end of each photo-ALE experiment in DI H_2O or NH_4OH. To adjust the results for dark corrosion, witness samples were immerged in DI H_2O or NH_4OH and kept in darkness for the same period of time as the photoetching samples. The ICP-MS experiments were carried out in a PerkinElmer ELAN DRC II ICP-MS equipped with an AS-93 auto sampler. Data were collected for 5 mL samples with 20 sweeps per reading, 1 reading per replicate and 3 replicates for each sample. The dwell time was 50 ms/AMU. Germanium was used as an internal standard. Both the internal standard and sample were introduced in the machine via a peristaltic pump and mixed in a T junction just before entering the nebulizer. The injection sequence was a 45 sec wash with 2% nitric acid, followed by a 75 sec flush with sample. A 15 sec delay was applied before taking a reading. Standard curve for calculation was prepared from 1000 ppm ICP-MS grade single element standard (Isospec, Delta Scientific) and 2% nitric acid as diluting solvent. Calibration was carried out for the 1 to 500 ppb range. Diluting solvent and wash solution were prepared from Aristar plus nitric acid (BDH ARISTAR) and ultrapure water (18.2 MΩ/cm, ELGA purifying machine). Samples were kept at room temperature between reception and ICP-MS analysis.

3.4.6. Fourier-Transform Infrared Spectroscopy (FTIR)

The analysis of surface chemistry of photoetched samples was carried out based on the FTIR absorption data collected with a Vortex 70 v instrument (FTIR Bruker, Germany). Typically, an absorption spectrum was constructed based on 512 scans collected with a mercury cadmium telluride (MCT) detector. Measurements started with a 15 min delay after evacuation of the sample compartment to minimize the influence of moisture on the collected data. A freshly prepared (degreased, then immersed for 2 min in NH_4OH, rinsed with DI H_2O and dried with nitrogen flow) J0152 GaAs/AlGaAs sample was used to determine an FTIR absorption baseline. FTIR data were analyzed to resolve the peaks using OPUS software (version 7.2).

3.4.7. Atomic Force Microscopy (AFM)

Surface morphology of processed samples was studied using an atomic force microscopy (AFM) technique (Digital Instrument, Nanoscope III). The AFM instrument operated in a tapping mode. All images were collected over a 10 μm × 10 μm surface area with 512 points per line for 512 lines, using tip velocity of 12 μm/s and at a scan rate of 0.598 Hz. A freshly prepared (degreased, then immersed for 2 min in NH_4OH, rinsed with DI H_2O and dried with nitrogen flow) J0152 GaAs/AlGaAs sample was used as the reference surface.

3.4.8. X-ray Photoelectron Spectroscopy (XPS)

The XPS Kratos Axis Ultra DLD spectrometer was utilized to determine the elemental composition of the sample surface. Samples were excited with the Al$K\alpha$ monochromatized line (1486.6 eV) of a 225 W source. The analyzer was operated in a constant pass energy mode of 160 eV for the survey scans, and 20 eV for the high resolution scans. The work function of the instrument was calibrated to give a binding energy (BE) of 83.96 eV for the Au $4f_{7/2}$ line of metallic gold. The dispersion of the spectrometer was adjusted to give a BE of 93.62 eV for the Cu $2p_{3/2}$ line of metallic copper. The samples were mounted on a non-conductive tape. A charge neutralizer was used on all samples to compensate for the charging effect. Charge corrections were done using the adventitious carbon peak set at 284.8 eV. The analyzed area was an oval with approximate dimensions of 300 μm × 700 μm. Data analysis was conducted using the Casa XPS software (version 2.3.18). The relative sensitivity factors used for quantification purpose are the experimental RSF given by Kratos Analytical for their machines.

3.5. Results

Figure 3-3 shows examples of the integrated temporal PL intensity from four individual samples of the J0152 wafer that underwent photo-ALE in DI H_2O following 90, 266, 450 and 720 cycle numbers (CN) for duty cycle ($DC = T_{ON}/T_{TOT}$) equal to 3/60 and $P = 20$ mW/cm^2. While **Figure 3-3** illustrates viable reproducibility of the photo-ALE process, the formation of well-defined PL maxima could be clearly observed in agreement with the previously reported results [104, 105, 108, 109]. As a guide to an eye, the zones of photoetching GaAs and $Al_{0.35}Ga_{0.65}As$ layers extending up to 56 nm, i.e., deep inside of the 100 nm thick $Al_{0.35}Ga_{0.65}As$ layer were

indicated in this figure. The initial increase of the PL signal, observed in **Figure 3-3** for CN ≤ 100, is related to formation of Ga_2O_3 that is known to reduce the concentration of nonradiative recombination centers (NRRC) and chemically passivate the GaAs surface [112]. As the GaAs layer was dissolved, the formation of an electrolytic junction involving DI H_2O and $Al_{0.35}Ga_{0.65}As$ revealed an interface with a significantly greater surface concentration of NRRC. It was reported that the surface recombination velocity of AlGaAs is near 10^7 cm/s in comparison to that of 10^5 to 10^6 cm/s observed for the GaAs surface [113, 114]. This led to a reduced intensity of the PL emission each time the $Al_{0.35}Ga_{0.65}As$ surface was exposed to DI H_2O. The PL signal was recovered only when a new electrolytic junction involving DI H_2O and GaAs was revealed *in situ* (observed for CN > 210). Consequently, temporal position of the PL maxima can be accurately correlated with the position of GaAs-AlGaAs interface, as demonstrated with AFM-measured depth of photocorroded craters created on GaAs/AlGaAs quantum wells [108]. Furthermore, position of PL maxima versus time is directly related to the rate of material removal, which can be controlled by power and sequence (duty cycle) of the excitation photons [108] as well as the *p*H of surrounding solution [105].

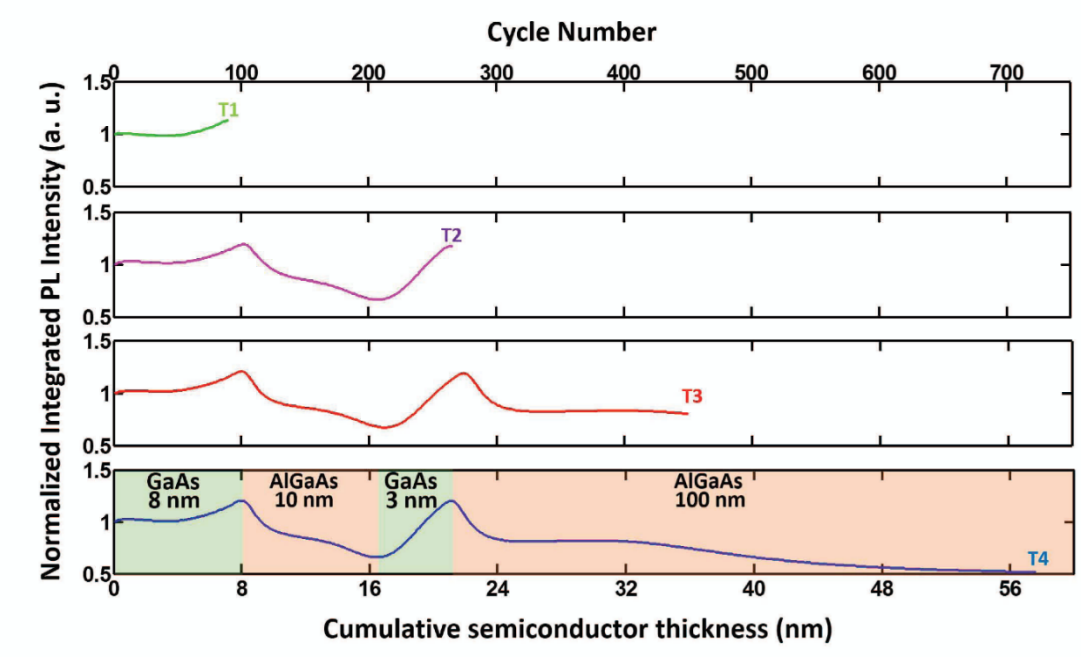

Figure 3-3. *In situ* monitored depth of photo-ALE in DI H_2O. Temporal oscillations of the PL emission intensity at λ ≈ 870 nm from four independent J0152 samples photo-etched in DI H_2O as a function of the semiconductor thickness and the cycle number for DC = 3/60. The zones of etched GaAs and AlGaAs layers are indicated approximately with distinctively different colors.

Figure 3-4 displays temporal PL of J0152 samples photoetched at different rates in DI H_2O and aqueous solutions of NH_4OH. As it can be seen in **Figure 3-4 (a)**, the PL intensity of the sample photoetched in DI H_2O stabilized at ~ 50% of the initial intensity, after ~ 600 cycles, however photoetching in NH_4OH, with ~ less than 600 cycles (**Figure 3-4 (b)**) and less than 400 cycles (**Figure 3-4 (c)**), resulted in the PL signals too weak to be detected with the employed PL setup. Under the employed excitation conditions, the PL measurement setup displayed in **Figure 3-2** does not respond to the weak PL emission from a single layer of GaAs (500 nm PL emitter), unless the carrier confinement is provided by the top GaAs and AlGaAs epitaxial layers. Therefore, intensity of the PL signals in **Figure 3-4 (b)** and **Figure 3-4 (c)** fell below the sensitivity of the measuring setup, when the the four top GaAs and AlGaAs epitaxial layers were entirely etched. This feature allows determining deceleration of the material removed rate per photo-ALE cycles. **Figure 3-4 (d)** and **Figure 3-4 (e)** show the photo-ALE rate of J0152 in DI H_2O and NH_4OH, respectively, estimated from the slope of cumulative semiconductor thickness versus position of PL-revealed interfaces of GaAs-AlGaAs. Accordingly, the photo-ALE rate of J0152 samples in DI H_2O was 0.08 ± 0.005 nm/cycle (approximately 0.3 monolayer/cycle [115]) that was ~ 4-time slower, compared to the samples photoetched in NH_4OH (28%). It is noteworthy that the etch rate in NH_4OH (**Figure 3-4 (e)**) was constant, whereas the etching rate in DI H_2O (**Figure 3-4 (d)**) was decelerating, consistent with saturation of PL signal in **Figure 3-4 (a)**. This data specified that, even though, the J0152 nanoheterostructure exhibited similar temporal PL profile in the employed environments, the stoichiometry and/or properties of the produced surfaces could be considerably dissimilar.

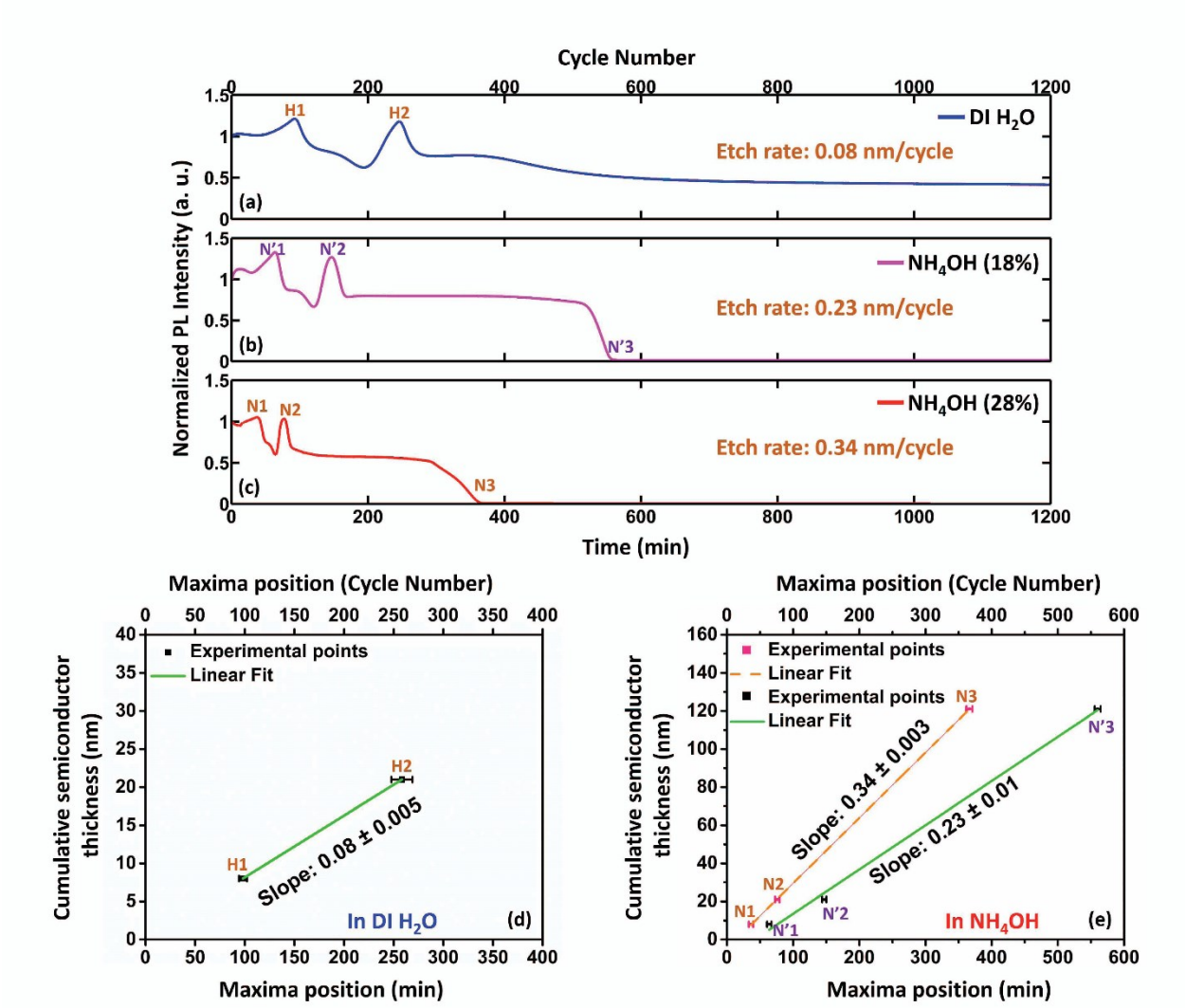

Figure 3-4. Regulating photo-ALE rate of J0152 samples in different aqueous solutions. Representative temporal PL intensity of J0152 samples in DI H_2O (a), NH_4OH solution 18% (b), and NH_4OH solution 28% (c). Photo-ALE rate in DI H_2O was estimated at 0.08 ± 0.005 nm/cycle, based on the positions of the 1st and the 2nd PL maxima (d). Photo-ALE rate in NH_4OH solution 28% was estimated at 0.34 ± 0.003 nm/cycle, based on the positions of the 1st and the 2nd PL maxima as well as the last AlGaAs-GaAs interface (e).

To investigate the underlying mechanisms responsible for inconstant etch rate in DI H_2O, and in an attempt to describe conditions leading to formation of stoichiometric surfaces, ICP-MS measurements were conducted on the photo-ALE solutions. The number of As^{3+} and Ga^{3+} ions expected to be released by photo-ALE of GaAs/$Al_{0.35}Ga_{0.65}As$ nanoheterostructures of known thicknesses were compared to those determined by ICP-MS, as shown in **Figure 3-5**. The

calculations of As^{3+} and Ga^{3+} ions concentration were based on the empirically determined etch rates, shown in **Figure 3-4 (d)** and **Figure 3-4 (e)**, as well as the known thickness of GaAs/$Al_{0.35}Ga_{0.65}As$ nanoheterostructures (see Supporting Information for details). **Figure 3-5 (a)** and **Figure 3-5 (b)** show this comparison for samples underwent photo-ALE in DI H_2O, besides **Figure 3-5 (c)** and **Figure 3-5 (d)** show such a data for samples underwent photo-ALE in 28% of NH_4OH. Notice that different concentrations of ions calculated in DI H_2O and NH_4OH for the same amount of photoetched material are due to different molecular weights of the investigated solutions. It can be seen that ICP-MS detected As^{3+} and Ga^{3+} ions at 110 and 18 parts per billion (ppb), respectively, were released from the nanoheterostructure photoetched in DI H_2O by 60 nm. Data were adjusted for the dark corrosion that revealed up to ~ 20 and ~ 5 ppb of As^{3+} and Ga^{3+} ions, respectively, released during the same period of time (see **Figure 3-11**). While a growing deficit of As^{3+} ions was detected for the samples photoetched deeper than 60 nm, a deficit of Ga^{3+} ions was already observed for a sample photoetched by less than 8 nm (T1). In contrast, the photo-ALE process in NH_4OH released both As^{3+} and Ga^{3+} ions at ICP-MS detected concentrations in an excellent agreement with the calculated data for the investigated nanoheterostructure photoetched by at least up to ~ 110 nm (**Figure 3-5 (c)** and **Figure 3-5 (d)**). The congruent character of material decomposition in this case suggests that stoichiometric surfaces of GaAs and AlGaAs were formed at the end of each photoetching cycle. However, for samples photoetched in DI H_2O, the congruent character of material decomposition was only preserved for less than 8 nm (merely the top GaAs layer). Furthermore, no trace of Al was found in DI H_2O photoetching products and, in spite of a reasonable agreement between the calculated and ICP-MS detected As^{3+} and Ga^{3+} ions observed for the NH_4OH photoetching products, no such agreement could be demonstrated for Al ions.

Such distinctive photo-ALE performances are associated with the oxidation/dissolution kinetics of these materials in aqueous solutions. In the case of an n-type III-V semiconductor, the presence of holes is required for the initiation of a dissolution process, with the main products of GaAs photoetching in water being $[Ga(OH)_4]^-$, GaO, Ga_2O, Ga_2O_3 and AsO [116, 117]. The oxidation/decomposition process of GaAs in water is described by the following reaction [118]:

$$2GaAs + 3h^+ + 3H_2O \rightarrow Ga_2O_3 + 2As(0) + 6H^+ \qquad (3\text{-}1)$$

where h^+ represents the hole carriers. Following the absorption of e-h^+ forming photons, Ga^{3+} ions produced at the GaAs surface could react with dissolved oxygen or oxygen of water molecules and produce Ga oxides. Among As-oxides and Ga-oxides, Ga_2O_3 represents a relatively stable form of a compound that is insoluble in water, thus, it could pile up at the GaAs surface [119]. Furthermore, some of the Ga^{3+} ions could diffuse out from the surface and form oxides in the solution. Ultimately, contribution of these two processes leads to the presence of Ga^{3+} ions in the aqueous environment. Photo-oxidation of GaAs also produces As oxides. The elemental As(0) formed at the surface in the first step (reaction 1) could react further, giving As_2O_3 as the main product of the following reaction [120]:

$$2As(0) + 3h^+ + 3H_2O \rightarrow As_2O_3 + 6H^+ \qquad (3\text{-}2)$$

Thus, As_2O_3 could also be formed in the solution. But, this compound is both volatile and water soluble under neutral *p*H conditions [120]. This leads to the decomposition of GaAs into Ga_2O_3 and formation of elemental As, as follows [121]:

$$2GaAs + As_2O_3 \rightarrow Ga_2O_3 + 4As \qquad (3\text{-}3)$$

The reaction (3-3) that is kinetically slow but thermodynamically favored [121] could increase concentration of As in a solution. Considering these reactions, Ga products in DI H_2O are expected to partially remain on the surface of III-V samples, whereas, in NH_4OH, such oxides pile up could be prevented [122]. Post-photoetching characterizations of J0152 samples were carried out to clarify the process of photo-ALE in DI H_2O and NH_4OH.

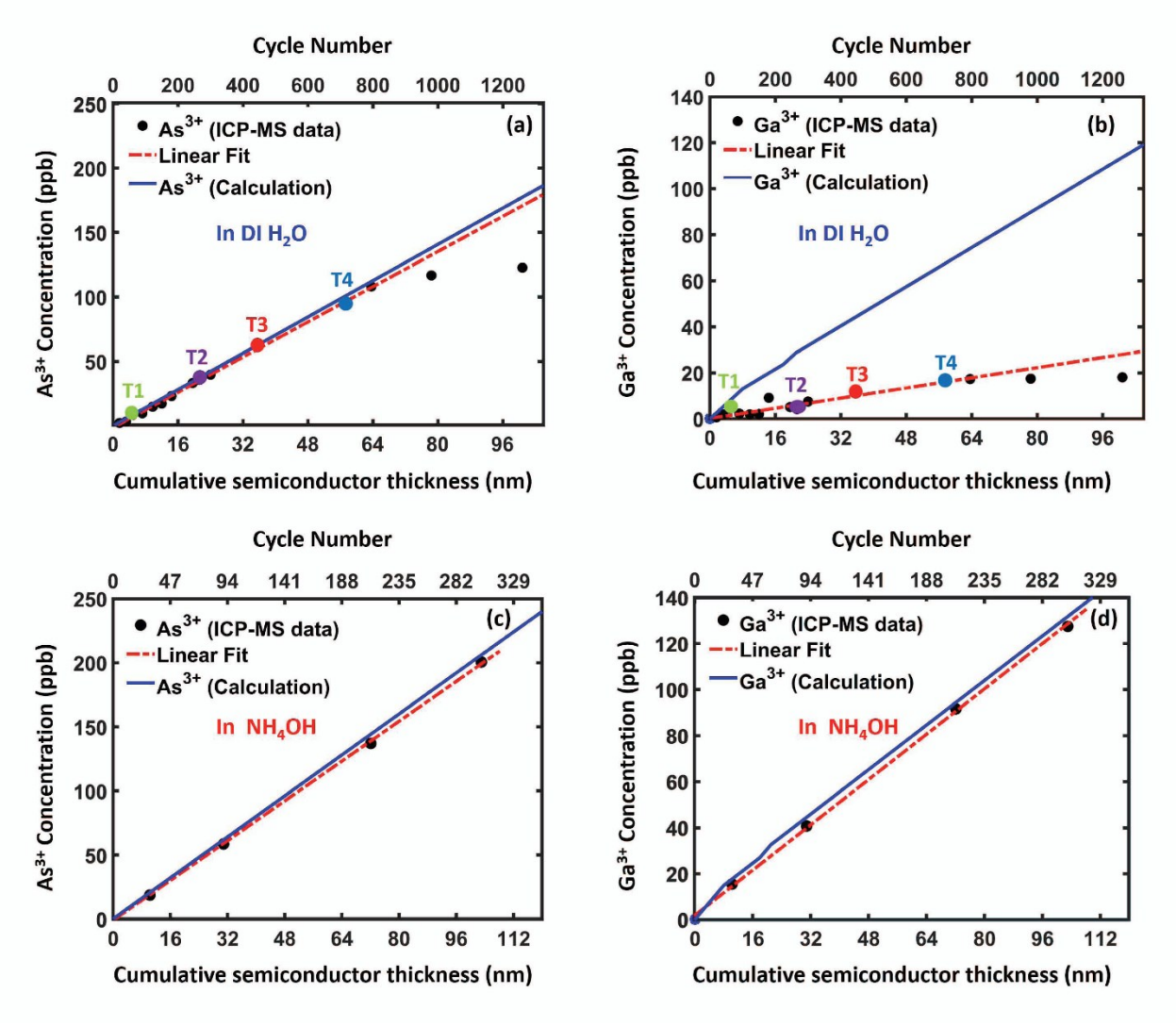

Figure 3-5. Stoichiometry assessment of J0152 samples photo-etched in DI H_2O and NH_4OH. Comparison of ICP-MS detected As^{3+} and Ga^{3+} ions with their calculated concentrations expected to be released during photo-ALE of GaAs/$Al_{0.35}Ga_{0.65}As$ nanoheterostructures in DI H_2O (a) and (b), respectively, and in NH_4OH (c) and (d), respectively. Data collected at the end of runs T1-T4, which were previously shown in Figure 3-3, are indicated here with large full circles, in Figure 3-5 (a) and Figure 3-5 (b).

Figure 3-6 displays FTIR absorbance data in the region of 450-800 cm^{-1} for four samples of the J0152 wafer that were photoetched in DI H_2O with 40-CN (S1), 120-CN (S2), 180-CN (S3) and 1320-CN (S4). The spectra for S2-S4 indicate the presence of a peak at 520 cm^{-1} identified as the aluminum oxide related Al-O stretching mode [123]. The absence of this peak for sample S1 is consistent with the position of the etching front, estimated at ~ 3.2 nm from the top of that sample

(initially, capped with an 8 nm thick GaAs). The photoetched surface of S2 was located within the 1st $Al_{0.35}Ga_{0.65}As$ layer (~ 9.6 nm from the top), while S3 was located in the middle of the 1st $Al_{0.35}Ga_{0.65}As$ layer (~ 14.4 nm from the top) and S4 was located at the bottom of the 2nd $Al_{0.35}Ga_{0.65}As$ layer (~ 105.6 nm from the top). Although presence of Al_2O_3 was confirmed, no FTIR peaks associated with Ga-O bond vibrations, expected at 463 and 764 cm^{-1} ([124]) were observed, likely due to the insufficient signal to noise ratio in these experiments.

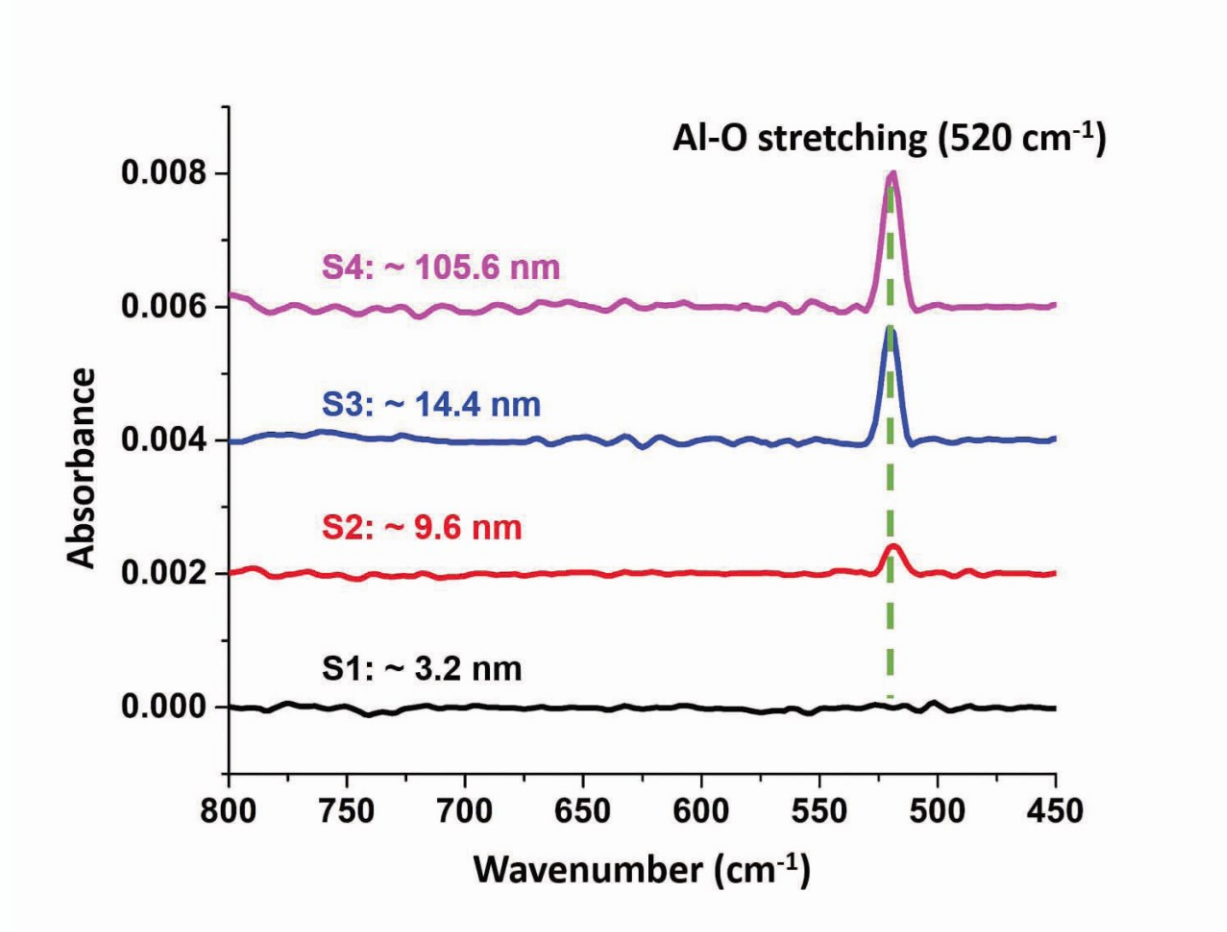

Figure 3-6. FTIR absorbance spectra of GaAs/AlGaAs (wafer J0152) photo-etched in DI H_2O. Al-O peaks at 520 cm^{-1} revealed at the surface of samples after photo-ALE front reached the AlGaAs layer, i.e., corresponding to S2 (120 CN), S3 (180 CN) and S4 (1320 CN). The spectra were shifted vertically for clarity.

Figure 3-7 compares high resolution XPS scans of four J0152 samples that underwent photo-ALE with the XPS scan for a freshly prepared reference sample partially covered with native oxide (following etching in NH_4OH, that sample was air exposed for ~ 30 min before being loaded

into the XPS chamber). **Figure 3-7 (a)** shows two peaks related to the Ga 3*d* transitions differentiated by a chemical shift. The peaks in the higher energy region of binding energy (BE) equal to 20.2 *eV* ([125]) and 20.5 *eV* ([126]) contribute to an integrated peak corresponding to the oxide state of GaAs. The lower energy peak at BE = 19.28 *eV* ([127]) corresponds to Ga bounded in GaAs. In the case of samples photoetched in H_2O, the Ga_2O_3 peak (BE = 20.5 *eV*) was always present and its intensity was much higher than that of the native oxide of the reference sample. In contrast, the intensity of this peak for samples photoetched in a NH_4OH environment was fairly similar to that of the reference sample. This is consistent with the dissolution and/or growth prevention of Ga-oxide in the NH_4OH environment. High resolution scans of Al 2*p*, displayed in **Figure 3-7 (b)**, indicated that two types of aluminum compounds, Al_2O_3 with BE = 74.7 *eV* ([128]), and $Al(OH)_3$ with BE = 73.9 *eV* ([129]), were formed at the surface of the investigated samples as a result of Al reacting with H_2O and Al and O_2. Due to the small difference between BEs corresponding to these compounds, they are known to be difficult to differentiate [130]. In the case of the GaAs/$Al_{0.35}Ga_{0.65}As$ nanoheterostructure etched with 120 CN in NH_4OH (~ 36nm deep according to **Figure 3-4(e)**), the XPS probed surface was mostly that of $Al_{0.35}Ga_{0.65}As$, and the corresponding amount of $Al(OH)_3$ was much higher than that of Al_2O_3. This suggested that accumulation of Al_2O_3 was somehow inhibited in the NH_4OH environment. Of particular importance to the constant etch rate is that the XPS Al $2p_{3/2}$ scan, as shown in **Figure 3-7 (b)**, revealed neither Al_2O_3 nor $Al(OH)_3$ related peaks for the sample photoetched with 1200 CN, i.e., up to ~ 411nm deep (based on the average photo-ALE rate of 0.34 nm/cycle, as shown in **Figure 3-4 (e)**). This suggests that a CN proportional concentration of Al ions should be expected in the photo-ALE product generated in the NH_4OH environment. However, such an agreement could not be demonstrated for Al ions, probably due to poor sensitivity of the ICP-MS method in this case. The possible reason of this difficulty could be a relatively high vapor pressure of NH_4OH, which is known to be the source of the ICP instability [131]. Alternatively, NH_4OH could induce precipitation of Al as an insoluble hydroxide [132].

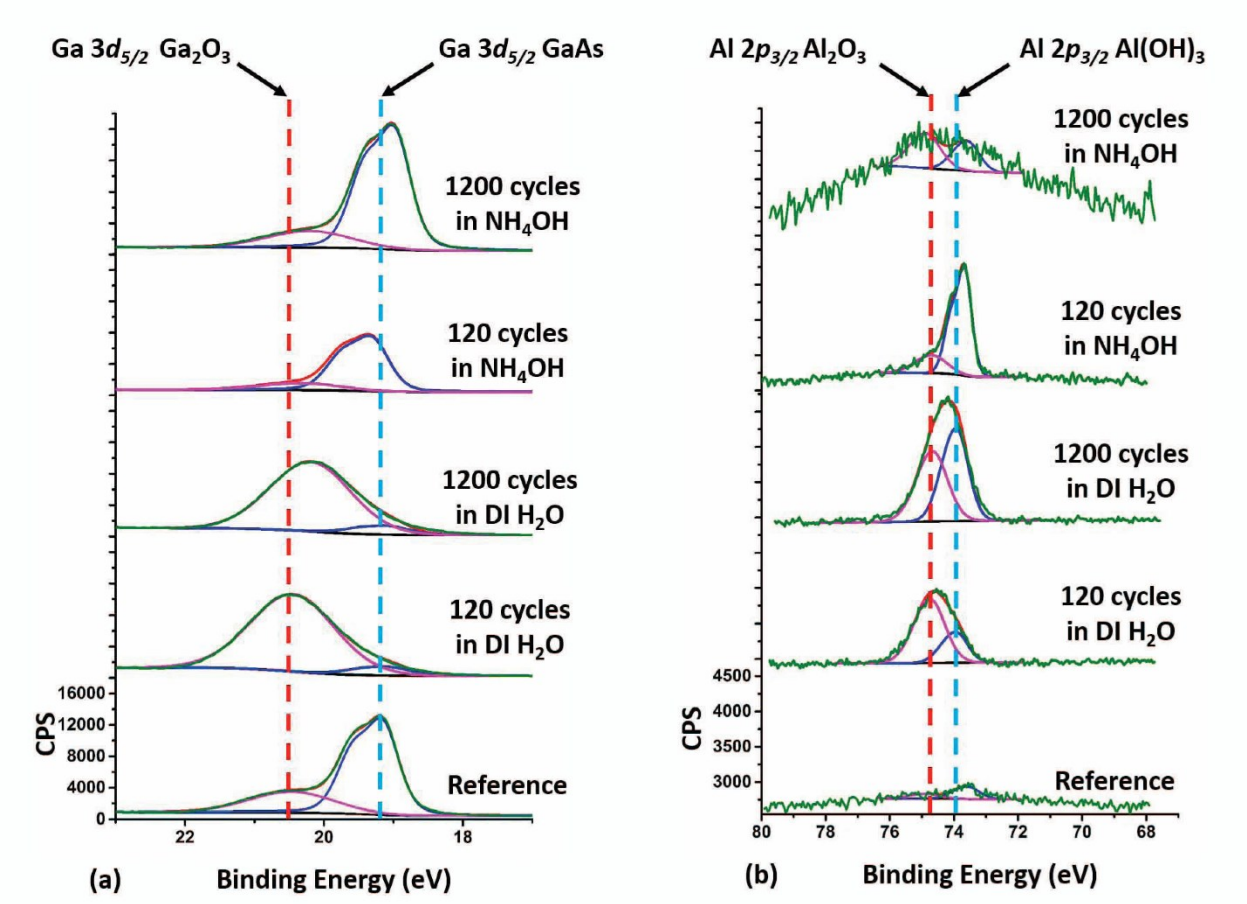

Figure 3-7. High resolution XPS scans of J0152 samples photoetched in DI H_2O and NH_4OH. Data shown for transactions corresponding to Ga 3d (a) and Al 2p (b).

Figure 3-8 shows AFM images of a J0152 reference sample (**Figure 3-8 (a)**) and S1-S4 samples after photo-ALE in DI H_2O with 40, 120, 180 and 322 CN (**Figure 3-8 (b) - Figure 3-8 (e)**), while **Figure 3-8 (f)** shows an AFM image of the sample S5 after photo-ALE in NH_4OH with 322 CN. The freshly prepared reference sample (see Experimental Section) was used to examine the effect of photo-ALE on roughness of the photoetched samples. It can be seen that samples photoetched in DI H_2O up to a depth of ~ 14.4 nm (S1-S3) exhibited surface morphology characterized by σ_{RMS} = 0.76 - 0.86 nm, which is fairly comparable to that of a reference sample (σ_{RMS} = 0.75 nm). However, the sample S4, photoetched to a depth of ~ 105.6 nm in DI H_2O, showed a surface roughness characterized by σ_{RMS} = 2.1 nm. The AFM image shown in **Figure 3-8 (e)** relates to the non-stoichiometric surface of J0152 etched in DI H_2O with 1325 CN to a depth

of ~105.6 nm, which is consistent with the XPS data (**Figure 3-7 (a)**) showing a significant surface accumulation of Ga_2O_3. Moreover, these are in agreement with PL data, shown in **Figure 3-4 (a)**, revealing inconstant etch rate in DI H_2O. In contrast, the surface of the sample S5 photoetched in NH_4OH to a comparable depth of ~ 105.6 nm (**Figure 3-8 (f)**) is characterized by σ_{RMS} = 0.93 nm, which is only minimally greater than σ_{RMS} = 0.75 nm of the reference sample (**Figure 3-8 (a)**). A possible reason for this increased roughness could be the presence of residual Al-based compounds formed on the surface of the 2nd AlGaAs layer of the J0152 nanoheterostructure mapped in this case with AFM.

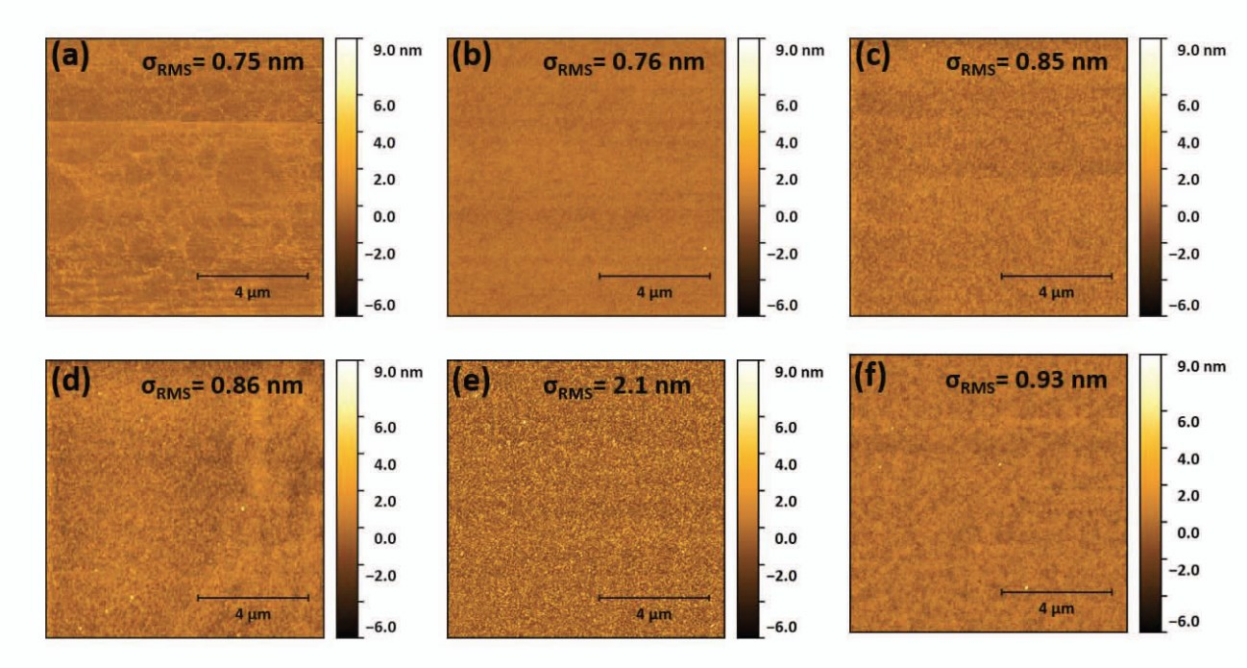

Figure 3-8. AFM images of J0152 samples, taken from a freshly prepared reference sample (a), and after photo-ALE in DI H_2O with depth of 3.2 nm (b), ~ 9.6 nm (c), ~ 14.4 nm (d), ~ 105.6 nm (e), and after photo-ALE in NH_4OH with depth of ~ 105.6 nm (f).

The ability of stoichiometric diagnostics with PL measurements was explored further by conducting photo-ALE on nanoheterostructures consisting of 6 pairs of nominally same thickness GaAs and $Al_{0.35}Ga_{0.65}As$ layers. **Figure 3-9** compares PL plots collected during photo-ALE of the D3422 wafer in DI H_2O (**Figure 3-9(a)**) and NH_4OH (**Figure 3-9(b)**). These experiments were carried out with LED power P ≈ 16 mW/cm^2 and DC = 3/25. It can be seen that it took ~ 1920 CN to reveal seven PL maxima of an 80 nm thick nanoheterostructure photoetching in DI H_2O, while

only 725 CN revealed the same number of peaks in NH_4OH. Furthermore, the photo-ALE in an oxide etching environment of NH_4OH ([98, 122]) allowed defining positions of each PL maxima more precisely than those in the DI H_2O environment. **Figure 3-9 (c)** shows that positions of the PL maxima detected in NH_4OH follow a straight line in function of the cumulative thickness of the nanoheterostructure photoetching at least up to 80 nm deep, which is indicative of the constant etch rate. In contrast, a growing deviation from such a linear behavior was already appeared for the same nanoheterostructure photoetching in DI H_2O at etch depth less than 40 nm. This is revealing formation of a non-stoichiometric surface in DI H_2O.

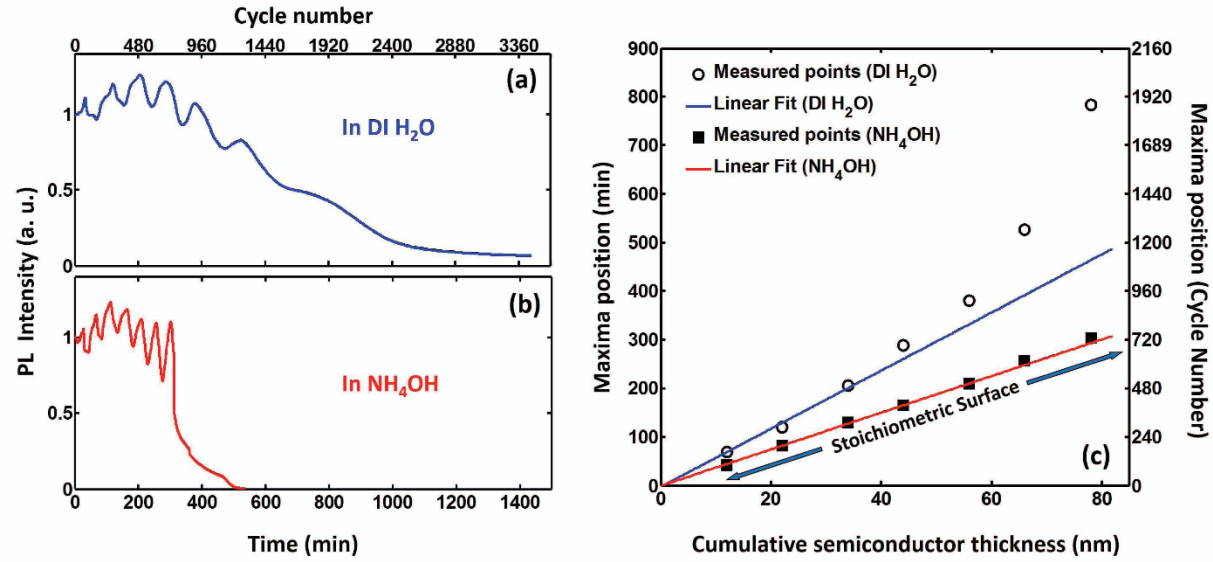

Figure 3-9. Photo-ALE of GaAs/AlGaAs nanoheterostructures (wafer D3422). Temporal PL plots from samples photo-etched in DI H_2O (a), and in NH_4OH (b). Linearly depending PL maxima positions on the cumulative thickness of the GaAs/$Al_{0.35}Ga_{0.65}As$ nanoheterostructure indicate formation of stoichiometric surfaces (c).

3.6. Discussion

The efficiency of generating PL signal by a semiconductor is related to the minority carriers lifetime, τ, and it could be expressed with the following relationship [133]:

$$\frac{1}{\tau} = \frac{1}{\tau_R} + \frac{1}{\tau_{nR}} + \frac{IRV}{d} \qquad (3\text{-}4)$$

where τ_R and τ_{nR} denote lifetime of radiative and nonradiative recombination processes, respectively, d is a thickness of the active (PL emitting) layer, and IRV (interface recombination velocity) represents processes related to the interface states of investigated materials. In the case of GaAs and $Al_{0.35}Ga_{0.65}As$ nanoheterostructures investigated in this report, the overall IRV is a sum of the recombination velocities, IRV_k, at interfaces of the PL emitting GaAs layer with $Al_{0.35}Ga_{0.65}As$ and AlAs, at interfaces between GaAs and $Al_{0.35}Ga_{0.65}As$ layers located above, as well as at the interface of the topmost layer with the etching solution, i.e., $IRV = \sum_{k=1}^{n} IRV_k$. In addition to the presence of the intrinsic surface states arising from the break in the translational symmetry of a bulk semiconductor at its surface, the impurities and other surface defects act as NRRC playing a critical role in the conversion efficiency of excited electron-hole pairs to the PL signal.

Subsequently, the oscillation of temporal PL intensity of GaAs/AlGaAs nanoheterostructures was induced by variations of surface states as a result of formation/dissolution of oxides, thus, the two PL maxima in **Figure 3-3** observed at ~ 110 CN and ~ 260 CN were related to the dissolution of 8 and 3 nm thick GaAs layers, respectively. In agreement with the structure of the D4322 sample (**Figure 3-1 (b)**), photo-ALE process revealed seven characteristic PL maxima shown in **Figure 3-9 (a)** (DI H_2O data) and **Figure 3-9 (b)** (NH_4OH data). Then, the amount of material removed per each photo-ALE cycle could be determined based on the positions of the PL maxima and the known thickness of GaAs/AlGaAs nanoheterostructures. This approach allowed following in real time the position of a photo-ALE front with a sub-monolayer resolution. It should also be emphasized that the temporal PL plots discussed in this report were collected with a relatively low excitation power density of ~ 20 mW/cm^2 designed to achieve slow photo-ALE of the investigated nanoheterostructures. Together with the intermittent mode of sample irradiation, PL signal allowed monitoring the photo-ALE with an enhanced sensitivity to contributions from the interface states and formation of Ga_2O_3 and other Ga-, Al- and As-based surface products [113]. Under the low excitation power conditions, the intensity of PL emission could fall below the sensitivity of the measuring setup, presented in **Figure 3-2**, whenever the oxides are dissolved homogenously. For instance, in **Figure 3-4 (a)**, commensurate with the growing concentration of surface oxides, the photo-ALE rate slowed down and PL intensity for the sample photoetched in excess of 60 nm

saturated at ~ 50% of its initial intensity, whereas in NH_4OH solutions (**Figure 3-4 (b)** and **Figure 3-4 (c)**) the absence of a surface passivating layer resulted in the PL signal too weak to be detected with the employed PL setup. In view of that, PL data could reveal, *in situ*, accumulation of oxides at the surface of the investigated nanoheterostructures, in DI H_2O, and it could indicate homogenous and constant photo-ALE of GaAs and AlGaAs layers in NH_4OH, under the applied experimental conditions.

This was corroborated with ICP-MS data, shown in **Figure 3-5**. A linear dependence between calculated and ICP-MS detected As^{3+} ions was observed for the samples photoetched up to 60 nm deep in DI H_2O (**Figure 3-5 (a)**), however experimental data started to deviate from calculation points at etch depth deeper than 60nm, in agreement with saturation of PL data at this etch depth. At the same time, a large deficit of Ga^{3+} ions detected in the photo-ALE product from the early stage of the photoetching process in DI H_2O (**Figure 3-5 (b)**), which is consistent with the formation/accumulation of Ga_2O_3 in water on the surface of the above bandgap illuminated GaAs [121]. This suggests that it is impossible to produce stoichiometric surfaces of GaAs or AlGaAs dissolving in DI H_2O, beyond etch depth of ~ 8 nm. In contrast, the ICP-MS results of photo-ALE in 28% of NH_4OH presented in **Figure 5 (c)** and **Figure 5 (d)** demonstrated an excellent agreement between the concentrations of As^{3+} and Ga^{3+} ions detected in the photo-ALE product with those expected for these ions released by the photoetching nanoheterostructures, at least up to ~ 110 nm deep. The congruent character of the observed decomposition is consistent with the formation of a stoichiometric surfaces of GaAs and AlGaAs at the end of each etching cycle.

The interaction of Al ions released by photoetching AlGaAs with H_2O and O_2 could lead to formation of Al_2O_3 and $Al(OH)_3$ [130]. Indeed, the Al-O stretching mode (520 cm^{-1}) identified with the FTIR data shown in **Figure 3-6** points out to the presence of Al_2O_3. Consistent with this are high resolution XPS scans for Ga 3*d* and Al 2*p* shown in **Figure 3-7** that confirm the presence of Ga_2O_3 as well as Al_2O_3 and $Al(OH)_3$. These compounds could prevent diffusion of O or H_2O molecules towards the oxide-semiconductor interface, resulting in reduced photoetching rates. However, no Al ion was detected in the photo-ALE product for the calibrated ICP-MS range. The absence of Al ions in the ICP-MS data of photo-ALE samples could imply that Al compounds, due to their poor solubility in NH_4OH [122, 134] and water [134] remained on the surface of

photoetching samples. Alternatively, the inability of detecting Al ions in NH_4OH could be related to the known difficulty of the ICP-MS technique in tracing metals in NH_4OH [131, 132].

The AFM data revealed that surface of the GaAs/AlGaAs nanoheterostructure photoetched in NH_4OH was smoother (**Figure 3-8 (f)**, $\sigma_{RMS} = 0.93$ nm) compared to the surface of that nanoheterostructure photoetched in DI H_2O to a comparable depth (**Figure 3-8 (e)**, $\sigma_{RMS} = 2.1$ nm). Furthermore, the photo-ALE process of J0152 etched in DI H_2O to less than ~14 nm (**Figure 3-8 (b)** to **Figure 3-8 (d)**) did not increase significantly the surface roughness of processes samples. Hence, consistent with the XPS and FTIR data, the source of the increased roughness must be related to surface accumulated oxides poorly dissolvable in DI H_2O. Clearly, while etching in NH_4OH eliminates accumulation of Ga- and As-oxides on the etched surfaces, the use of ammonia is not efficient in removing Al-oxides and Al-based compounds. As the accumulation of these products is expected in proportion to the overall thickness of photo-ALE GaAs/AlGaAs nanoheterostructures, it is reasonable to expect that the presence of these products is responsible for the increased surface roughness of the 105.6 nm deep etched sample ($\sigma_{RMS} = 0.93$ nm). The reported here σ_{RMS} values require additional discussion as it is known that high-quality GaAs (001) surfaces are characterized by $\sigma_{RMS} \leq 0.5$ nm (e.g., Karkare *et al.*[135]), and chemo-mechanical polished (CMP) epi-ready GaAs (001) could have $\sigma_{RMS} \leq 0.15$ nm ([136]). However, we note that the samples investigated in this report were diced out from a wafer that was photoresist coated to minimize the inclusion of semiconductor dust generated during dicing. This procedure was carried out in a fabrication environment class 10000, and no special surface treatment, such as CMP or thermal annealing, was applied to these samples after photoresist removal. Under these conditions, $\sigma_{RMS} = 0.75$ nm for the reference sample (**Figure 3-8 (a)**) seems a reasonable result.

The unique ability of the photo-ALE process in providing a rapid assessment of the semiconductor etching characteristics was further underscored by photo-ALE data of wafer with multiple nanoheterostructures (**Figure 3-9**). We argue that under constant photo-ALE rates, the positions of PL-revealed maxima (interfaces) depend linearly on the thickness of the investigated nanoheterostructures. This was achieved for D3433 sample etched in NH_4OH up to 80 nm deep, as presented in **Figure 3-9 (b)** (full squares). The constant etch rate during photo-ALE of a semiconductor nanoheterostructure is indicative of the congruent decomposition of material, consistent with the ICP-MS results reported in **Figure 3-5 (c)** and **Figure 3-5 (d)**. However, the

use of NH_4OH for deep photo-ALE of AlGaAs nanoheterostructures must be further explained as it is known that NH_4OH-based solutions were used for selective etching of GaAs over AlGaAs [122], [137]. This is because the Al–O bond is much stronger than that of Ga–O and As–O, which would lead to surface accumulation of Al_2O_3. Thus, it is plausible to expect that the linear (CN proportional) etching of the investigated here GaAs/AlGaAs nanoheterostructures, significantly thicker than 80 nm, would require Al-oxide etching solutions, such as hydrofluoric acid or phosphoric acid [122]. In contrast, PL data for the same nanoheterostructures photoetching in DI H_2O (**Figure 3-9 (c)**, open circles) suggest that non-linear photoetching takes place at depths exceeding 35 nm. This is consistent with the decelerating photo-ALE rate due to accretion of Ga_2O_3 (**Figure 3-7 (a)**) and with the significant deficit of Ga^{3+} ions detected with ICP-MS, for more than ~ 8 nm of etched GaAs (**Figure 3-5 (b)**). It seems that a more accurate PL-based assessment of the photo-ALE process would be still possible, e.g., by reducing the average amount of material etched in an individual photo-ALE cycle. Nevertheless, these results demonstrate the attractive application of a PL-based diagnostics for monitoring *in situ* formation of stoichiometric surfaces of nanoheterostructures of compound semiconductors.

3.7. Conclusion

Mechanisms of digitally photo-ALE of GaAs/$Al_{0.35}Ga_{0.65}As$ nanoheterostructures in DI H_2O and NH_4OH environments were investigated. The photoetching was induced with a low power 660 nm LED ($P \approx 16\text{-}20$ mW/cm^2) and monitored *in situ* with PL emitted by the investigated nanoheterostructures. The ICP-MS detected concentrations of the photo-ALE products were compared to the calculated concentrations of $As^{3+}$and Ga^{3+} ions expected to be released by photoetching GaAs and AlGaAs layers of known thickness. A deficit of Ga^{3+} ions in the photo-ALE product was detected for the nanoheterostructures photoetched in DI H_2O, suggesting that it is impossible to produce stoichiometric surfaces of GaAs or AlGaAs dissolving in such an environment, for photoetch depth over ~ 8 nm. In contrast, the ICP-MS results exhibited an attractive agreement between the concentrations of As^{3+} and Ga^{3+} ions in the photo-ALE products and those expected for As^{3+} and Ga^{3+} ions released by the nanoheterostructures photoetched in NH_4OH, at least up to ~ 110 nm deep. The congruent character of the decomposition in this case was consistent with the constant photo-ALE rate and formation of stoichiometric surfaces. The constant photo-ALE rate of GaAs was also demonstrated with PL

data for the nanoheterostructures photoetched in NH_4OH. The AFM data confirmed the formation of a relatively smooth surface (σ_{RMS} = 0.93 nm) of a GaAs/AlGaAs nanoheterostructure (J0152) photoetched in NH_4OH to a depth of 105.6 nm. In contrast, the surface of that nanoheterostructure photoetched to a comparable depth in DI H_2O was significantly rougher (σ_{RMS} = 2.1 nm), consistent with the surface accumulation of Ga_2O_3 and other Al-based compounds. Since $Al(OH)_3$ could pile up on the surface of GaAs/AlGaAs nanoheterostructures photoetched in NH_4OH, the fabrication of stoichiometric surface of nanoheterostructures photoetched significantly deeper than100 nm requires Al compound etching environments, such as those comprising hydrofluoric or phosphoric acids.

The concept of photo-ALE is similar to the conventional atomic layer etching of semiconductors. However, there are some fundamental differences pointing to the potential advantage of a photo-process in nanostructuring of compound semiconductors and fabrication of advanced nanoscale devices. Firstly, the photo-ALE allows a sub-monolayer precision of material removal without the need of changing the hardware that, normally, is required by the conventional digital etching methods. Secondly, the photo-ALE process can be monitored *in situ* with either photoluminescence of a processed wafer, or the open circuit potential of the photoetching material, as demonstrated by us recently [109]. Thirdly, since an enhanced dissolution of the surface accumulating photo-ALE products is expected in the forced flow of a photoetching liquid, a 2-step etching cycle could be reduced below the shortest cycle of 25 sec investigated in this report, which would result in an accelerated further photoetching process. These results demonstrate a relatively simple process for *in situ* chemical diagnostics of ALE and fabrication of compound semiconductor nanodevices that expands beyond, e.g., topographical characterization of etched semiconductor surfaces [138].

3.8. Associated Content

S1. PL spectroscopy at 20 K and during photo-ALE at 298 K (Wafer J0150); S2. Calculations of ions released from J0152 samples in DI H_2O and NH_4OH; S3. Dark corrosion data for J0152 in DI H_2O and NH_4OH

3.9. Author Information

Corresponding Author

*E-mail: jan.j.dubowski@usherbrooke.ca

Notes

The authors declare no competing financial interest.

3.10. Acknowledgments

This research was supported by the Canada Research Chair in Quantum Semiconductors Program (Grant no. 950-220304), the Natural Sciences and Engineering Research Council of Canada (Discovery Grant RGPIN-2015-04448 and Strategic Partnership Grant SPG-2016-494057). One of the authors (MRA) acknowledges the support received in the frame of the NSERC-CREATE Training Program in Integrated Sensor Systems. The fabrication of GaAs/AlGaAs wafers was subsidized by the CMC Microsystems (Kingston, Canada). The authors are indebted to Dr. Khalid Moumanis for collecting wavelength dependent PL spectra of the GaAs/AlGaAs wafers, Prof. Roland Leduc and Mr. Olivier Savary (Department of Civil Engineering, Faculty of Engineering, Université de Sherbrooke) for collecting ICP-MS data, and Mrs. Sonia Blais (Centre de caractérisation des matériaux, Université de Sherbrooke) for collecting XPS data and assisting in their analysis.

3.11. Supporting Information

3.11.1. PL spectroscopy at 20 K and during photo-ALE at 298 K (Wafer J0150)

Figure 3-10 (a) shows the low-temperature PL spectrum of J0152 excited with ~ 600 W/cm^2 power of a 532 nm diode laser. The signal was collected with a SPEX (Model 1704), a thermoelectrically cooled photomultiplier tube (Hamamatsu, model R2658) and a lock-in amplifier. **Figure 3-10 (b)** and **Figure 3-10 (c)**, respectively, illustrate spectral and temporal

variations of the PL emission from J0150 in DI H_2O. Measurements were carried out using a hyperspectral imaging photoluminescence mapper (HI-PLM), equipped with a 532 nm laser, computer-controlled volume Bragg gratings, beam homogenizing microlens array and a Peltier cooled high sensitivity CCD camera [139]. Pulses of 6 second duration with a 60 sec period (DC = 6/60) delivered an excitation power density of P = 70 mW/cm^2. Note that the J0150 wafer has nominally the same structure as that of J0152 [104].

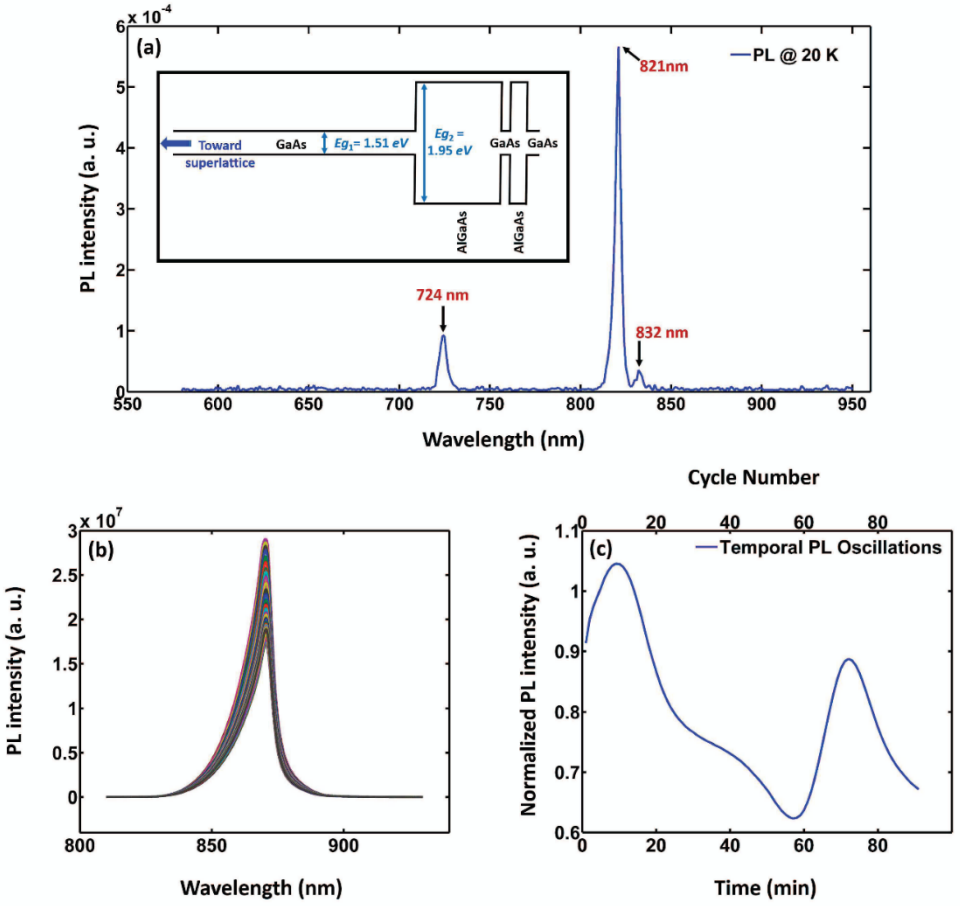

Figure 3-10. (a) Low temperature (20 K) PL spectrum showing a 724 nm peak, originating from the 3 nm GaAs layer, the 821 nm peak, originating from band-to-band transitions in GaAs, and the 832 nm peak related to donor-acceptor pair transitions (inset shows schematically the band diagram of the J0150 GaAs/AlGaAs nanoheterostructure). (b) A series of PL spectra measured with HI-PLM during photo-ALE of the nanoheterostructure in DI H_2O (DC = 6/60, P = 70mW/cm2). Note that it took ~ 60 sec to collect a single spectrum with HI-PLM. (c) Temporal plot of PL intensity variations for the spectra shown in Figure S1b.

3.11.2. Calculations of ions released from J0152 samples in DI H_2O and NH_4OH

GaAs and $Al_xGa_{1-x}As$ have a zinc blende crystal structure, with a lattice constant of 5.65325 Å and 5.65325+0.0078*x* Å, respectively. In case of GaAs, there are 4 Ga and 4 As atoms in the unit cell, and in case of $Al_xGa_{1-x}As$, since Ga atoms are substituted by mole faction of *x*, there are 4*x* of Al, 4 × (1-*x*) of Ga and 4 As atoms. Furthermore, the atomic weights of Ga, As and Al are 69.723 u, 74.9216 u and 26.9815 u, respectively, where 1 u = 1.66×10^{-27} kg. Individual mass of atoms in a unit cell is $M = NB \times MW \times 1.66 \times 10^{-27}[kg]$, where *NB* is number of atoms and *MW* is atomic weight. Then the atomic density is $p = \frac{M}{L.C.^3}[\frac{kg}{m^3}]$, where *L.C.* is lattice constant of related material in m [140, 141].

For GaAs, the total mass in a unit cell is:

$$M_{GaAs} = MGa_{GaAs} + MAs_{GaAs}[kg] \tag{3-5}$$

where $MGa_{GaAs}$and MAs_{GaAs} are as follow:

$$MGa_{GaAs} = 4 \times 69.723 \times 1.66 \times 10^{-27}[kg] \tag{3-6}$$

$$MAs_{GaAs} = 4 \times 74.9216 \times 1.66 \times 10^{-27}[kg] \tag{3-7}$$

Then the atomic density is:

$$pGa_{GaAs} = \frac{MGa_{GaAs}}{(5.65325 \times 10^{-10})^3}[\frac{kg}{m^3}] \tag{3-8}$$

$$pAs_{GaAs} = \frac{MAs_{GaAs}}{(5.65325\times10^{-10})^3}[\frac{kg}{m^3}] \quad (3\text{-}9)$$

Alternatively, for $Al_{0.35}Ga_{0.65}As$ the total mass in a unit cell is:

$$M_{AlGaAs} = MGa_{AlGaAs} + MAs_{AlGaAs} + MAl_{AlGaAs}[kg] \quad (3\text{-}10)$$

where MGa_{AlGaAs}, MAs_{AlGaAs} and MAl_{AlGaAs} are as follow:

$$MGa_{AlGaAs} = 0.65\times4\times69.723\times1.66\times10^{-27}[kg] \quad (3\text{-}11)$$

$$MAs_{AlGaAs} = 4\times74.9216\times1.66\times10^{-27}[kg] \quad (3\text{-}12)$$

$$MAl_{AlGaAs} = 0.35\times4\times26.9815\times1.66\times10^{-27}[kg] \quad (3\text{-}13)$$

Then again the atomic density is:

$$pGa_{AlGaAs} = \frac{MGa_{AlGaAs}}{(5.656\times10^{-10})^3}[\frac{kg}{m^3}] \quad (3\text{-}14)$$

$$pAs_{AlGaAs} = \frac{MAs_{AlGaAs}}{(5.656\times10^{-10})^3}[\frac{kg}{m^3}] \quad (3\text{-}15)$$

$$pAl_{AlGaAs} = \frac{MAl_{AlGaAs}}{(5.656\times10^{-10})^3}[\frac{kg}{m^3}] \quad (3\text{-}16)$$

By multiplying the atomic density with the volume of each GaAs and AlGaAs layer (in m^3), and considering the LED spot size of 3.2 mm^2, we can calculate the mass of each desired layer. Since we used 5 mL of each solution (0.005 kg of DI H_2O or 0.0044 kg of NH_4OH), for each layer of concern (layer *x*), the obtained numbers will be converted to parts per billion as follows:

$$\frac{Mass\ of\ Element_{layer\ x}}{Mass\ of\ layer\ x + \text{Mass of solution}}[ppb] \qquad (3\text{-}17)$$

Figure 3-11 shows the calculated number of ions released from photoetching J0152 sample (down to the bottom of 2nd AlGaAs layer) in 5 mL of DI H_2O (**Figure 3-11 (a)**) and in 5mL NH_4OH (**Figure 3-11 (b)**). The photo-ALE rates of 0.08 ± 0.005 nm/cycle, in DI H_2O, and 0.34 ± 0.003 nm/cycle, in NH_4OH, were taken into account (data are presented in **Figure 3-4**). It must be noted that the number of Ga atoms in AlGaAs is reduced in comparison to those in GaAs due to the stoichiometric ratio of AlGaAs, which is 0.35:0.65:1. This results in sub-liner evolution of Ga in the calculated data, presented in **Figure 3-11 (a)** and **Figure 3-11 (b)**.

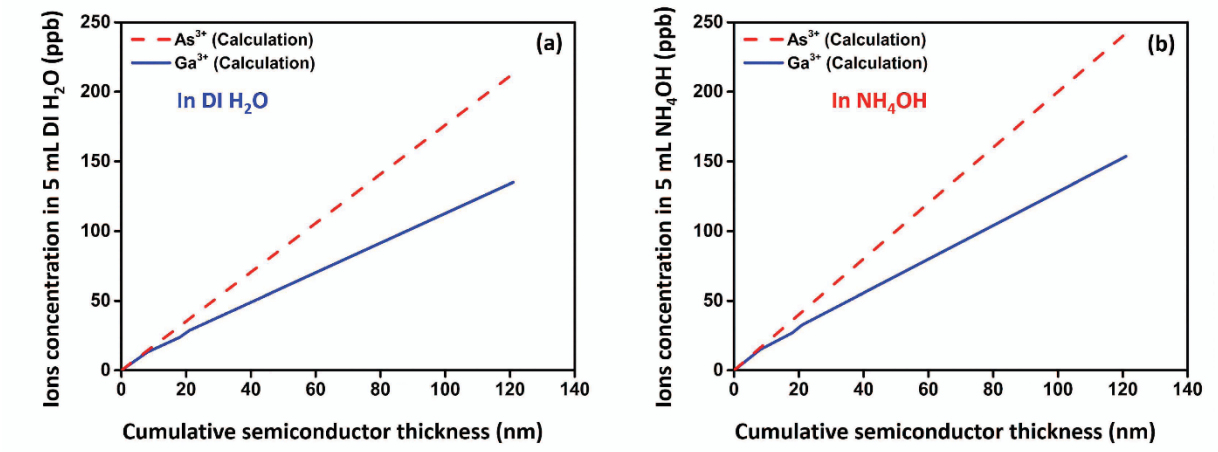

Figure 3-11. Calculated concentration of As^{3+} and Ga^{3+} ions released by GaAs/$Al_{0.35}Ga_{0.65}As$ samples (wafer J0152) versus cumulative sample thickness, in 5 mL of DI H_2O (a) and in 5mL of NH_4OH (b).

3.11.3. Dark corrosion data for J0152 in DI H2O and NH4OH

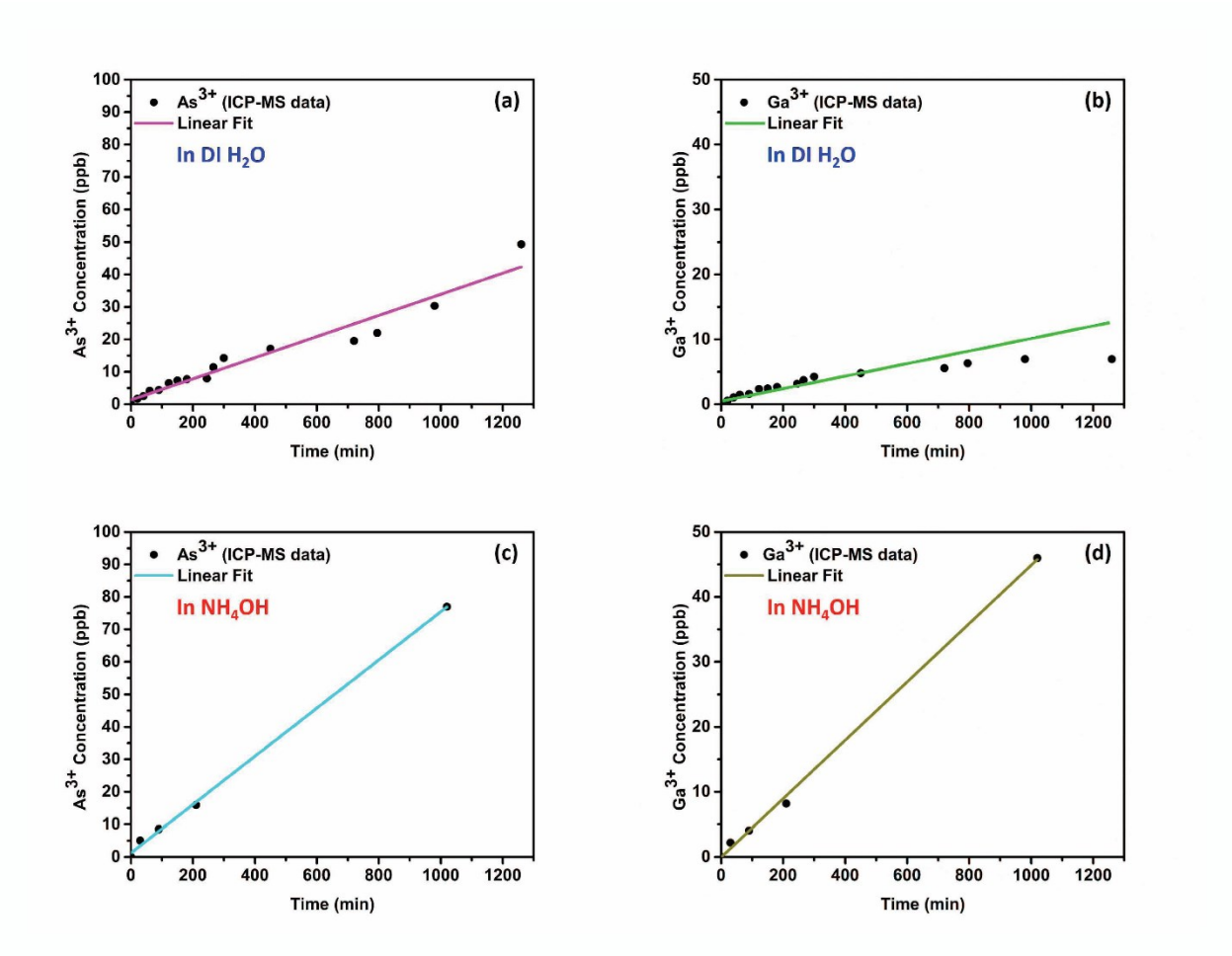

Figure 3-12. Concentration of ICP-MS detected As^{3+} and Ga^{3+} ions released in darkness during the same period of time as that of photo-ALE experiments of GaAs/$Al_{0.35}Ga_{0.65}As$ nanoheterostructures in DI H_2O (a) and (b), respectively, and in NH_4OH (c) and (d), respectively.

CHAPTER 4. Photonic Biosensor Based on Photocorrosion of GaAs/AlGaAs Quantum Heterostructures for Detection of *Legionella pneumophila*

4.1. AVANT-PROPOS

Auteurs et affiliation:

- Mohammad Reza Aziziyan : Étudiant au doctorat, Université de Sherbrooke, Faculté de génie, Département de génie électrique et informatique.
- Walid M. Hassen : Assistant de recherche, Université de Sherbrooke, Faculté de génie, Département de génie électrique et informatique.
- Denis Morris : Professeur titulaire, Université de Sherbrooke, Faculté des sciences, Département de physique.
- Eric H. Frost : Professeur titulaire, Université de Sherbrooke, Faculté de médecine et des sciences de la santé, Département de microbiologie et d'infectiologie.
- Jan J. Dubowski : Professeur titulaire, Université de Sherbrooke, Faculté de génie, Département de génie électrique et informatique.

Titre français : Biocapteur photonique basé sur la photocorrosion des hétérostructures quantiques GaAs/AlGaAs pour la détection de *Legionella pneumophila*

Date d'acceptation : 2 février 2016

État de l'acceptation : version finale publiée

Revue : Biointerphases

Référence : M. R. Aziziyan, W. M. Hassen, D. Morris, E. H. Frost, and J. J. Dubowski, "Photonic biosensor based on photocorrosion of GaAs/AlGaAs quantum heterostructures for detection of Legionella pneumophila," Biointerphases, vol. 11, no. 1, pp. 019301, 2016.

Contribue au document : Ce chapitre décrit, pour la première fois, la détection de *L. pneumophila* à l'aide de la réponse photonique des nanohétérostructures GaAs/AlGaAs. Nous avons démontré que la longueur de Debye joue un rôle important dans le contrôle des performances du biocapteur et qu'elle pourrait être modifiée pour intensifier davantage l'effet de charge des bactéries. En outre, une évaluation approfondie est fournie, en particulier dans le contexte des propriétés biophysiques de différentes bactéries et de leurs différentes charges électriques de surface et efficacité d'immobilisation. Les problèmes et obstacles potentiels restreignant la limite de détection de la technologie QSPB pour la détection de *L. pneumophila* sont détaillés.

Résumé français : Le processus de photocorrosion de semi-conducteurs est très sensible à la présence d'états de surface, et il peut être influencé par les molécules chargées électriquement immobilisées à proximité de l'interface du semi-conducteur/électrolyte. Le mécanisme principal est lié à la flexion de la bande d'énergie de la structure du semi-conducteur à proximité de sa surface et aussi à la distribution des électrons et des trous excités associées à la flexion de la bande d'énergie. Nous avons étudié la photoluminescence des hétérostructures quantiques GaAs/AlGaAs pour le monitoring «*in situ*» de la photocorrosion, ce qui nous a permis de démontrer la détection de *Legionella pneumophila* non-croissante en suspension dans une solution saline tamponnée au phosphate. Des biopuces fonctionnalisées par des anticorps ont permis la détection directe de ces bactéries à 10^4 bactéries/ml. Nous discutons de la sensibilité de ce processus relié à la possibilité de créer des conditions appropriées pour le processus de la photocorrosion à des taux lents ainsi que l'interaction d'une charge électrique de bactéries avec la surface d'un semi-conducteur bio-fonctionnalisé.

4.2. Abstract

Photocorrosion of semiconductors is strongly sensitive to the presence of surface states, and it could be influenced by electrically charged molecules immobilized near the semiconductor/electrolyte interface. The underlying mechanism is related to band bending of the semiconductor structure near the surface and the associated distribution of excited electrons and holes. The authors have employed photoluminescence of GaAs/AlGaAs quantum heterostructures for monitoring *in situ* the photocorrosion effect, and demonstrating detection of nongrowing *Legionella pneumophila* suspended in phosphate buffered saline solution. Antibody functionalized samples allowed direct detection of these bacteria at 10^4 bacteria/ml. The authors discuss the sensitivity of the process related to the ability of creating conditions suitable for photocorrosion proceeding at extremely slow rates and the interaction of an electric charge of bacteria with the surface of a biofunctionalized semiconductor.

4.3. Introduction

Reduction in the risk of diseases associated with growth and propagation of pathogenic bacteria in water supplies requires frequent and rigorous assessment of the bacteriological quality of drinking and industrial water [1, 3, 4]. Certain conditions make our plumbing systems and cooling towers an attractive habitat for *Legionella pneumophila*. These bacteria have been recognized as the source of infection through inhalation of aerosols from contaminated water leading to outbreaks of Legionellosis and of Pontiac fever [5, 142-144]. Thus, regular monitoring and frequent *L. pneumophila* testing should be conducted to ensure that these bacteria are not present in water systems.

To detect the presence of pathogenic bacteria or microorganisms in aqueous solutions, conventional methods have been applied for a long period of time; however, they are normally time consuming and relatively expensive, making them unsuitable for frequent analysis of water. Full description of the performance of these techniques and detailed comparison of their pros and cons are extensively discussed in literature [1, 2, 33, 43, 143, 145]. Both academia and R&D sectors of industrial companies have spent a great deal of effort to develop low cost and fast biosensing methods, specifically for detection of pathogens in water. Nevertheless, up until now,

few biosensing platforms have been found attractive and achieved commercial success, such as those for point-of-care diagnostics [146-148]. Biosensors use biologically sensitive bioreceptors together with suitable transducers [149]. Among techniques explored for detection of *L. pneumophila* and *Escherichia coli*, the most popular are surface plasmon resonance [13], surface acoustic wave [14], and electrochemical impedance spectroscopy [15]. Significant attention has been paid toward the development of transducers since they could determine the overall performance and detection limit of a biosensor. Some transducers are relatively fast and sensitive, but often technical complexity or excessive price of such biosensors prevent them from replacing traditional methods of detection.

Studies of semiconductor photoluminescence (PL) based biosensors have demonstrated the potential of this approach for sensitive detection of biomolecules [25, 55, 57, 150]. The PL effect has also been employed for the investigation of a slow photocorrosion process of GaAs/AlGaAs quantum heterostructures. Progress with monitoring the process of semiconductor/electrolyte interface formation has allowed development of methods for selective area etching of GaAs [65], and photo-assisted etching of GaAs and AlGaAs with an etch depth resolution down to the micrometer level [151]. The current approach employing the photocorrosion process for biosensing, however, is based on the ability to control etch depth resolution pushed down to the nanometer level. Since GaAs and AlGaAs have nearly identical lattice constants, the band-gap of these heterostructures could be flexibly engineered to provide two dimensional electron gas based devices [26, 27], which could also be of potential interest for biosensing. Furthermore, the optically confined GaAs/AlGaAs epitaxial heterostructure exhibits strong PL in the near-infrared window, where the biological materials have minimal absorption (700–1300 nm) [28]. This makes GaAs/AlGaAs and other semiconductor microstructures emitting in the near infrared region potentially attractive for developing photonic nanobiosensors designed for monitoring biological processes *in vivo*. The electrostatic interaction between bacteria and the semiconductor depends on the bacteria charge, concentration, average distance between immobilized bacteria and semiconductor surface, and a dielectric constant of the environment. Thus, the investigation of these parameters is of paramount importance for the development of attractive photoelectrochemical biosensors. Recently, we have demonstrated that the photocorrosion process of GaAs/AlGaAs heterostructures could be used to carry out the direct detection of electrically

charged *E. coli* bacteria interacting with the semiconductor surface at 10^3 colony-forming units per milliliter (CFU/ml) [30]. Given that the proposed detection is a relatively new approach, while the electric charge on the surface of a bacterial cell and bacterial zeta potential depend on the biophysical properties of bacteria, it would be important to evaluate the proposed technology for detection of different bacteria.

In this paper, we investigate the photocorrosion process of GaAs/AlGaAs quantum well heterostructures, and we examine the photocorrosion based biosensing approach for detection of heat-killed *L. pneumophila* diluted in phosphate buffered saline (PBS) solution.

4.4. Experimental Approach

4.4.1. Materials and Apparatus

A detailed structure of two wafers investigated in this work is shown in **Figure 4-1**. For both wafers, an undoped 500 nm thick GaAs buffer layer was first grown on a semi-insulating GaAs (001) substrate. One structure (wafer V0881) is terminated by a 116 nm-thick $Al_{0.35}Ga_{0.65}As$ barrier capped with a 10 nm-thick GaAs layer (**Figure 4-1 (a)**). For the second wafer (J0150), a GaAs/AlGaAs quantum well structure was grown on the GaAs buffer layer (**Figure 4-1 (b)**) and capped by an 8 nm-thick GaAs layer.

Biotinylated polyethylene glycol (Bio-PEG) was obtained from Prochimia Surfaces (Gdansk, Poland) and hexadecanethiol (HDT) was bought from Sigma-Aldrich (ON, Canada). Neutravidin was bought from Molecular Probes (Invitrogen, Burlington, Canada). Polyclonal biotinylated antibody against *L. pneumophila* was purchased from ViroStat, Inc. (Portland, Maine). PBS 10X, *p*H 7.4, was purchased from Sigma (Oakville, Canada). OptiClear was obtained from National Diagnostics (Mississauga, Canada), acetone from ACP (Montréal, Canada), and isopropyl alcohol (IPA) from Fisher Scientific (Ottawa, Canada). Ammonium hydroxide 28% (NH4OH) was purchased from Anachemia (Richmond, Canada). We used deionized water (DI-water), 18.2 MX, produced with Millipore purification custom system build by Culligan (PQ, Canada). Gold chloride was purchased from Sigma-Aldrich (ON, Canada). The *L. pneumophila* ssp1 was provided from industrial water by Magnus Chemicals Ltd. (Boucherville, Canada) and

cultured in buffered charcoal yeast extract agar medium. About six colonies were suspended in 5ml PBS, and their concentration was measured by an optical densitometer operating at 600 nm. To prevent infection, we heated *L. pneumophila* containing solutions at 90 °C for 20min [152]. The initial concentration was 8×10^7 CFU/ml. *Bacillus subtilis* bacteria were obtained from the Department of Biology of the University of Sherbrooke (Québec, Canada). These bacteria were grown in minimal broth and stored in 50% glycerol at -22 °C. Before usage, bacteria were aliquoted at 10^6 CFU/ml and centrifuged for 25min at 3000 rpm. The medium was removed, and bacterial pellets were suspended in PBS. The pellets were washed by a second centrifugation for 15 min followed by pellets' resuspension in PBS. Finally, the suspension was heated at 90 °C for 20 min to arrange for a sound comparison with heat-treated *L. pneumophila*. For heat-treated bacteria, we will use term "bacteria/ml" instead of "CFU/ml" throughout this report.

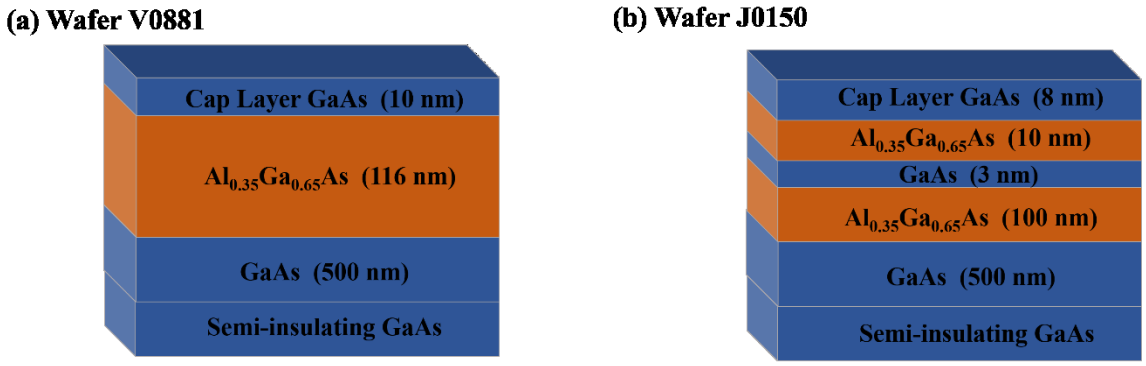

Figure 4-1. Schematics of GaAs/Al0.35Ga0.65As quantum-heterostructures studied in this work.

The low-temperature (20 K) PL measurements were carried out using a diode laser emitting at 532 nm. The laser power was kept at 50 mW, and the chopped excitation beam (at 300 Hz) was focused on a spot diameter (at 1/e) of about 100 µm. The PL emission was collected and refocused on the entrance slit of a 1 m-spectrometer (SPEX, model 1704). The PL signal was measured using thermoelectrically cooled photomultiplier tube (Hamamatsu, model R2658) and a lock-in amplifier.

Bacteria detection experiments were conducted at room temperature using a custom designed quantum semiconductor photonic biosensor (QSPB) reader. A schematic of the QSPB reader is shown in **Figure 4-2**. It employs a 660 nm light emitting diode (LED) source for excitation of samples and a CCD camera for recording PL signal. A long pass filter with a

transmission wavelength range of 840–1650 nm (Edmunds 86–070) was used to collect PL signal dominated by 870 nm emission from the 500 nm thick GaAs layer of the investigated microstructures. All PL plots were collected for samples irradiated, typically, at 20 mW/cm^2.

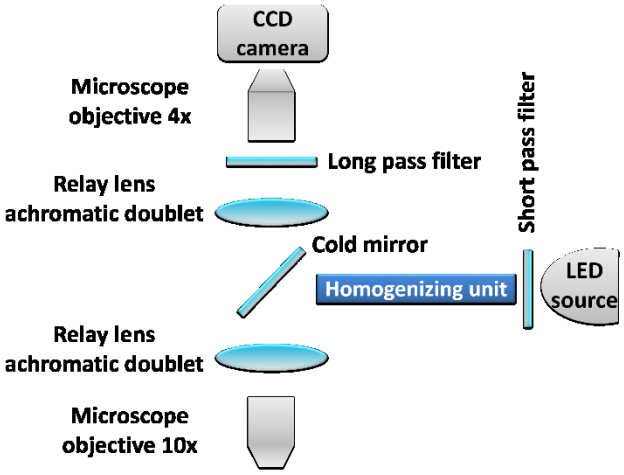

Figure 4-2. Schematic diagram of the QSPB reader employed for collecting PL signal from biofunctionalized GaAs/AlGaAs samples.

4.4.2. Sample Preparation Steps and Conditions

Semiconductor chips of 2×2 mm dimensions were diced from a 4-in. wafer whose surface was protected by spin-coated photoresist. The samples were sequentially cleaned in OptiClear and IPA for 5min and anhydrous ethanol and DI-water for 2 min, all using an ultrasonic bath. Afterward, they were dried by high purity nitrogen flow and immersed in ammonium hydroxide (28%) for 1-min, rinsed with DI-water, and dried with a nitrogen flow. Next, the bottom surface of the chips was immediately exposed to a solution of gold chloride (2mM in DI-water) with a three-time repetition of the following sequences: 3 min exposure to gold chloride, rinsed with DI-water, and dried with nitrogen flow. Then, chips were exposed to acetone to remove the protective photoresist layer from their top surfaces (active area). Degreasing steps were carried out in an ultrasonic bath of OptiClear, acetone, and IPA, each 5min. Following this step, chips were dried by nitrogen flow and immersed in ammonium hydroxide for 1.5 min to remove a native oxide layer. Next, chips were rapidly rinsed with anhydrous ethanol and directly transferred to a thiol solution consisting of 0.15mM biotinylated PEG thiol and 1.85mM HDT diluted in deoxygenized ethanol. The samples were incubated in the thiol solution for 20 h at room temperature and in

darkness. After the thiolation process, chips were rinsed with anhydrous ethanol to remove physisorbed thiols and rinsed with 1X PBS and incubated with neutravidin, 0.2 mg/ml in 1X PBS, for 2 h. Next, the chips were rinsed with 1X PBS and incubated with an antibody solution, 0.1 mg/ml in 1X PBS, for 1 h. Finally, the chips were rinsed with 0.1X PBS and transferred to a flow cell. For bacteria detection tests, the biofunctionalized chips were first exposed to bacteria solution (in 0.1X PBS) for 25min at a flow rate of 0.04 ml/min, then for 5min in a without flow condition. Afterward, 0.1X PBS was injected continuously for another 30 min. At the final stage, the chips were transferred from the flow cell into a petri dish, where they were rinsed with DI-water while slowly shaking the petri dish. This process was repeated three times in an effort to remove physisorbed bacteria from the semiconductor surface prior to counting bacteria by optical microscopy. **Figure 4-3** shows a schematic view of a GaAs/AlGaAs biochip after being exposed to bacteria.

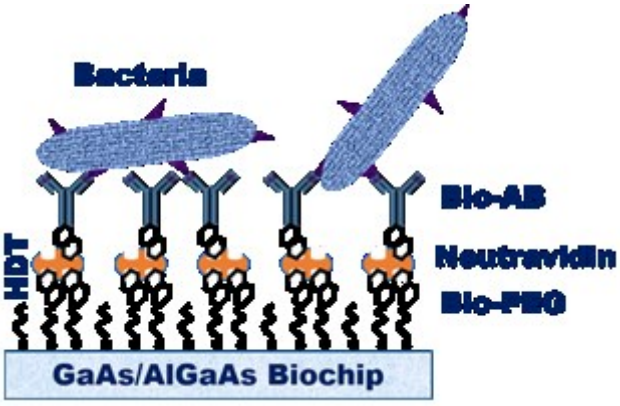

Figure 4-3. Schematic view of a GaAs/AlGaAs biochip functionalized with a Bio-PEG/HDT/Neutravidin/antibody architecture.

4.5. Temporal Evolution of PL Emission from Quantum Heterostructure

When a semiconductor surface is in contact with an electrolyte, the difference between the work function of these two materials will impose a transient charge transfer, until a thermodynamic equilibrium is reached. At equilibrium, the Fermi level in the semiconductor is aligned with the electrochemical potential (redox) level. The charge transfer process will lead to band bending at the interface of the semiconductor-electrolyte. The band bending is normally upward for n-type

semiconductor. The built-in electric field tends to separate the electron-hole pairs generated in the depletion region near the interface and this may cause a reduction of the PL signal [61, 62]. Moreover, absorption of ions on the surface of the semiconductor leads to the formation of a double layer and generation of some extrinsic surface states depending on the type of the electrolyte [153]. Now, at the GaAs/electrolyte interface, the semiconductor surface chemistry will be affected and GaAs could begin corroding.

4.6. Photocorrosion Concept

It is generally accepted that in case of III–IV semiconductors the holes are responsible for initiation and progression of the corrosion process, which for GaAs is described by the following reaction formula [154]:

$$GaAs + 2H_2O + 6h^+ \rightarrow Ga^{3+} + HAsO_2 + 3H^+ \qquad (4\text{-}1)$$

This process, normally inefficient in the dark, for n-type semiconductor can be photoactivated. In such a case, the built-in electric field will drive the photogenerated holes toward the semiconductor/electrolyte interface and the electrons in the opposite direction [64]. The excess density of holes will speed up the photocorrosion process. The dynamics of this process depends on the built-in potential (concentration of reduced ions) as well as the illumination level. It is therefore possible to regulate the rate of the electrolytic decomposition reaction by controlling these quantities [155]. This concept becomes more important when discussing photodecomposition of semiconductors in an electrolytic solution exposed to charged particles. If charged particles approach the semiconductor surface and change its band bending condition, this could affect the rate of semiconductor decomposition. The surface recombination velocity (SRV) and band bending are important factors influencing PL intensity of semiconductors. In general, surface recombination is nonradiative and band bending separates electron-hole pairs, both resulting in reduced PL intensity [55]. Marshall *et al.* argued that an interfacial dipole layer near the surface of GaAs upon chemisorption of thiols reduces SRV causing increased PL intensity [57]. Since PL of GaAs is strongly correlated with the presence of surface states, we can track PL variations as an indicator of SRV changes. **Figure 4-4** displays a schematic band structure diagram of a semiconductor/electrolyte interface for an n-type semiconductor. Miller and Richmond

experimentally demonstrated that the photocorrosion rate is higher for upward band bending in n-type GaAs than that observed under flat band condition [60].

To investigate the photocorrosion process, we studied optical spectroscopy of V0881 and J0150 samples at 20K. These results were compared with the photocorrosion of J0150 observed at 300K with the QSPB reader. A 12-h exposure to a train of 3 s pulses delivered every 60 s was employed to demonstrate the removal of the second GaAs layer (3 nm thick quantum well) of the J0150 nanostructure. We have estimated that the cap layer of J0150 functionalized with the antibody photocorroded at a rate of 0.25 ± 0.01 nm/min.

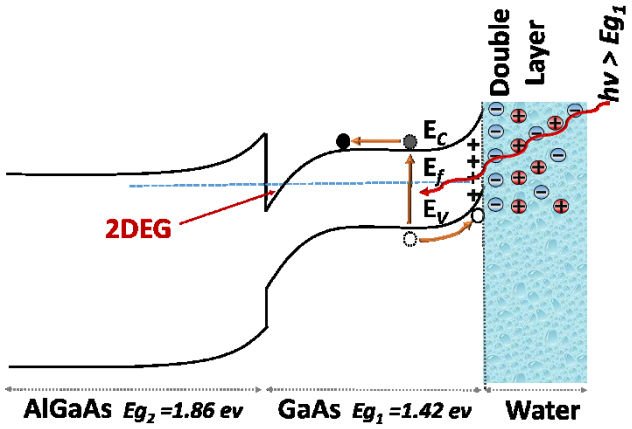

Figure 4-4. Schematic band structure diagram of illuminated semiconductor/ electrolyte interface, showing upward band bending and formation of an electric double layer.

4.7. Bacteria Immobilization

When bacteria are suspended in a PBS solution, the protonation and deprotonation of its surface groups results in charging of the bacteria surface. This surface charge affects the distribution of counter ions in the solution and attracts them around bacteria creating a double layer region over which the influence of surface charge is extended. At normal physiological *p*H between 5 and 7, the surfaces of almost all bacteria are negatively charged owing to the presence of proteins and other wall and cell membrane components containing phosphate, carboxyl, and other acidic groups [53]. The capture of bacteria could be achieved by functionalization of the semiconductor surface with specific antibody. Once molecular interactions between bacteria and antibody become dominant, the negative charge of bacteria repels the negative ions (responsible

for hole drag from semiconductor toward its surface) at the surface of n-type GaAs leading to reduced band bending and depletion region depth [156]. Hence, lower amount of holes are able to reach the surface and the rate of photocorrosion decreases. The effect of a decreasing photocorrosion rate of GaAs/AlGaAs heterostructures has been observed following the exposure of antibody functionalized chips to increasing concentrations of *E. coli* bacteria [30]. For detection of *L. pneumophila*, we first biofunctionalize GaAs/AlGaAs wafers with antibodies directed against this bacteria, as explained in Sec. 4.3. Next, we exposed a series of biofunctionalized chips to prearranged concentrations of bacteria and simultaneously collect PL data from the chips. The samples were irradiated with 3-s pulses (delivered in every 60-s period) of the 20 mW/cm^2 radiation of an LED operating at 660 nm wavelength.

4.8. Results and Discussion

4.8.1. PL Spectra and Temporal Behaviour

The 20 K-PL spectra of the functionalized samples are presented in **Figure 4-5**. The PL peak at 821 nm (band-to band transition) and an associated peak at 832 nm (donor–acceptor pair) both originate from photons emitted by the GaAs buffer layer [157]. The J0150 wafer exhibits similar PL peaks at 821 and 832 nm and an extra peak at 724 nm, which originates from photons emitted by the thin GaAs quantum well (QW). For sample J0150 immersed in 0.1X PBS, this PL feature vanishes after a 12 h exposure to 660 nm radiation at 20 mW/cm^2 (see **Figure 4-5 (b)**). Thus, the photocorrosion process must have removed at least 21 nm of the investigated GaAs/AlGaAs heterostructure.

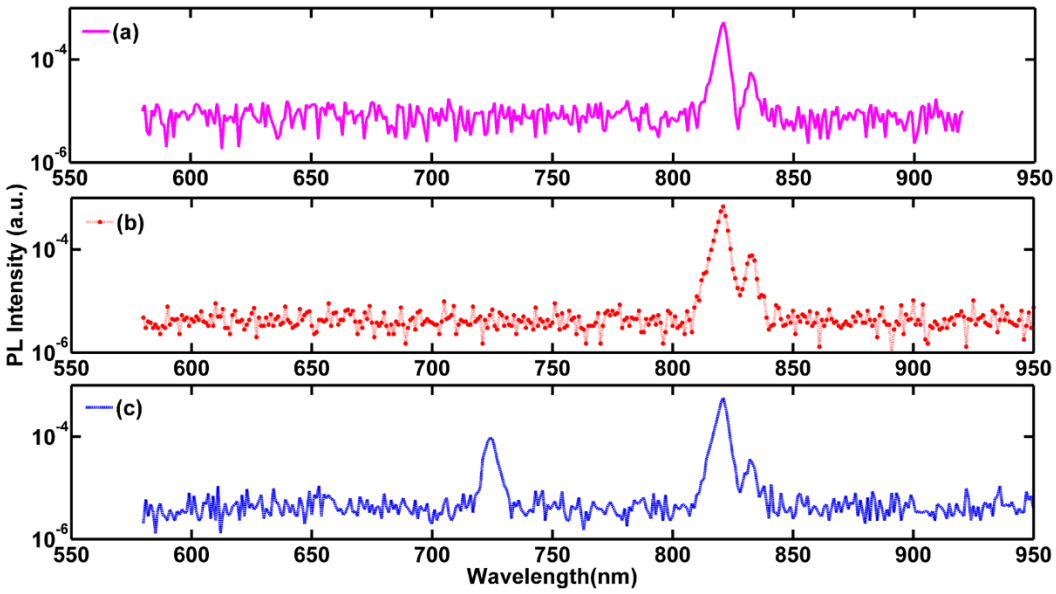

Figure 4-5. Low-temperature PL spectra of fresh V0881 (a), photocorroded J0150 (b) and fresh J0150 (c) wafers.

Figure 4-6 shows the time-dependent GaAs PL signal collected during the photocorrosion process of J0150 wafers at 300K. Two clearly distinguishable maxima are visible at $t = 31$ and $t = 229$min. The initial rise of the PL signal was attributed to the photoinduced formation of a Ga_2O_3 oxide layer on the GaAs surface exposed to water environment, often referred to as the photowashing effect [112, 158]. Offsey *et al.* [159] showed that photostimulated washing of n-GaAs and p-GaAs increased PL intensity of such samples as a result of the reduced surface state density. These investigations have also indicated that removal of As and As oxide leads to band flattening of GaAs and increased PL intensity. It has commonly been reported that oxidation of GaAs surfaces results in the formation of Ga_2O_3 (Refs. [159, 160]) that reduces nonradiative recombination centers on the surface of this material [161]. The passivation process of GaAs surfaces through formation of Ga_2O_3 has been studied by ab initio molecular-orbital calculations. Simulation results provide theoretical support that formation of Ga_2O_3 results in reduced density of surface states. It is argued that this is derived from the initial near bridge bonded O atoms and surface state energy gap moving outside of the bulk energy gap [162]. The Ga_2O_3 oxide, due to its thermodynamic instability in a water environment [99] is slowly dissolved leading to a decreasing PL signal as the GaAs cap layer is photocorroded away. A slow dissolution of this oxide and progressing photocorrosion of the GaAs cap material lead to the onset of PL signal decay as the

photocorroding front approaches the GaAs-AlGaAs interface. Thus, PL maxima observed from photocorroding GaAs/AlGaAs samples are markers indicating a transition from GaAs layer to AlGaAs layer. We attribute the formation of maxima observed at $t = 31$ and $t = 229$min in **Figure 4-6** to the dissolution of 8 and 3 nm thick layers of GaAs, respectively. The formation of a PL maximum in temporal plots of PL emission from GaAs/AlGaAs quantum-heterojunctions has previously been used for detection of *E. coli* K12 bacteria [30], and the dynamics of formation of such maxima in GaAs/AlGaAs QW has recently been investigated [163]. We note that Fink and Osgood used electrical current measurement to monitor corrosion of GaAs/AlGaAs multilayers, but the sensitivity of their technique was not sufficient to resolve layers thinner than approximately 1 μm [151].

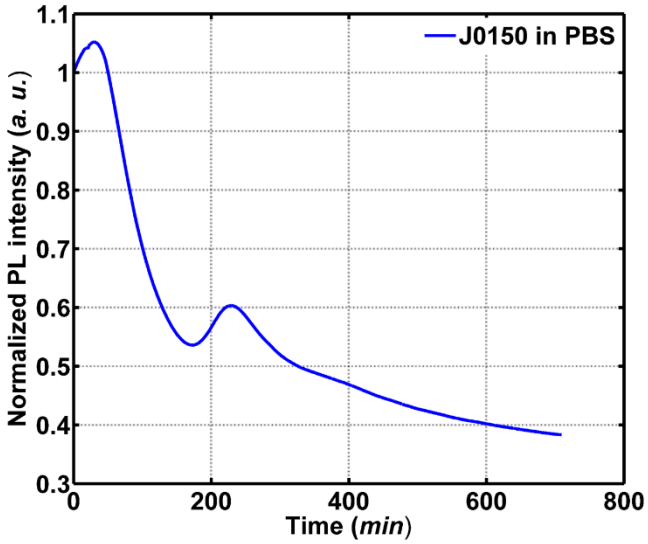

Figure 4-6. Temporal PL profile of J0150 photocorroding in 0.1X PBS.

4.8.2. Bacteria Detection

Figure 4-7 displays examples of time dependent PL plots collected for biofunctionalized chips exposed to 0.1X PBS and different concentrations of bacteria diluted in 0.1X PBS. The formation of a clear maximum is observed in each investigated case. It can be seen that the position of these maxima shifts from ~ 32 min for the sample exposed to 0.1X PBS (solid curve) to 42, 52, and 62 min for the samples exposed to solutions of *L. pneumophila* at 10^4, 10^5, and 10^6 bacteria/ml, respectively. The delay of the PL maximum with increasing concentration of bacteria is consistent with photocorrosion of the GaAs cap material and the role negatively charged bacteria play in the

semiconductor-electrolyte interaction. A specificity of the *L. pneumophila* binding architecture was examined by exposing it to a solution of *B. subtilis* at 10^6 bacteria/ml. As it can be seen in **Figure 4-7**, the associated PL plot (solid circles) exhibits the same position maximum as that observed for the sample exposed to 0.1X PBS (solid line). Note that the kink features observed in this figure near 25-30 min are related to a transition from the flow to stagnant and back to flow conditions in the flow cell.

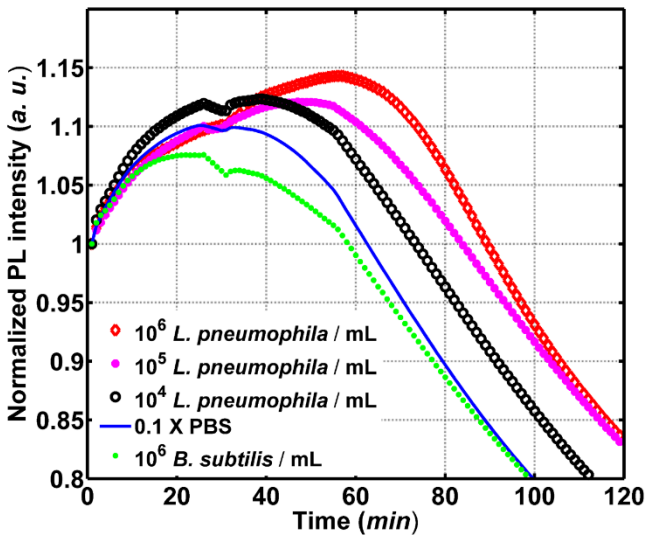

Figure 4-7. Temporal behavior of the PL signal from Bio-PEG/HDT/Neutravidin/antibody biofunctionalized chips (J0150) exposed at 0.1X PBS to different concentrations of *L. pneumophila* and *B. subtilis* at 10^6 CFU/ml.

It should be mentioned that we were not able to detect *L. pneumophila* in the 1X PBS environment that previously was employed for successful detection of *E. coli* [30]. In the case of *L. pneumophila*, the positions of the PL maxima on the PL versus time plots were undistinguishable from those of the biofunctionalized chips exposed to 1X PBS only for bacterial solutions of up to 10^6 bacteria/ml. It seems that this result is related to an excessive ionic strength of the 1X PBS medium and screening of bacteria charge from the semiconductor surface [68]. Consistent with this are our zeta potential measurements. While zeta potential of *E. coli* K12 in 0.1X PBS was found equal to - 53 mV, in agreement with literature data [164], we observed zeta

potential of - 24mV for *L. pneumophila* in the same PBS environment. This parameter is consistent with the weaker response of the investigated biochips to *L. pneumophila*.

Due to the complexity of the biofunctionalization procedure and a limited accuracy in the preparation of bacterial solutions, a temporal appearance of the PL maximum may vary among different experiments. By collecting a series of PL runs, repeated 3-4 times for each concentration of *L. pneumophila*, we were able to construct a calibration plot exhibiting PL maxima positions versus concentration of bacteria, as shown **Figure 4-8**. It can be seen that the error in determining the position of PL maxima does not exceed 5%. However, the sensitivity of the current biosensing architecture does not allow resolving PL maxima corresponding to biochips reacting with 0.1X PBS and a bacterial solution at 10^3 bacteria/ml. Given that GaAs/AlGaAs quantum heterostructures respond to the average density of the bacteria immobilized on their surface, it is the limited ability of the investigated antibody binding architecture that seems to be the main factor limiting the biochip sensitivity level.

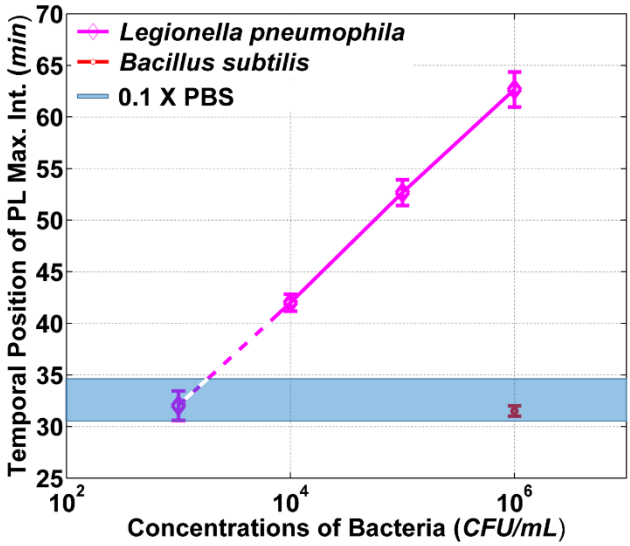

Figure 4-8. PL intensity maximum vs time for numerous repeated detection runs.

A systematic analysis of optical microscopic images, with area of 3720±7 μm^2, allowed to determine that the biochip surface coverage with *L. pneumophila*, following the immobilization procedure described in Sec. 4.3.2, was ~ 0.09, ~ 0.28, and ~ 0.45 per 100 μm^2 for the volume concentrations of 10^4, 10^5, and 10^6 bacteria/ml. In contrast, only few *B. subtilis* bacteria were captured by the biochips functionalized with *L. pneumophila* antibody, confirming specificity of

the applied bacteria binding architectures. **Figure 4-9** shows examples of optical microscopic images of the surface of biofunctionalized J0150 chips exposed to *L. pneumophila* and *B. subtilis* at 10^6 bacteria/ml. The elongated shape of *L. pneumophila* bacteria, typically of 2 μm in length and 0.3-0.9 μm in width are clearly observed in (**Figure 4-9 (a)**). This shape is consistent with images of *L. pneumophila* published in literature [165]. **Figure 4-9 (b)** shows a control result of weakly present rod shaped *B. subtilis* bacteria on the surface of a biochip designed for detection of *L. pneumophila*.

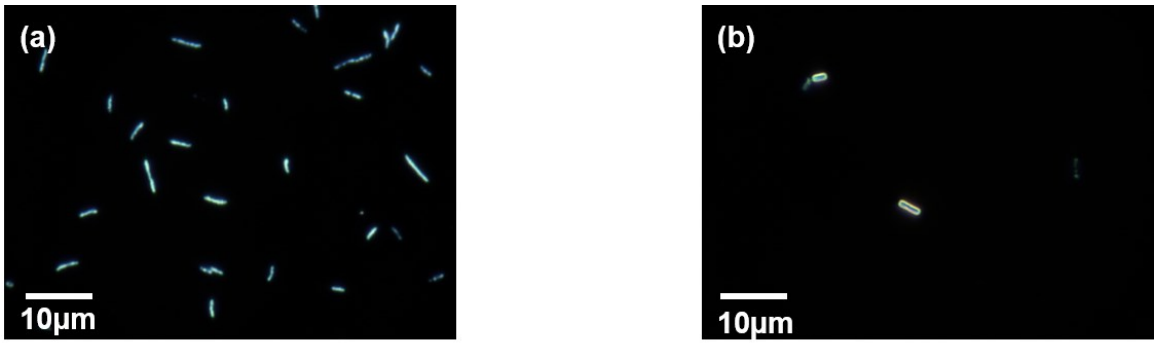

Figure 4-9. Optical microscopy of biofunctionalized chips exposed to 106 bacteria/ml of *L. pneumophila* (a) and *B. subtilis* bacteria (b).

Optical microscopy of biochips for different concentrations of *L. pneumophila* provides systematic information about the bacteria immobilization efficiency under varying conditions, as well as quantitative statistics required for further assessment and modeling of system performance. Given that optical microscopy images of surfaces shown in **Figure 4-9** were captured after three washings with DI-water, it is reasonable to assume that this procedure resulted in the removal of most unattached (physisorbed) bacteria [166]. Thus, it is reasonable to assume that *L. pneumophila* found on the surface of these biochips has been tethered by the strong bacteria-antibody interaction.

4.9. Conclusions

We have employed a photocorrosion-based method for detection of *L. pneumophila* bacteria in phosphate buffered saline solution. The approach is based on monitoring the photocorrosion of GaAs/AlGaAs heterostructures with photoluminescence originating from a

GaAs epitaxial layer buried under heterostructures. The slow rate of photocorrosion is achieved by exposing PBS surrounded chips to low-intensity radiation (~ 20 mW/cm^2) that also serves to excite the PL signal. To shed some light on the resolution of the investigated photocorrosion process, we studied low temperature PL spectroscopy of a GaAs/AlGaAs quantum heterostructure comprising a 3 nm thick GaAs QW located 18 nm below the surface, as well as a time dependent PL during photocorrosion of such a heterostructure. The appearance of two maxima in a time dependent PL plot could be linked to the dissolution of an 8 nm thick GaAs cap and a 3 nm thick GaAs QW, consistent with vanishing of the QW PL emission from a similar sample that underwent photocorrosion for 12 h. Given that the photocorrosion rate of GaAs depends on the concentration of holes appearing at its surface, the electrostatic interaction between the bacteria and the semiconductor could affect that rate and, consequently, change position of PL maxima observed on time dependent plots.

The photocorrosion-based detection of *L. pneumophila* in 0.1X PBS has been demonstrated between 10^4 and 10^6 bacteria/ml. The tenfold diluted PBS in comparison to 1X PBS we used recently for detection of *E. coli* K12 (Ref. [30]) was dictated by our inability to distinguish between the position of PL maxima of biochips photocorroding in 1X PBS (reference test) and different *L. pneumophila* bacterial solutions. This seems to be related to the reduced interaction with the semiconductor surface of *L. pneumophila* bacteria that are characterized by significantly weaker zeta potential than that of *E. coli* K12. Indeed, our measurements carried out for heat-killed *E. coli* K12 in 0.1X PBS indicated a zeta potential equal to - 53 mV in agreement with literature data, while a zeta potential of - 24mV was measured for heat-killed *L. pneumophila* in the same PBS environment. This property might explain the weaker sensitivity level of detecting *L. pneumophila* (10^4 bacteria/ml) in comparison to that of *E. coli* K12 (10^3 bacteria/ml) with the investigated biofunctionalized GaAs/AlGaAs quantum heterostructures. However, other parameters, such as binding affinity of the employed antibodies, could also influence the sensitivity level observed with current experiments. We note an excellent specificity achieved with the investigated *L. pneumophila* antibodies as only few *B. subtilis* bacteria were observed on the investigated biochips exposed to 10^6 bacteria/ml of those bacteria diluted in PBS.

4.10. Acknowledgments

This project was supported by the Canada Research Chair in Quantum Semiconductors Program, the CRIBIQ-MITACS-FRQNT Project on “Development of a miniaturized device for optical reading of the QS biosensor,” the NSERCCRD Project No CRDPJ 452455-13, and the NSERC-CREATE Training Program in Integrated Sensor. The financial support and participation of Magnus Chemicals, Ltd. (Boucherville, Québec) in addressing technical challenges of the project is greatly appreciated. The authors thank Khalid Moumanis, Gabriel Laliberté, and the technical staff of 3IT for providing technical assistance to the project, and CMC Microsystems (Kingston, Ontario) for subsidizing the manufacturing cost of some of the GaAs/AlGaAs epitaxial quantum heterostructures used in this work. The authors also thank Zbigniew Wasilewski of the University of Waterloo for providing some of the GaAs/AlGaAs microstructures used in our work, François Malouin of the Université de Sherbrooke for kindly supplying *Bacillus subtilis* bacteria, and Carmel Jolicoeur of the Université de Sherbrooke for allowing us to use their zeta potential measurement setup.

CHAPTER 5. Electrically Biased GaAs/AlGaAs Heterostructures for Enhanced Detection of Bacteria

5.1. AVANT-PROPOS

Auteurs et affiliation:

- Mohammad Reza Aziziyan : Étudiant au doctorat, Université de Sherbrooke, Faculté de génie, Département de génie électrique et informatique.
- Walid M. Hassen : Assistant de recherche, Université de Sherbrooke, Faculté de génie, Département de génie électrique et informatique.
- Jan J. Dubowski : Professeur titulaire, Université de Sherbrooke, Faculté de génie, Département de génie électrique et informatique.

Titre français : Hétérostructures GaAs/AlGaAs électriquement polarisées pour une détection améliorée des bactéries

Date d'acceptation : 25 mars 2016

État de l'acceptation : version finale publiée

Revue : Synthesis and Photonics of Nanoscale Materials XIII (Proceeding of SPIE)

Référence : M. R. Aziziyan, W. M. Hassen, and J. J. Dubowski, "Electrically biased GaAs/AlGaAs heterostructures for enhanced detection of bacteria," Synthesis and Photonics of Nanoscale Materials XIII, vol. 9737, pp. 97370E-97370E-6, 2016.

Contribution au document : Ce chapitre décrit la mise en œuvre d'une technique électrochimique destinée à améliorer l'adhésion des bactéries à la surface d'un biocapteur dans le but d'améliorer la limite de détection. On discute ici des conditions permettant de réduire l'effet de répulsion de surface et, éventuellement, de faciliter l'immobilisation bactérienne à la surface des semi-

conducteurs bio-fonctionnalisés. Le processus d'adhésion bactérienne est étendu sur la base de la théorie DLVO et de la structure d'énergie des bandes des semi-conducteurs dans un environnement électrolytique.

Résumé français : Nous avons examiné l'influence de la polarisation électrique sur l'immobilisation des bactéries à la surface des hétérostructures GaAs/AlGaAs, fonctionnalisées avec une architecture à base d'alkanethiols. Un mélange de polyéthylène glycol (PEG) thiol biotinylés et d'hexadécanethiol a été appliqué pour fixer la neutravidine et des anticorps ciblant une immobilisation spécifique de *Legionella pneumophila*. Une installation électrochimique a été conçue pour polariser des échantillons bio-fonctionnalisés avec l'électrode de référence potentielle par rapport à l'électrode d'argent/chlorure dans un système de configuration à trois électrodes. L'efficacité de l'immobilisation a été examinée avec la microscopie à fluorescence après marquage des bactéries capturées avec des anticorps marqués à la fluorescéine. Nous démontrons plus de 2 fois la capture de *Legionella pneumophila*, ce qui amène à penser que les biopuces électriquement polarisées pourraient accroître la sensibilité à la détection de ces bactéries.

Note : À la suite des corrections demandées par les membres du jury, le contenu de cet article diffère de celui qui a été accepté.

5.2. Abstract

We have examined the influence of electrical bias on immobilization of bacteria on the surface of GaAs/AlGaAs heterostructures, functionalized with an alkanethiol based architecture. A mixture of biotinylated polyethylene glycol (PEG) thiol and hexadecanethiol was applied to attach neutravidin and antibodies targeting specific immobilization of *Legionella pneumophila*. An electrochemical setup was designed to bias biofunctionalized samples with the potential measured versus silver/silver chloride reference electrode in a three-electrode configuration system. The immobilization efficiency has been examined with fluorescence microscopy after tagging captured bacteria with fluorescein labeled antibodies. We demonstrate more than 2 times enhanced capture of *Legionella pneumophila*, suggesting the potential of electrically biased biochips to deliver enhanced sensitivity in detecting these bacteria.

Keywords: Biosensing, Bacteria Detection, Band Engineering, Debye Length, GaAs/AlGaAs Heterostructure, Surface assembly monolayer (SAM), *Legionella pneumophila*

5.3. Introduction

Detection of bacteria with biosensors has been investigated as an attractive alternative to traditional methods of bacteria counting due to its potential for a cost effective, rapid and specific analyte recognition [43]. Rapid detection becomes critical especially when dealing with outbreaks of diseases characterized by high mortality rates induced by bacteria, such as *Legionella pneumophila* (*L. pneumophila*). This pathogen can be dispersed via aerosol of hot-water systems and cooling tower water [167]. Numerous biosensing systems have been investigated for rapid detection of bacteria based on a variety of transducer effects that determine their sensitivity [33]. Recently, a photoluminescence (PL) monitored photocorrosion of GaAs/AlGaAs biochips has emerged as an attractive approach for rapid detection of bacteria [25, 30, 104]. The PL effect can provide remarkable information due to the sensitivity to surface and interfaces located phenomena. Generally, optical excitation and photonic data collection does not impose complicated prearrangements, such as creation of high quality ohmic contact; hence, PL based study becomes convenient and useful specifically for studying with high resistivity materials [55]. It has been suggested that PL of epitaxial quantum dots provides a novel platform for optical biosensing

capable of rapidly detecting pathogens captured on the surfaces of III–V semiconductors [168]. Moreover, PL of GaAs/AlGaAs nano heterostructures has been used for detection of *Escherichia coli* and *L. pneumophila* suspended in phosphate buffered saline solutions [25, 30, 104]. Thus, photonics of nanoscale materials such as semiconductor quantum heterostructures and quantum dots has become an attractive tool for biosensing.

A primary step of bacteria detection with biosensor systems is an efficient immobilization of the bacteria on the transducer part. Most of bacteria are negatively charged under normal physiological conditions and at *p*H around 5 to 7 [53]. Furthermore, formation of a semiconductor/electrolyte interface is associated with redistribution of ions and, at equilibrium, semiconductor energy bands bend upward in an n-type semiconductor creating a negatively charged surface [104]. Thus, before immobilization with an antibody (Ab) through intermolecular interactions, bacteria experience an electrostatic interaction that plays an important role in their adhesion to the biosensor surface, or in the interaction with an Ab functionalized surface. A reasonable model of bacteria interaction with the surface could be provided using colloidal particles described by the DLVO (Derjaguin, Landau, Vervey, Overbeek) theory [72] that, in its simplest form, considers only van der Waals attraction and double layer repulsion forces to give a picture of how colloidal particles and surface interact electrostatically [169]. By theoretical plot of these two forces, Yuehuei *et al.* [71] explained how a double layer repulsion limits the particles that undergo Brownian thermal fluctuation from reaching the surface. The repulsion between a charged surface and bacteria could be decreased by increasing the ionic strength of the solution [73], however, this could limit the performance of biosensing systems based on the electrostatic interaction due to reduction of the Debye length [68].

Band bending of semiconductors and its consequences on electronic state of surfaces and interfaces has been extensively discussed in literature, indicating that tuning of this parameter could lead to formation of an electrostatic interaction facilitating bacteria immobilization [61, 156]. In view of this, one can create conditions where less negative surface of electrically biased GaAs could attract a greater number of bacteria. However, selection of a bias potential for a GaAs/AlGaAs biochip plays an important role since at high anodic potentials, and transport of electrons to the GaAs valence band results in decomposition of this material, while at high cathodic potentials hydrogen evolution could occur [170].

In this paper we report on the role of electrical bias of GaAs/AlGaAs biochips, biofunctionalized against *L. pneumophila,* in achieving an enhanced immobilization of this pathogen. An electrochemical analyser was used for precisely applying electrical bias and, concurrently, voltage was monitored using an Ag/AgCl reference electrode, which provided a well-defined and stable potential.

5.4. Materials, Preparation and Characterization Details

5.4.1. Materials

Samples used in this experiment were GaAs/AlGaAs nano-heterostructures (Wafer J0152) consisting of undoped epitaxial layers of GaAs and $Al_{0.35}Ga_{0.65}As$ grown on a semi-insulating GaAs (001) substrate. **Figure 5-1** presents details of this multilayer structure along with its energy band diagram. We note that similar nano-heterostructures were used for detection of bacteria in phosphate buffered saline (PBS) solutions [30, 104]. The chemical reagents were obtained as follow: biotinylated polyethylene glycol (Bio-PEG) from Prochimia Surfaces (Gdansk, Poland), hexadecanethiol (HDT) from Sigma-Aldrich (Ontario, Canada), neutravidin from Molecular Probes (Invitrogen, Burlington, Canada), polyclonal biotinylated and fluorescein isothiocyanate (FITC) conjugated antibodies against *L. pneumophila* from ViroStat, Inc. (Portland, Maine), PBS 10X, *p*H 7.4 from Sigma (Oakville, Canada), OptiClear from National Diagnostics (Mississauga, Canada), acetone from ACP (Montréal, Canada), isopropyl alcohol (IPA) from Fisher Scientific (Ottawa, Canada), ammonium hydroxide 28% (NH_4OH) from Anachemia (Richmond, Canada). Deionised (DI) water, 18.2 MΩ, was produced with a Millipore purification system built by Culligan (Quebec, Canada). The *L. pneumophila* ssp1 samples were provided by Magnus Chemicals Ltd. (Boucherville, Canada). For the reported here experiments, we worked with UV light killed bacteria. Throughout the text, we use term “bacteria/mL” for UV-treated bacteria.

Description	Material	X	T [nm]
GaAs (Cap layer)	GaAs		8
Barrier	$Al_xGa_{1-x}As$	0.35	10
Well	GaAs		3
Barrier	$Al_xGa_{1-x}As$	0.35	100
GaAs (Emitter)	GaAs		500

(a)

(b)

Figure 5-1. Details of J0152 GaAs/AlGaAs nano-heterostructure (a), and corresponding energy band diagram (b)

5.4.2. Functionalization Process of Biochips

We used 2 mm × 2 mm chips diced from a GaAs/AlGaAs wafer. The backside of the chips was coated with gold before the biofunctionalization step. Details on creating Au contact at the backside of chips can be found elsewhere [104]. Gold coated chips were all degreased sequentially in ultrasonic bath of OptiClear, acetone and IPA for 5 min each, then dried with flow of nitrogen and immersed in ammonium hydroxide (28%) for 2-min, in order to remove their native oxide layer. Next, they were immersed in deoxygenized anhydrous ethanol and immediately transferred to solution of thiol (0.15 mM Bio-PEG and 1.85 mM HDT diluted in deoxygenized anhydrous ethanol) and kept there around 20 hours. Then, biochips were rinsed with anhydrous ethanol and 1XPBS then post processed with neutravidin (0.2 mg/mL in 1XPBS for 1h) and then, after rinsing with 1XPBS, incubated for 1 h in a solution of Ab against *L. pneumophila* (0.1 mg/mL in 1XPBS). At this stage, the biochips were rinsed with 1XPBS and transferred to microfluidic setup for bacteria immobilization tests. At the end of bacteria incubation process, biochips were exposed for 1 h to FITC conjugated antibodies (50µg/ml in 1XPBS) to survey presence of bacteria via fluorescence microscopy. As illustrated in **Figure 5-2**, *L. pneumophila* will be sandwiched between two antibodies.

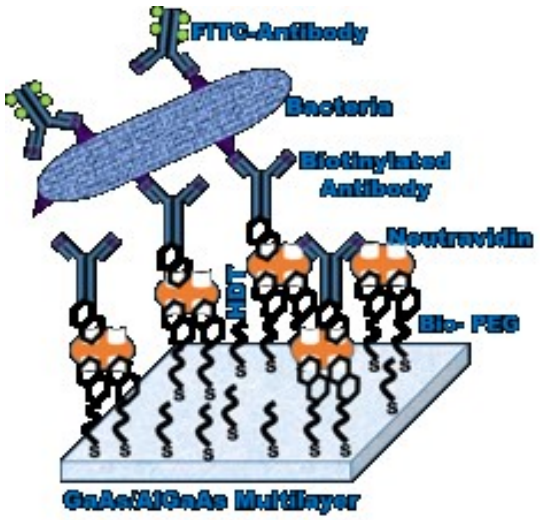

Figure 5-2. Bioarchitecture of Bio-PEG/HDT/Neutravidin/Antibody for immobilization of *L. pneumophila*. After trapping the bacteria, they are stained with FITC conjugated antibodies for fluorescence microscopic identification.

The influence of electric bias on GaAs biochips was studied for biochips biased at E= -0.2, 0 and 0.2 volts and exposed for 30 min to a solution containing *L. pneumophila* with concentration at 10^5 bacteria/mL. For the applied bias voltages, the current-voltage characteristics of GaAs/AlGaAs heterostructures suggests that anodic dissolution or hydrogen evolution reactions of this material play a negligible role [151].

5.4.3. Immobilization Experiments with Biased Biochips

After the Ab coated biochips were rinsed with 1XPBS, they were placed inside a flow cell, which allowed for exposure to different environments facilitated with a peristaltic pump. **Figure 5-3** displays a schematic view of the flow cell setup. After biasing a biochip, we injected *L. pneumophila* suspended in 1XPBS at, 10^5 bacteria/mL and incubated for 30 min under a continuous flow of a bacterial solution at 0.04 mL/min. Next, the biochip was removed from the flow cell and rinsed with DI water to wash salts and physisorbed bacteria from surface of GaAs. Bacteria immobilized on the surface of biofunctionalized GaAs were stained with FITC conjugated antibodies, and characterized by a fluorescence inverted microscope (Olympus, IX71). The light source emits between 450 and 490 nm (blue light) and images were observed at 515 nm using a DP71 digital camera [171]. For characterization of electrically biased biochips, we used an electrochemical analyser (CH Instruments, CHI604C) and in all tests, the working electrode was

GaAs with an Au contact, counter electrode was also Au, while the reference electrode was Ag/AgCl.

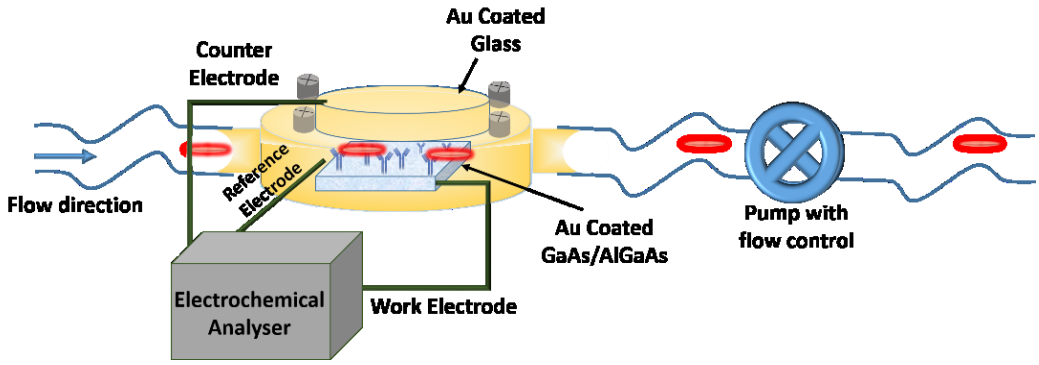

Figure 5-3. Schematic view of employed microfluidic setup connected to pump and electrochemical analyser.

5.5. Experimental Results and Discussions

Figure 5-4 shows fluorescence microscopy image of a GaAs surface after FITC tagging and systematic analysis of bacteria immobilization. The florescence image is obtained by 3 seconds exposure time. FITC dyes are clearly observed on the surface of GaAs, representing the *L. pneumophila*. We systematically assessed the number of FITC dyes and compared obtained numbers to verify influence of each bias point on the trapping process. As shown by **Figure 5-4** (b), for sample biased at 0.2 V we could increase the surface coverage more than 2 times relative to sample biased at 0 V. Conversely, we degraded bacteria immobilization efficiency for sample biased at -0.2 V. The anodic potential actually increased the band bending of the GaAs/AlGaAs heterostructure at its interface with the electrolyte; hence, it depletes more charge carriers from space charge and creates a more positive depletion region. While the variation of the Helmholtz layer, responsible for double layer repulsion, is small compared to variations of the space charge region due to applied bias [170], presumably, anodic bias provides more attraction force for deflection of negatively charged bacteria towards the GaAs surface. We also carried out a control test by exposing a biofunctionalized biochip directly to FITC conjugated antibodies (no bacteria were immobilized initially). As shown by the inset of **Figure 5-4 (a)**, there was no noticeable unspecific binding of FITC conjugated antibodies to the surface of that biochip.

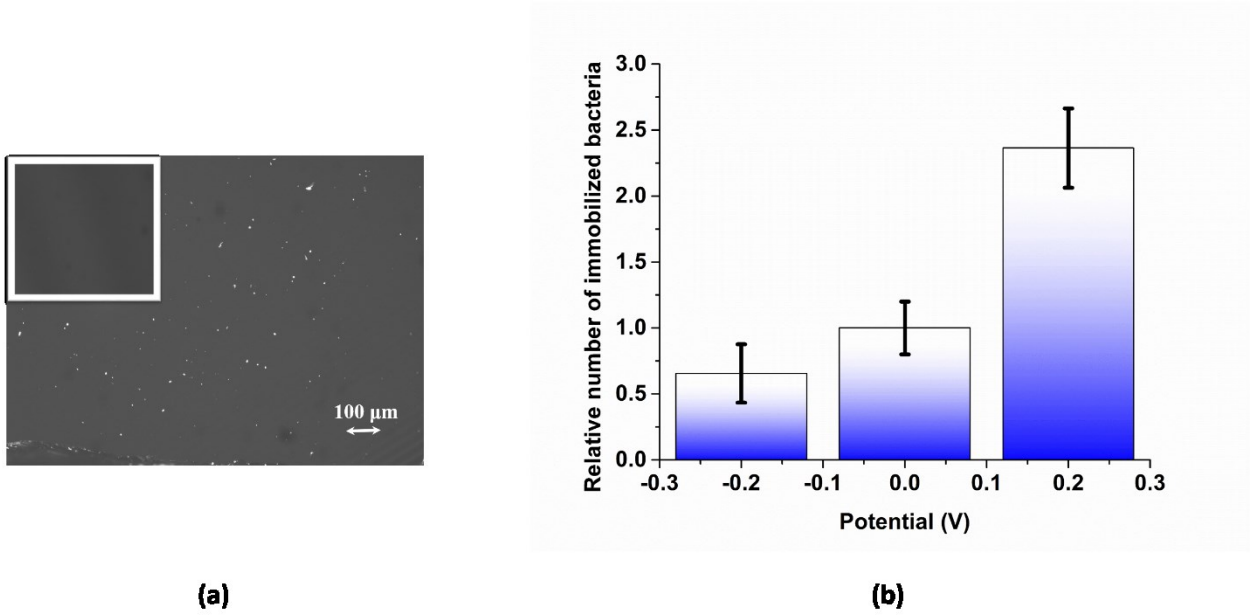

Figure 5-4. Fluorescence microscopic image showing the presence of *L. pneumophila* on the surface of Ab functionalized biochip exposed to 10^5 bacteria/mL in comparison to a control sample exposed to FITC conjugated Ab only, as shown by the inset (a), relative number of bacteria captured at different electrical bias conditions normalized to bacteria counted for an unbiased (E = 0 V) sample (b)

5.6. Conclusion

We studied the impact of an electrical bias on immobilization of *L. pneumophila* on the surface of biofunctionalized GaAs/AlGaAs nano-heterostructures. We used bio-PEG/HDT/Neutravidin/Antibody architectures to specifically capture *L. pneumophila*. Electrical bias was realized in an electrochemical cell with a 3-electrode configuration employing Ag/AgCl as a reference electrode. The presence of immobilized bacteria was studied by employing FITC conjugated antibodies and fluoresce microscopy technique. We demonstrate that electrical control of band bending could be applied to moderate bacteria-semiconductor interaction. Under increased band bending conditions achieved with E = 0.2 V, the repulsion semiconductor-bacteria could be reduced, leading to a 2X increased surface concentration of the negatively charged *L. pneumophila*. Given that the limit of detection with GaAs/AlGaAs nano-heterostructure biochips is determined by the critical number of bacteria immobilized on the biochip surface, our

investigations suggest that an enhanced sensitivity of detection could be achieved by electrical biasing of the biochip.

5.7. Acknowledgments

This project was financially supported by the Canada Research Chair in Quantum Semiconductors Program, the CRIBIQ-MITACS-FRQNT project on “Development of a miniaturized device for optical reading of the QS biosensor”, the NSERC-CRD project CRDPJ 452455 - 13 and the NSERC-CREATE Training Program in Integrated Sensor systems. Technical support provided by the staff of 3IT and the help of Dr. Khalid Moumanis are greatly appreciated.

CHAPTER 6. Sodium Dodecyl Sulfate Decorated *Legionella pneumophila* for Enhanced Detection with a GaAs/AlGaAs Nanoheterostructure Biosensor

6.1. AVANT-PROPOS

Auteurs et affiliation:

- Mohammad Reza Aziziyan : Étudiant au doctorat, Université de Sherbrooke, Faculté de génie, Département de génie électrique et informatique.
- Walid M. Hassen : Assistant de recherche, Université de Sherbrooke, Faculté de génie, Département de génie électrique et informatique.
- Hemant Sharma : Stagiaire postdoctoral, Université de Sherbrooke, Faculté de génie, Département de génie électrique et informatique.
- Ehsan Shirzaei Sani : Étudiant au doctorat, Université de Californie - Los Angeles (UCLA), Faculté de génie, Département de génie chimique et biomoléculaire.
- Nasim Annabi : Professeur assistant, Université de Californie - Los Angeles (UCLA), Faculté de génie, Département de génie chimique et biomoléculaire.
- Eric H. Frost : Professeur titulaire, Université de Sherbrooke, Faculté de médecine et des sciences de la santé, Département de microbiologie et d'infectiologie.
- Jan J. Dubowski : Professeur titulaire, Université de Sherbrooke, Faculté de génie, Département de génie électrique et informatique.

Titre français : *Legionella pneumophila* Décoré par Dodécylsulfate de Sodium pour une Détection Améliorée avec un Biocapteur de Nanohétérostructure GaAs/AlGaAs

Date de soumission : Janvier 2018

Revue : Biosensors and Bioelectronics

Contribution au document : Ce chapitre décrit une nouvelle technique permettant d'améliorer la limite de détection des biocapteurs à base de photocorrosion en modifiant la charge électrique

bactérienne. Il a été démontré que la charge électrique de surface des bactéries pourrait être modifiée de manière à ce que la charge bactérienne négative augmente, entraînant l'amélioration de limite de détection. La conjugaison de molécules synthétiques portant de multiples charges négatives à la surface des bactéries est élaborée et les mécanismes d'interaction des bactéries avec la surface du biocapteur et d'autres aspects critiques de la décoration des bactéries sont discutés.

Résumé français : La charge électrique nette associée à une souche bactérienne est principalement définie par le nombre de groupes fonctionnels disponibles à sa surface et peut déterminer la limite de détection des biocapteurs à charge. Nous avons étudié la dynamique des variations des charges électriques bactériennes par la liaison de molécules synthétiques chargées négativement, telles que l'acide aspartique, la sérum-albumine bovine (BSA) et le dodécylsulfate de sodium (SDS), dans le but d'améliorer la LOD des biocapteurs plates-formes, en particulier pour la détection de *L. pneumophila*. Les mesures du potentiel zêta ont confirmé un accroissement substantiel du potentiel zêta bactérien négatif jusqu'à ~ 2 fois dans une solution salée tamponnée au phosphate (PBS), à pH 7,4, en utilisant du SDS, tandis que l'acide aspartique et le BSA présentaient des résultats prometteurs. Une détection améliorée de *L. pneumophila* inactivée par la chaleur à des concentrations de 10^3 UFC/ml en utilisant la photocorrosion des nanohétérostructures de GaAs/AlGaAs a également été observée avec le SDS. Nous discutons des mécanismes d'interaction des bactéries avec ces fractions organiques et des aspects critiques des décorations des bactéries.

Note : Après la publication, le contenu de ce chapitre peut différer de celui publié.

6.2. Abstract:

The net electric charge associated with a bacteria strain is primarily defined by the number of available functional groups at its surface and we observed that it can determine the limit of detection of a quantum semiconductor biosensor. We have investigated the dynamic range of bacterial electric charge variations through binding negatively charged sodium dodecyl sulphate (SDS) molecules, with the objective of improving the detection limit of a charge-sensing platform, particularly for detection of *Legionella pneumophila* using digital photocorrosion of GaAs/AlGaAs nanoheterostructures. Zeta potential measurements confirmed up to ~ 2-fold increment of bacterial negative zeta potential in phosphate buffered saline solution at *p*H 7.4. By applying Gouy-Chapman model on spectrophotometric data, it was estimated that 2-fold increment of zeta potential for *L. pneumophila*, at SDS concentration of 0.02 mg/mL, corresponded to adding $\sim 1.2 \times 10^5$ *e* to each bacterium, indicating that each SDS molecule contributed in supplying 0.0035 *e*. Subsequently, it was possible to detect SDS decorated and heat-inactivated *L. pneumophila* at 10^3 CFU/mL. This further advocated the fundamental role of bacterial electric charge in altering the photoetching rate of III-V semiconductor biochips. We discuss mechanisms of bacterial interaction with SDS, critical aspects of decorating bacteria with this anionic surfactant and the channels responsible for enhanced detection.

Keywords: Electric-charge biosensor, Bacterial zeta-potential, *Legionella pneumophila*, Sodium dodecyl sulfate, Photoluminescence, Digital photocorrosion, GaAs/AlGaAs nanoheterostructures, Quantum semiconductor

6.3. Introduction

Outbreaks of *Legionella* from contaminated water sources, resulting in mortality and morbidity, have been recorded periodically in numerous countries. Inhalation of *Legionella*-contaminated aerosols causes Legionnaires' disease and Pontiac fever. Among the about 60 known-species of *Legionella*, *L. pneumophila* ssp1 have been identified as the most common cause of severe pneumonia, or Legionnaires' disease [7, 143, 172]. Since conventional bacteria detection techniques were not effective in preventing *Legionella* speared, numerous biosensing platforms

have been investigated and proposed with the aim of providing prospective identification of *L. pneumophila* [173]. Sensors addressing detection of electrically charged molecules represent a significant portion of the biosensing filed. For instance, electrochemical impedance spectroscopy [174] and field effect transistor [175] immunosensors have been investigated for detection of electrically charged biomolecules. In photonic materials, such as III-V semiconductors, adsorption of electrically charged biomolecules at the surface of a semiconductor in an electrolytic environment can induce perturbation of the near-surface band structure [61, 156, 176], which could be monitored with the photoluminescence (PL) effect.

The photonic characteristics of GaAs/AlGaAs nanoheterostructures has provided a compelling platform for detection of electrically charged bacteria [25, 30, 104]. This technique relies on the PL-monitored photo-dissolution of III-V semiconductors through, so-called, digital photocorrosion (DIP) in electrolytic environments at rates that could be controlled with a nanoscale precision [108]. The perturbation of GaAs-electrolyte and AlGaAs-electrolyte interfaces by the negatively charged bacteria resulted in reduced photocorrosion rates, which allowed detection of *Escherichia coli* K12 at 10^3 CFU/mL [30] and heat-inactivated *L. pneumophila* at 10^4 CFU/mL [104]. Though, the mechanism of interaction of bacteria with the semiconductor biosensor is not clear yet.

The limit of detection (LOD) is one of the most important parameters for biosensing devices, thus numerous techniques, e.g. charged self-assembled monolayers [177], electrophoresis [106], chemotaxis [178], three-dimensional polymer brushes [179] or centrifugation [180] were examined to enhance this aspect. Most bacteria are known to be negatively charged under physiological *p*H conditions [53] and the amplitude of bacterial zeta potential could reflect LODs achievable with a charge sensing device. Previously, we reported that heat-inactivated *L. pneumophila*, extracted from industrial water, carried a smaller negative charge compared to that of *E.coli* K12 [104], which was considered as one of the reasons of the inferior LOD for *L. pneumophila*. Then, conjugation of synthetic molecules that carry multiple negative charges to the surface of bacteria seems a viable approach for enhancing performance of electric charge transducers. Whereas many studies have focused on modifying bacterial membrane properties to improve bio-production or drug delivery [181, 182], amplifying bacterial negative charge with the purpose of achieving enhanced LOD has not been addressed. We note that, recently, anionic

surfactants have been used for amplifying signal of electrochemical field effect transistors detecting buckwheat allergenic proteins [183].

In this study, we investigated decoration of *Legionella pneumophila* with sodium dodecyl sulfate (SDS) in order to increase bacterial negative charge and eventually enhance the LOD of GaAs/AlGaAs biosensors. We utilized zeta potential measurements to assess the charge modification of the decorated bacteria and studied the effect of SDS on bacterial immobilization with the employed bio-architecture. Here, we report detection of SDS decorated *L. pneumophila* (heat-inactivated) with an enhanced LOD reaching 10^3 CFU/mL based on *in situ*-monitored DIP of GaAs/AlGaAs nanoheterostructures.

6.4. Materials and Chemicals

Semi-insulating undoped GaAs (001) wafer (AXTG108, AXT Inc., USA) and molecular beam epitaxy fabricated GaAs/$Al_{0.35}Ga_{0.65}As$ nanoheterostructures (CPFC, National Research Council of Canada, Ottawa) were utilized. Details of III-V nanoheterostructure can be found in Supplementary Information (SI) section.

The following chemical/biological compounds were used in our experiments: OptiClear (National Diagnostics, Mississauga, Canada), acetone (ACP, Montréal, Canada), isopropyl alcohol (Fisher Scientific, Ottawa, Canada), ammonium hydroxide 28% (Anachemia, Richmond, Canada), anhydrous ethanol (Commercial Alcohols Inc., Brampton, Canada), biotinylated polyethylene glycol (Prochimia Surfaces, Gdansk, Poland), hexadecanethiol (Sigma-Aldrich, ON, Canada), neutravidin (Molecular Probes, Burlington, Canada), polyclonal biotinylated antibody and Fluorescein isothiocyanate (FITC) antibody against *L. pneumophila* and *E.coli* (ViroStat, Portland, Maine), aspartic acid, 1-Ethyl-3-(3-dimethylaminopropyl)carbodiimide (EDC), N-Hydroxysuccinimide (NHS), SDS, Dimethylformamide (DMF), Stains-All (all from Sigma-Aldrich, ON, Canada), FITC (Sigma-Aldrich, MO, USA), BSA, Dimethyl sulfoxide (DMSO) and bicarbonate buffer (all from Thermo Fisher Scientific, USA). In all experiments, we used deionized (DI) water with resistivity of 18.2 MΩ.

E. coli ATCC 25922 (*E. coliA)* and *S. aureus* ATCC 43300 were cultured overnight in Tryptic Soy Broth medium. *E. coli* K12 *(E. coliK)* was grown overnight in Luria-Bertani nutrient

broths and colonies of *L. pneumophila* ssp1 were cultured on L-cysteine BCYE agar medium. All bacteria were suspended in 1X phosphate-buffered saline (PBS) solution at a concentration of 10^9 CFU/mL. To inactivate bacteria, *E. coliK* and *L. pneumophila* were either exposed to UV light (λ = 250-260 nm, P = 100 mW/cm^2) or were heat-treated (90 °C, for 20 min). In either case, the efficiency of inactivation was verified by culture method (data not shown here).

6.5. Experimental methods

6.5.1. Decorating Bacteria with SDS

Bacterial samples were exposed to various concentrations of SDS (0.001 mg/mL to 0.02 mg/mL in PBS), while reference bacterial samples were kept in PBS, all for 30 min in a thermomixer (at 37 °C and 175 rpm). The rinsing procedure to remove excess reactants from bacterial solutions consisted of two steps. First, centrifugation at 3000 rpm for 25 min, removal of the supernatant and resuspension of the pelleted bacteria in 1 mL of PBS, followed by a second centrifugation at 3000 for 15 min and resuspension in 1 mL PBS.

6.5.2. Zeta Potential Measurements

Zeta potential of bacteria was measured with a Zetasizer Nano system (Malvern Instruments) and analyzed using the Helmholtz-Smoluchowski equation [53]. Measurements were carried out in folded capillary cells (DTS 1064) using 1 mL of bacterial suspension at 10^6 CFU/mL, with a 180-second delay before each run.

6.5.3. Spectrophotometric measurements

An optimized method developed by Rupprecht et al was adopted [184]. The absorbance was determined using a UV-1800 UV-Vis Spectrophotometer (SHIMADZU) at λ = 453 nm. Measurements were carried out with a mixture of 25% Stains-All solution (storing solution at 2 mg/mL in DMF and then diluted 20 times in 1 X PBS) and 75% SDS solution in 1X PBS (v/v). A solution of 1X PBS was used to determine the zero optical density (reference). A 10^9 CFU/mL suspension of heat-inactivated *L. pneumophila* in 1X PBS was exposed to 0.02 mg/mL of SDS for 30 min and then bacteria were filtrated using a PVDF membrane 0.22 μm filter (Millex-GV, Millipore, Canada).

6.5.4. Fourier transform infrared spectroscopy (FTIR)

E. coliA at a concentration of 10^9 CFU/mL was exposed for 30 min to 0.02 mg/mL of SDS in 1X PBS, and rinsed twice with 1X PBS. FTIR data of liquid samples were collected with a Perkin-Elmer Spectrum 100, using standard PTFE membranes cards. A solution of 1X PBS was used to determine the baseline. Measurements were conducted with a 1 cm^{-1} resolution.

6.5.5. Bio-functionalization and PL based detection

Bulk GaAs biochips were used for enumerating captured bacteria and GaAs/$Al_{0.35}Ga_{0.65}As$ nanoheterostructures were used PL based detection tests. Surfaces of 2 mm by 2 mm biochips were thiolated with a mixture of 0.15 mM biotinylated polyethylene glycol thiol and 1.85 mM hexadecanethiol in anhydrous ethanol, which had been deoxygenated with ultra-high purity nitrogen (5.0 UHP) prior to the thiolation process. The thiolated biochips were exposed for 2 h to 0.2 mg/mL neutravidin, and for 1 h to 0.1 mg/mL polyclonal biotinylated antibody against *L. pneumophila* or *E. coli*. Detailed procedures of biochip preparation can be found in reference [104]. PL data was recorded *in situ* using a quantum semiconductor photonic biosensor (QSPB) reader [104] designed for collecting PL maps of semiconductor samples under weak excitation conditions [30, 139, 185]. The QSPB reader employed in this work used a 660 nm light emitting diode (LED) for the intermittent excitation of GaAs/AlGaAs biochips (3-s in every 60-s period) at P = 25 mW/cm^2.

6.5.6. Fluorescence Microscopy

An Olympus IX71 fluorescence microscope was used to collect images of bio-functionalized GaAs biochips exposed to *L. pneumophila* or *E. coli* (30-min incubation). Surface of biochips, coated with bacteria, were rinsed with 1X PBS and exposed in the dark to 0.05 mg/mL of FITC-antibody against *L. pneumophila* or *E. coli* for 1 h. Next, the samples were rinsed with DI water and dried with a gentle flow of high-purity nitrogen (4.8 HP).

6.6. Results and Discussion

Figure 6-1 shows the zeta potential measurement results for *L. pneumophila* and *E. coliK* in 1X and 0.1X PBS (*p*H 7.4). In 1X PBS, *E. coliK* had a negative zeta potential of around -30

mV, which increased to about -50 mV in 0.1X PBS. The zeta potential values for *L. pneumophila* were close to -10 and -20 mV in 1X and 0.1X PBS, respectively. It can be seen that zeta potentials of UV- and heat-inactivated *E. coliK* were in the same range as that of live bacteria. Due to safety precautions, we were unable to measure zeta potential of live *L. pneumophila*, however considering *E. coliK* results, it seems reasonable to assume that the zeta potential of live *L. pneumophila* would be very close to that of UV- or heat-inactivated bacteria. Notice that Halder *et al.* observed a reduction of zeta potential in 0.5 mM potassium phosphate buffered solution (*p*H 7.4) for heat treated (100 °C for 10 min) *E.coli* (MTCC 2939) versus live bacteria, whereas a 10-min heat exposure at 100 °C had no significant impact on the zeta potential of *S. aureus* (MTCC 96), which was attributed to the thicker peptidoglycan layer of Gram-positive bacteria [186]. Since in the present study bacteria were heat-inactivated at only 90 °C, this might explain why a zeta potential difference between live and dead *E. coli* was not observed.

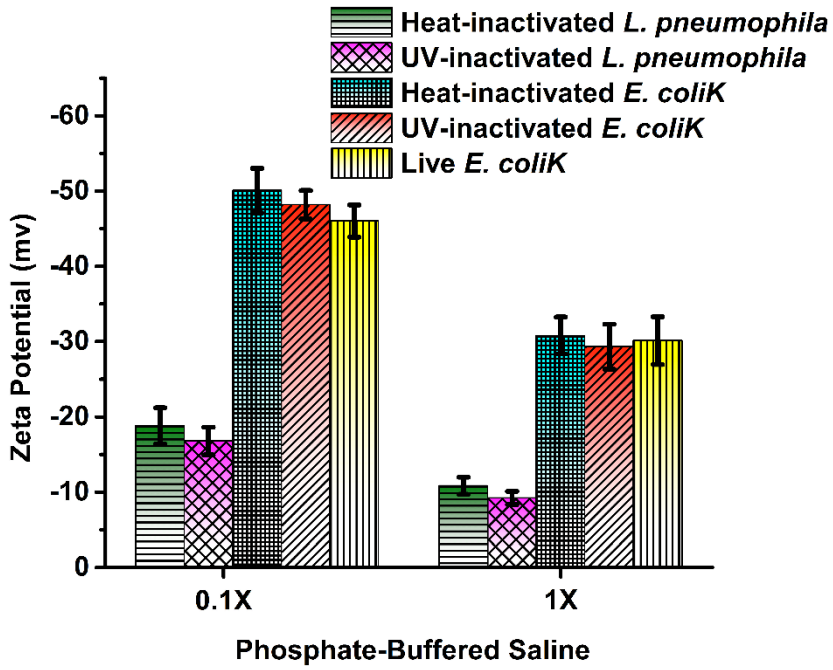

Figure 6-1. Zeta potential of *L. pneumophila* and *E. coliK* in two different concentrations of PBS.

As it can be seen in **Figure 6-1**, both bacteria exhibited higher negative zeta potentials in 0.1X PBS. This feature, potentially important for the performance of an electric charge biosensor, could be explained by the dependence of bacterial cell surface electric charge on the ionic strength

of the surrounding solution [53]. Zeta potential of bacteria increases in the solution of a reduced ionic strength, however further reduction of the ionic strength strongly diminishes the buffering capacity of PBS [187] and undermines its *p*H stabilizing performance. It was reported that *p*H condition can directly affect photocorrosion of GaAs/AlGaAs nanoheterostructures [105]. Thus, it more desirable to increase the negative charge of bacteria, without further reducing ionic strength of PBS (less than 0.1X), by decorating them with materials and molecules providing an excessive negative charge.

Figure 6-2 displays zeta potential measurements for *L. pneumophila* (heat-inactivated), *E. coliA*, and *S. aureus*, all decorated with SDS molecules after premixing the bacteria with SDS solutions at concentrations ranging from 0.001 mg/mL to 0.02 mg/mL. It has been reported that SDS at a concentration of 0.05% resulted in destruction of the bacterial membrane accompanied by a displacement of the nuclear material [188]. To avoid this problem and maintain the integrity of a bacterium cell membrane, the maximum concertation of 0.02 mg/mL was utilized in these experiments. For *L. pneumophila,* as shown in **Figure 6-2 (a)**, the negative zeta potential of bacteria versus SDS concentration was amplified by 1.9 times, from - 10.8 mV in 1X PBS, and by 1.8 times, from - 18.8 mV in 0.1X PBS. The zeta potential of *E. coliA*, as it can be seen in **Figure 6-2 (b)**, was improved by 2 times, from -9.3 mV in 1X PBS, and by 1.7 times, from -20.5 mV in 0.1X PBS. However, increment of zeta potential for *E. coliA* continued only up to 0.01 mg/mL of SDS and, from this point, no significant changes of zeta potential were observed for *E. coliA* exposed 0.02 mg/mL of SDS. Zeta potential values of *S. aureus*, as shown in **Figure 6-2 (c)**, increased by 2 times, from ~ -7.1 mV in 1X PBS, and by 1.6 times, from ~ -17.7 mV 0.1X PBS, though zeta potential increment continued merely up to 0.005 mg/mL of SDS and further increment of SDS concentration exhibited no major effect on zeta potential values of this Gram-positive bacteria, compared to 0.005 mg/mL concentration.

Electric charge of each bacteria strain is determined by the available surface groups at its surface and its hydrophobicity [53]. Consistent with the literature, our results revealed that the zeta potential of Gram-positive bacteria was less than that of Gram-negative bacteria, probably related to the presence of an additional negatively charged lipopolysaccharide (LPS) layer in Gram-negative bacteria [186, 189]. Furthermore, we observed that under the same conditions, the increment of zeta potential for *S. aureus* was saturated at a much lower concentration of SDS,

starting from 0.005 mg/mL, compared to that of *E. coliA*, starting from 0.01 mg/mL. Such a trend of zeta potential variations in Gram-negative bacteria could be due to the higher density of anionic groups and O-antigen in their LPS membrane, as well as their thin peptidoglycan layer [190]. The interaction between SDS and membrane proteins is not well understood, however SDS has been modeled as a 'lipid-like' amphiphile affecting helical rearrangements of proteins, resulting in protein denaturation [191]. It is relevant to mention that the concentrations of SDS utilized in our experiments were not enough to induce protein denaturation [188]. Binding of SDS to bacteria is mainly governed by hydrophobic interactions between long hydrophobic chains of SDS and the proteins at the surface of the bacteria [192]. Since LPS of *L. pneumophila* is hydrophobic, due to the presence of the deoxy groups and N- and O-acyl substituents in polylegionaminic acid [193], it may promote adherence of SDS molecules to the bacterial surface. It was reported that the highly hydrophobic surface of *L. pneumophila* promoted their adherence to alveolar macrophages [194] that contain negatively charged sialic acid on their membranes [195].

Figure 6-2 (d) compares the results for zeta potential measurements for two different incubation times, for *L. pneumophila* exposed to 0.02 mg/mL of SDS. Comparable zeta potential values obtained for different exposure times suggested the rapid formation of a stable *L. pneumophila*-SDS hybrid. Notice that the decreased and stable zeta potentials of *E. coli* and *S. aureus* have been reported for low concentrations of cetyl trimethyl ammonium bromide (CTAB), however at higher concentrations of CTAB, zeta potential changed over time [186].

We have investigated other negatively charged molecules for modulation of bacterial electric charge. We observed that electrostatic interaction of aspartic acid with *L. pneumophila* was much less stable and efficient compared to hydrophobic interaction of SDS (**Figure 6-8** in SI section). Specific binding of BSA showed low efficiency and involved extra chemical steps (**Figure 6-9** in SI section). Consequently, it was deduced that SDS provided the best solution in providing extra negative charge to bacteria. This approach was also much simpler and faster to apply, therefore it was further investigated for enhanced detection of *L. pneumophila*.

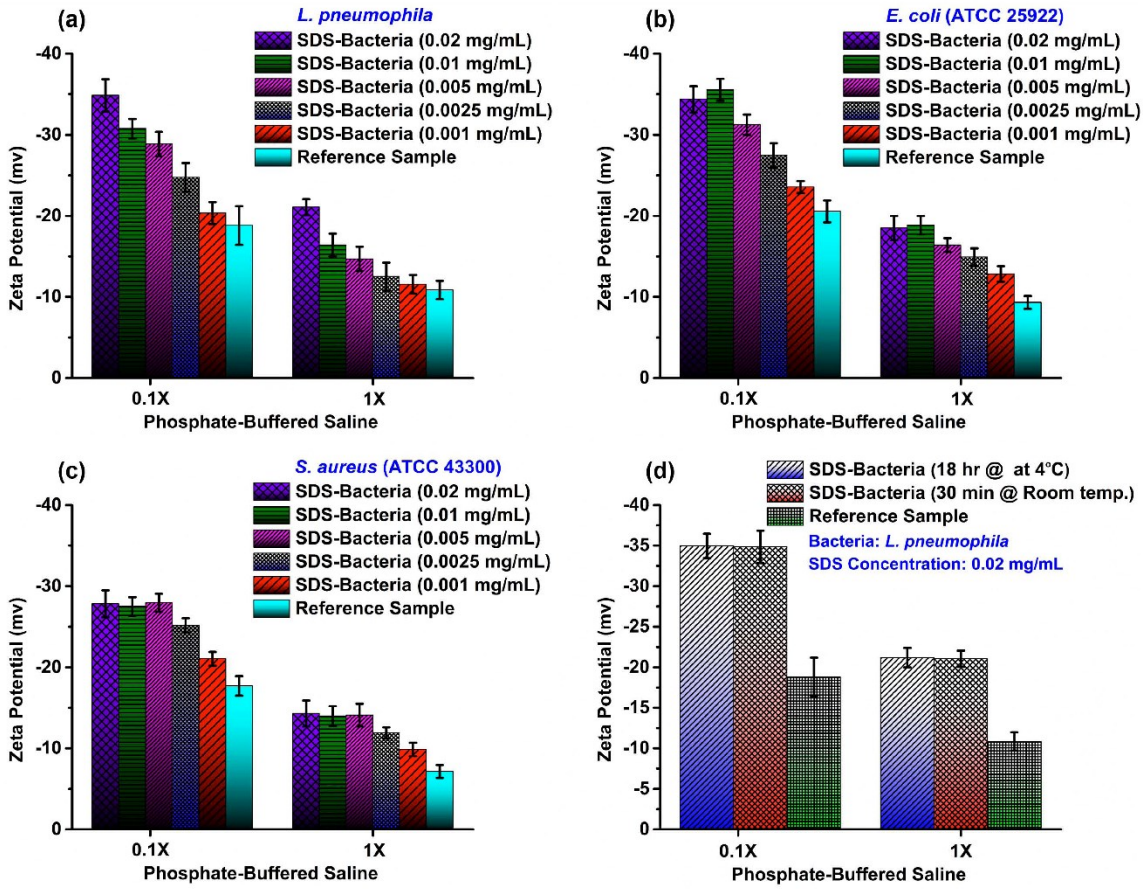

Figure 6-2. Effect of various concentrations of SDS on negative zeta potential of heat-inactivated *L. pneumophila* (a), live *E. coliA*, (b) and live *S. aureus* (c) and effect of incubation time on negative zeta potential of heat-inactivated *L. pneumophila* (d).

The spectrophotometry experiments were carried out to determine the incorporation of SDS molecules with bacteria. A linearly depending absorbance was observed for SDS concentrations between 0.0025 mg/mL to 0.01 mg/mL, in 1X PBS solution, with a background absorbance of 0.042 for the reference sample, as shown in **Figure 6-3**. After exposing 10^9 CFU/mL of heat-inactivated *L. pneumophila* to SDS at concentration of 0.02 mg/mL in 1X PBS, the non-interacted SDS were extracted by filtering the bacteria. The absorbance data of this solution is presented with a bold (green) square. These data indicated that concentration of SDS in supernatant fluid was ~ 0.003 mg/mL, while the rest of SDS molecules must have bound to bacteria, assuming negligible loss of molecules during experimental procedure. Quantification of SDS molecules

using conductivity measurements in DI H_2O resulted in comparable numbers (**Figure 6-10** in SI section). Given that the number of SDS molecules in the initial solution (0.02 mg/mL) was ~ 41.76 × 10^{15}, it was revealed that in average ~ 35.5 × 10^6 SDS molecules were attached per each bacterium (at concentration of 10^9 CFU/mL). As expected, such a number of SDS molecules had no effect on bacterial viability, which was confirmed by live/dead assay (**Figure 6-11** in SI section). Theoretical calculations based on Gouy-Chapman model showed that the surface charge density of *L. pneumophila*, exposed to 0.02 mg/mL of SDS, was almost doubled from ~ - 0.01 C/m^2, i.e. ~ 1.3×10^5 electrons (**Figure 6-12** in SI section). Even though the absolute values could be underestimated, the ratio of the final charge density per initial number was relatively accurate, considering that the employed model predicted the proper trend of charge variation as reported in [196, 197]. This information is of importance for molecular simulations as well as fundamental study of interaction of SDS with proteins and other biochemical compounds [198].

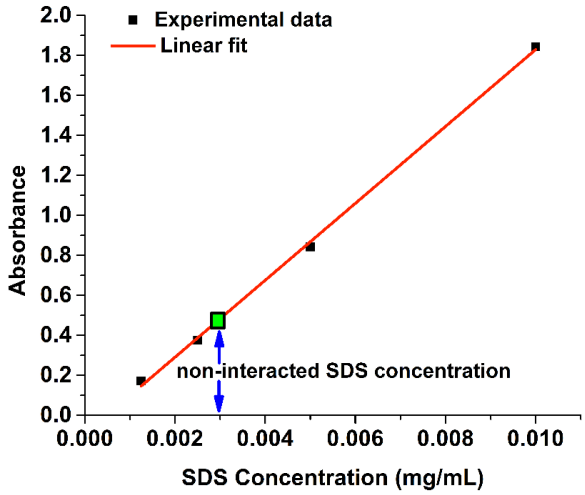

Figure 6-3. Quantification of SDS molecules using spectrophotometry in 1X PBS. The supernatant of bacterial solution is presented with bold (green) square.

Figure 6-4 shows FTIR spectra of *E. coliA* and SDS conjugated *E. coliA*. The FTIR spectra of bacteria contains overlapping signals that originate from different biomolecules and appear distinctively in five main regions (**Figure 6-4 (a)**) as defined in [199]. Full FTIR spectra of *E. coliA* and that of SDS conjugated bacteria, shown in **Figure 6-4 (a)**, looked very similar, because SDS molecules have CH_2, CH_3, S-O and S=O groups that are also common in bacterial cells. However, **Figure 6-4 (b)** and **Figure 6-4 (c)** shows that in the region I the CH_3 asymm stretch, the

CH_2 asymm stretch and the CH_2 symm stretch bands were more intense, well-defined and clearer in SDS conjugated compared to unconjugated *E. coliA*.

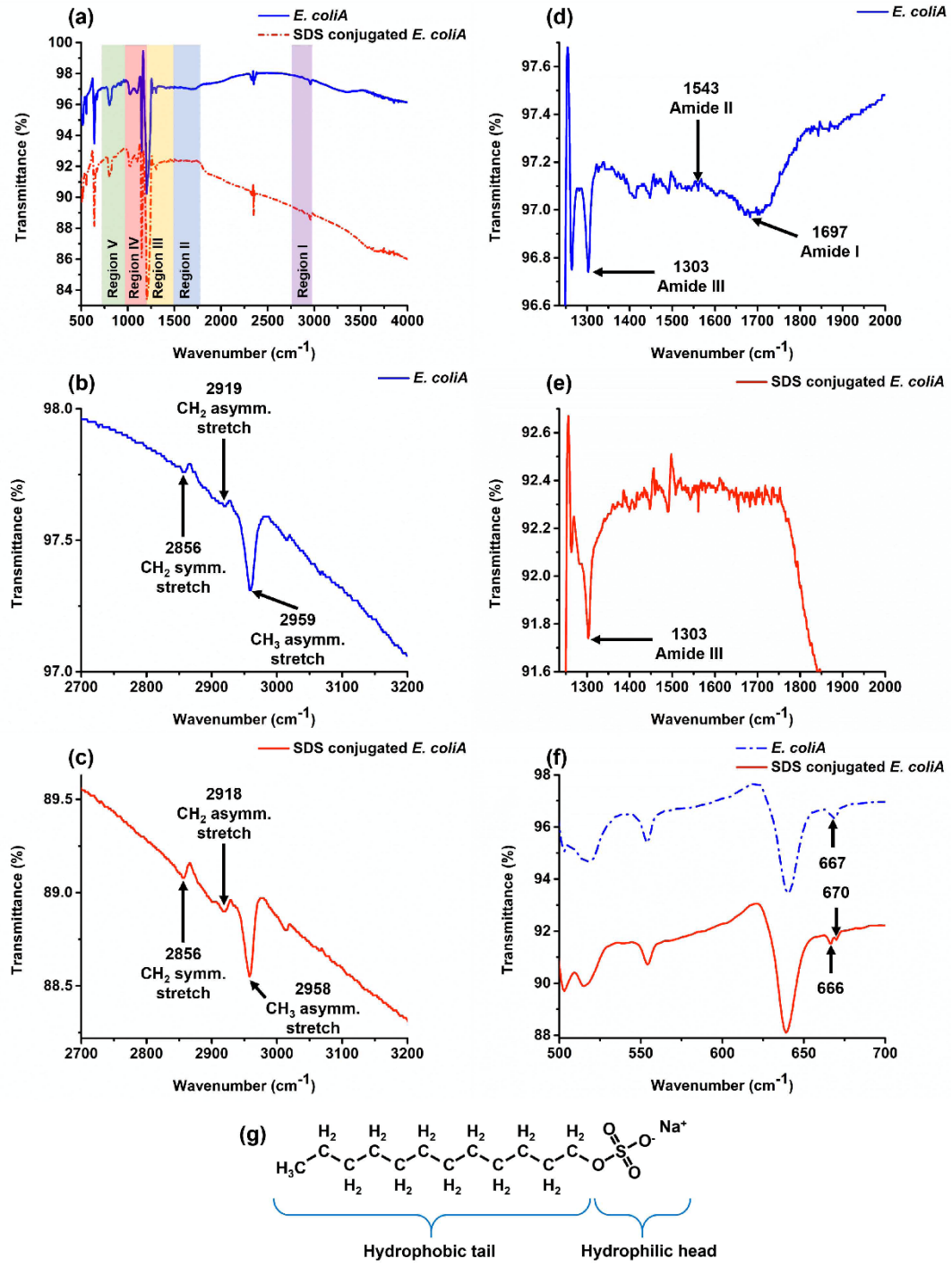

Figure 6-4. FTIR characterization of SDS conjugated *E. coliA* versus unconjugated bacteria, full spectra (a), magnified spectra of 2700-3200 cm^{-1} (b) and (c), magnifies spectra of 1250-2000 cm^{-1} (d) and (e), magnified spectra of 500-700 cm^{-1} (f), chemical structure of SDS (g).

These are the characteristic peaks related to the fatty acid region of bacterial FTIR spectra [200] and, in case of SDS coated bacteria, the long CH_2 chain of SDS could lead to an increased signal-to-noise ratio in this region. Moreover, the FTIR spectra of bacteria include amide I, II and III peaks, but the signal from these peaks were masked due to presence of SDS on the surface of bacteria, as shown in **Figure 6-4 (d)** and **Figure 6-4 (e)**. In **Figure 6-4 (a)**, the intensity ratio between peaks in regions III and IV has also been changed upon binding of SDS to *E. coliA*. The peaks associated with SO_3^- group of SDS could be indicative of interaction between the SDS and bacteria. The asymmetric or antisymmetric stretching and symmetric stretching vibration of SO_3^- groups overlapped with those peaks of bacteria, as shown in **Figure 6-4 (a)**. However, a new distinguishable peak was observed in the case of SDS conjugated bacteria at 670 cm^{-1}, which was related to the symmetric stretching vibration of SO_3^- group [201], as it can be seen from magnified portion of spectra, presented in **Figure 6-4 (f)**. The preceding dataset confirmed the presence of SDS on the bacterial surface, while it pointed to the fact that there was no chemical binding/shifting for the two involved components. This is consistent with the literatures reporting that the interaction between the negatively charged SDS and proteins only involves electrostatic and mainly hydrophobic interactions [192, 202].

Figure 6-5 compares the number of heat-inactivated *L. pneumophila* and *E. coliK* immobilized at the surface of GaAs biochips for both bare and SDS conjugated bacteria. In the case of *L. pneumophila*, **Figure 6-5 (a)**, no statistically significant differences were found between the two experiments, indicating that SDS did not impact bacterial coverage. However, in the case of *E. coliK*, a substantial decrease in bacterial capture was observed. Hassen *et al.* reported that *E. coliK* has strong affinity toward the neutravidin coated surface of GaAs biochips [178]. This was verified for the employed bio-architecture by exposing surface of GaAs biochips, only coated with SAM and neutravidin without grafting antibody, to the *E. coliK* and *L. pneumophila* (**Figure 6-13** of SI section). Thus, the difference observed in the capturing results of *E. coliK*, shown in **Figure 6-5 (b)**, could be associated with the reduced non-specific binding. Alternatively, reduced affinity between SDS decorated *E. coliK* and antibodies, in **Figure 6-5 (b)**, might also have an impact. As established by the live/dead assay (**Figure 6-11** in SI section), at an SDS concentration of 0.02 mg/mL, the loss of bacteria through lysis by SDS could not be considered as a major parameter in capture efficiency of bacteria. Moreover, disaggregation of the bacterial cell walls requires a much higher concentration of SDS, typically 0.2% (w/v) [203]. These results showed that SDS did not

interfere with the immobilization of *L. pneumophila* and they suggested that it can improve the selectivity of the employed bioreceptor architecture in the case of a solution containing mixture of *E. coli* and *L. pneumophila*. However, for other types of bacteria commonly found in the industrial water samples more investigation is required.

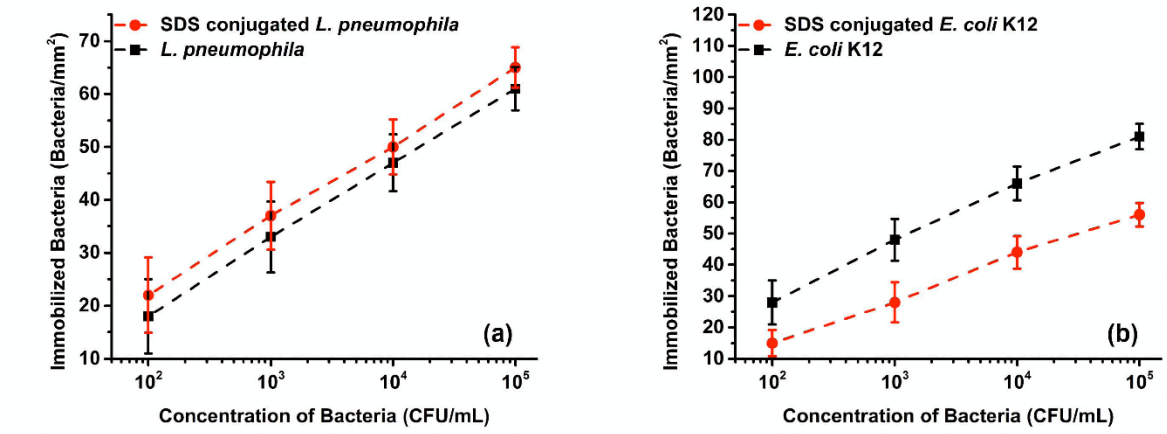

Figure 6-5. Surface coverage of bio-functionalized GaAs biochips exposed to heat-inactivated *L. pneumophila* (a) and *E. coli K12* (b), determined by fluorescence microscopy.

Figure 6-6 presents PL data for detection of SDS conjugated *L. pneumophila* (heat-inactivated) in 0.1X PBS, and the calibration curve of the biosensor. This technique relies on *in situ* monitoring the photocorrosion rate of GaAs/AlGaAs nanoheterostructures. The time of appearance of the PL maximum-intensity has been used as an indicator of the photon-induced etching rate. The presence of negatively charged bacteria resulted in a reduced photocorrosion rate and ultimately delayed the appearance of the PL maximum-intensity [30, 104]. In **Figure 6-6 (a)**, the blue curve (solid line) corresponds to a biochip exposed to a solution of 0.1X PBS, as the reference test, and the resultant PL maximum-intensity occurred at around $t = 43$ min. The green (full triangles), purple (full circles) and red (full rectangles) show data corresponding to individual biochips exposed to, respectively, 10^2, 10^3 and 10^4 CFU/mL of SDS decorated *L. pneumophila*. These biochips had PL maxima positioned at 55, 70 and 120 min, respectively. It can be seen in **Figure 6-6 (b)** that the temporal delay of the PL maximum-intensity position increased linearly with the concentration of *L. pneumophila*. This enable us to correlate the appearance of PL maximum-intensity to the concentration of *L. pneumophila* in a given solution. **Figure 6-6 (c)**

compares the delay of PL maximum-intensities obtained for unconjugated and SDS decorated *L. pneumophila* using GaAs/AlGaAs nanoheterostructure biosensors. It shows that exposing biochips to SDS-*L. pneumophila* resulted in a noticeable shift of the detection signal, compared to unconjugated *L. pneumophila* at the same concentration. For biochips exposed to 10^4 CFU/mL of SDS-*L. pneumophila*, an average delay of ~ 70-min versus reference biochip was observed. For the same concentration of bacteria, only a ~ 10-min delay was observed for the unconjugated *L. pneumophila*. Most importantly, we were unable to resolve the difference between PL maximum-intensity of reference biochips and that of biochips exposed to the unconjugated *L. pneumophila* at 10^3 CFU/mL, however for biochips exposed to 10^3 CFU/mL of SDS decorated bacteria we observed ~ 30 min delay of PL maximum-intensity. The surface coverage data, presented in **Figure 6-5**, indicated that decorating *L. pneumophila* with SDS had no effect on the bacterial surface coverage, compared to unconjugated bacteria, whereas the PL data, shown in **Figure 6-6**, revealed a substantial difference in appearance of PL maximum-intensity for these two cases. This pointed out the role of bacterial electric charge in decreasing the photoetching rate of GaAs/AlGaAs nanoheterostructure.

Chemical dissolution of III-V materials is, for the most part, governed by the number of hole carriers drifted into the interface of solid/electrolyte [155]. The excess hole carriers generated by photoexcitation of semiconductor can either contribute in the surface states mediated recombination [204] or participate in the charge transfer reaction with the surrounding electrolyte, via surface states [170]. While the recombination by means of surface states is non-radiative and independent of the surface band bending [55], the hole-driven photoetching reactions can be changed according to band bending conditions. It was observed that photocorrosion of n-GaAs was slower under flat band condition, compared to n-GaAs with upward band bending [60]. Chemical- and physical-induced band bending variation of semiconductors has been studied extensively [156]. Hilal *et al.* studied Mott-Schottky behavior of n-GaAs and reported that attachment of positively charged metalloporphyrin shifted the flat band voltage of semiconductor toward positive values by 200-300 mV [205]. Moreover, it has been reported that adsorption of electron acceptor molecules, such as Cl_2 and O_2, and electron donor molecules, such as CH_3OH, affected band bending of titanium oxide (TiO_2) and regulated the rate of hole transfer at the surface of TiO_2 [206]. In more than a few studies charge transfer between bacteria and a conducting or semiconducting substrate was observed [207, 208]. It has been experimentally demonstrated that,

on average, around 10^{-14} C of charge per single bacterium has been exchanged up on bacterial adhesion to the semiconducting indium tin oxide surface. This amount corresponds to only a fraction the total charge at the surface of bacteria [208].

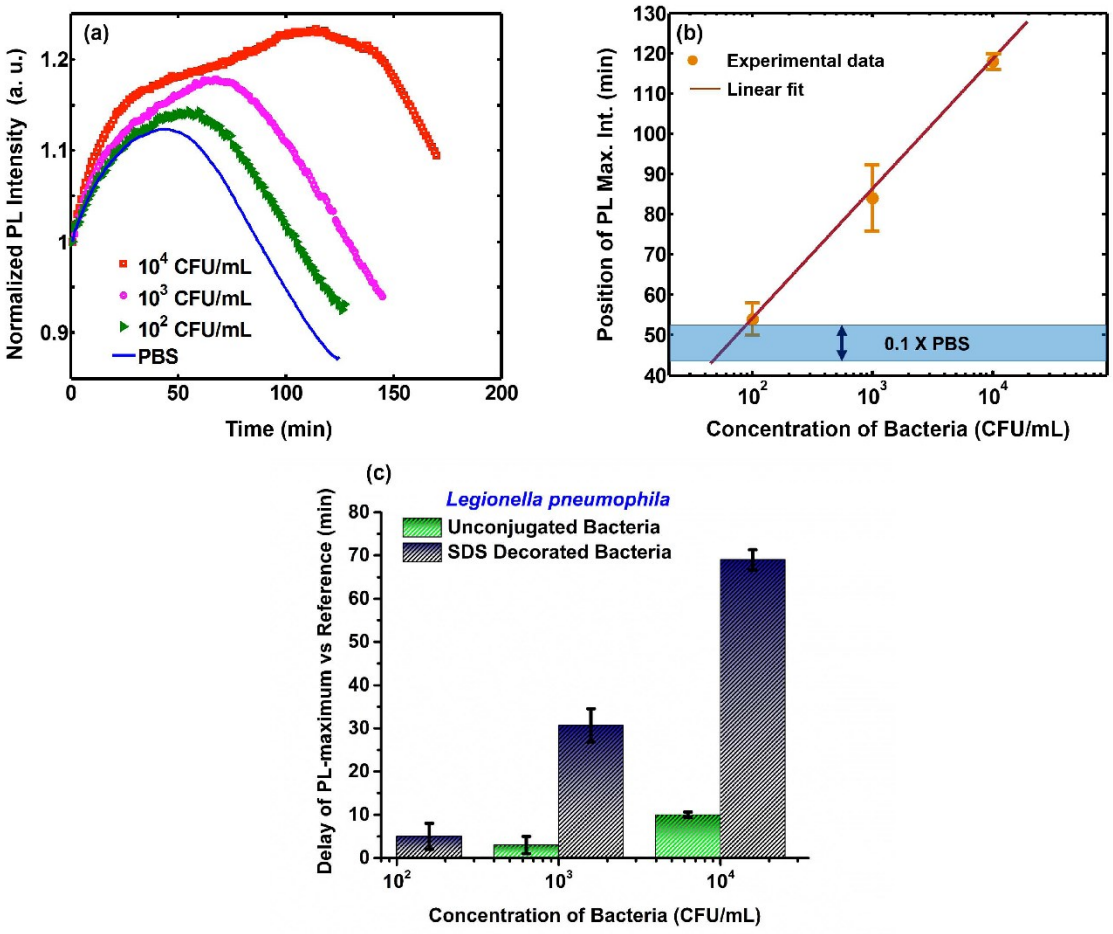

Figure 6-6. Representative PL data from bio-functionalized samples exposed to different concentration of SDS decorated *L. pneumophila* (a), statistical analysis of PL intensity maximum vs time for numerous repeated detection tests (b) and comparison of PL maximum-intensity delay versus reference sample for unconjugated and SDS decorated *L. pneumophila* (c).

In the case of GaAs/AlGaAs biosensor, adsorption of bacteria can electrostatically affect the band bending at the surface of semiconductor and influence the efficiency of charge transfer between an adsorbed bacterium and semiconductor. The degree of these variations is related to the

length of bioreceptor (the distance between bacteria and surface of biochips), the Debye length in the employed electrolytic environment [68] and conductivity of interfacial layer. Here, the surface of biochips were covered with thiols, neutravidin and antibodies prior to detection experiments. The evidence of charge transport by thiol has already been reported [209, 210]. Moreover, it has been shown that passivation of GaAs with thiols will not exceed 50% of the whole surface [211], therefore the uncovered area could also support the charge transfer between bacteria and semiconductor.

The foregoing discussion underlines that the increased negative zeta potential of SDS-*L. pneumophila* clearly improved the electrostatic interaction of bacteria with biochips by influencing the semiconductor band bending and/or charge transfer process, however elucidating detailed impact of these mechanisms requires further investigations. PL results confirmed that decorating *L. pneumophila* with SDS (at 0.02 mg/mL), enhanced the LOD of the photocorrosion based biosensor by one order of magnitude, regarding previously reported data [104]. According to the error bars of **Figure 6-6 (b)** and **Figure 6-6 (c)** detection of 10^2 CFU/mL of SDS-*L. pneumophila* was not significant. It is possible to reduce the error bars using a slightly acidic or basic solution, which showed to provide better conditions for homogenous GaAs photoetching [105, 212], then in due course better circumstances for detection of *L. pneumophila* at concentrations lower that 10^3 CFU/mL could be met.

6.7. Conclusion

We have investigated bacterial surface charge amplification by decorating *L. pneumophila*, *E. coliA* and *S. aureus* with negatively charged biomolecules. The results of alteration were studied using zeta potential measurements. Hydrophobic interactions of SDS molecules resulted in a nearly twofold increase in the negative zeta potential of both Gram-negative (*L. pneumophila, E. coliA*) and Gram-positive (*S. aureus*) bacteria, with an attractive stability of molecular binding. We were able to increase the zeta potential of *L. pneumophila* from - 10.8 mV to -21.05 mV in 1X PBS, and from - 18.8 mV to -34.85 mV in 0.1X PBS, by exposing bacteria to 0.02 mg/mL solution of SDS. Spectrophotometry data showed that such an improvement of zeta potential originated from attachment of ~ 35.5×10^6 SDS molecules per bacterium. By employing Gouy-Chapman

equation, it was determined that, at concentration of 0.02 mg/mL SDS, the surface charge density of *L. pneumophila* in 1X PBS increased from ~ - 0.01 C/m^2 to ~ - 0.02 C/m^2. This enabled us to estimate that ~ 35.5×10^6 SDS molecules added 1.2 10^5 *e* per bacterium, namely each SDS molecule provided 0.0035 *e*. Furthermore, using a maximum concentration 0.02 mg/mL of SDS caused no major damage to the cell membrane of *E. coliA* and *S. aureus*. Hydrophobic interaction of SDS with the surface of *E. coliA* was confirmed by FTIR-revealed traces of SDS molecules. Moreover, SDS assisted in reducing the nonspecific interaction of bacteria with the employed bio-architecture. In correlation with the zeta potential results, PL measurements confirmed that LOD of the GaAs/$Al_{0.35}Ga_{0.65}As$ nanoheterostructure biosensor for *L. pneumophila* was enhanced to 10^3 CFU/mL, which is one order of magnitude better than the previously reported results. The fundamental role of electrostatic interaction, between bacteria and surface of biochips, in performance of quantum biosensor was also advocated by PL data. We argue that this relatively simple approach could find application in the operation of enhanced-sensitivity biosensors targeting detection of a variety of electrically charged biomolecules.

6.8. Supplementary material

6.8.1. Wafer structure and room temperature PL spectra

An un-doped 500 nm thick GaAs layer was grown on a semi-insulating GaAs (001) substrate. Then a GaAs/AlGaAs quantum well was grown on the buffer layer. Finally, this structure was capped with an 8 nm-thick GaAs layer. **Figure 6-7** shows the schematic view and the room temperature PL profile of the employed GaAs/AlGaAs nanoheterostructure. PL spectra was measured using a Philips PL mapper (PLM-150), equipped with a second harmonic of Nd:YAG laser source (λ = 532 nm) for excitation of samples and an InGaAs photodiode detector array for collection of PL signal.

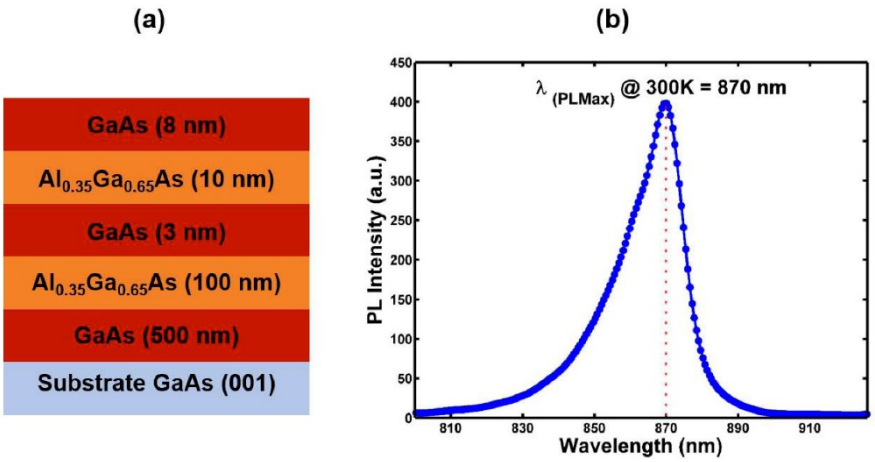

Figure 6-7. Schematic cross-section view of the GaAs/$Al_{0.35}Ga_{0.65}As$ nanoheterostructure (a), and room temperature PL emission of wafer, irradiated with a 532 nm laser (b).

6.8.2. Decorating bacteria with aspartic acid

Sample preparation: Different concentrations of aspartic acid (1mM, 5mM and 10 mM) were prepared in 1X PBS. Bacteria (10^9 CFU/mL) were suspended in these solutions and incubated for 2 h. Bacterial solutions were then rinsed twice with 1X PBS, as explained section 6.4.1 of this chapter, and diluted in either 1X PBS or 0.1X PBS to reach concentration of 10^6 CFU/mL, for zeta potential measurements.

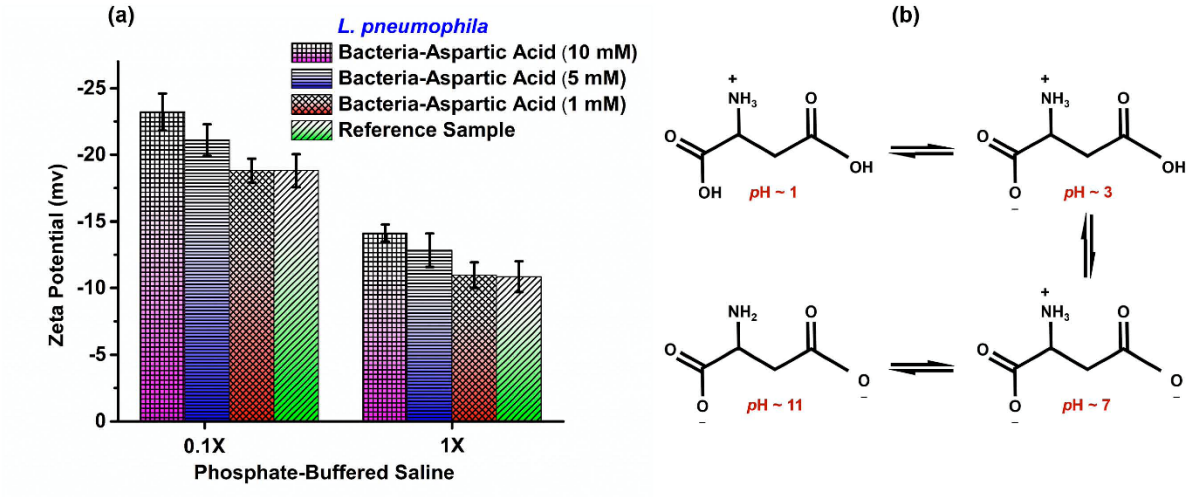

Figure 6-8. Zeta potential of heat-inactivated *L. pneumophila* in PBS, *p*H 7.4, exposed to aspartic acid (a), and chemical structure of aspartic acid at various *p*H levels (b).

Results: Figure 6-8 shows zeta potential data for heat-inactivated *L. pneumophila* exposed to 1 mM, 5 mM and 10 mM aspartic acid, as well as the chemical structure of aspartic acid at different *p*H values. At *p*H over 7, aspartic acid (pK_a 3.9), which is an amino acid with a polar side chain, appears in zwitterion form with two deprotonated carboxylic groups ($–COO^-$) and one protonated amine group ($–NH_3^+$) [213]. It was reported that electrostatic interaction was the major force between the aspartic acid and anionic phosphatidylglycerol moieties of bacterial cell surface lipid [214]. Therefore, while the positively charged $-NH_3^+$ group of aspartic acid could electrostatically attach to the bacterial phospholipid bilayer, and perhaps neutralized some negative charges, the two $-COO^-$ groups would provide the extra negative charge. For *L. pneumophila*, we observed that the decorated bacteria carried higher negative charge compared to the reference sample, only when it was exposed to 10 mM aspartic acid. Then, zeta potential of *L. pneumophila* increased 1.3-time, from -10.8 mV in 1X PBS and 1.23-time, from -18.8 mV in 0.1X PBS. This suggested that the electrostatic interaction of aspartic acid molecules and bacteria was not very efficient.

6.8.3. Decorating bacteria with BSA and labeling BSA with FITC for quantification

Sample preparation: First, 0.01 mg/mL of BSA (or FITC conjugated BSA) in 1X PBS was exposed to EDC/NHS (2mM/5mM in 1X PBS) for 30-min, then added to the bacterial solution at 10^9 CFU/mL and again incubated for 30-min. Then bacterial solution was rinsed twice with 1X PBS, as explained in section 6.4.1 of this chapter. For zeta potential measurements bacterial solution, exposed to BSA, was diluted to reach 10^6 CFU/mL, whereas for fluorescence intensity measurements bacterial solution, exposed to FITC-BSA, remained at 10^9 CFU/mL.

The efficiency of BSA binding to bacteria was evaluated using a microplate reader (SpectraMax® M3, Molecular Devices) with fluorescence intensity measurements taken in 96-well black polystyrene microplates (Thermo Fisher Scientific, USA). For this purpose, BSA molecules were conjugated with FITC prior to the fluorescence measurements (all steps in darkness). FITC:BSA ratio of 6:1 was selected to provide adequate labeling of all BSA molecules [215]. FITC was dissolved in DMSO (18 mg in 500 µL) and 158 mg of the BSA was dissolved in 25 mL of bicarbonate buffer (250 mg $KHCO_3$ in 25 mL DI H_2O). The BSA solution was stirred in

a glass vial and the FITC-DMSO solution was added, dropwise. This mixture was incubated for 1 h at room temperature with continuous stirring. In order to remove the unreacted FITC, the solution was dialyzed for 48 h against 1X PBS, which was changed frequently. The prepared solution was freeze-dried and stored at 4 ºC in the dark. A calibration curve was created using fluorescence intensity measurements on the FITC-BSA solutions (in 1X PBS) at concentrations ranging from 0.0005 mg/mL to 0.0045 mg/mL and then compared with the fluorescence intensity data from solutions containing *E. coliA* and *S. aureus*, decorated with FITC-BSA at concentration of 0.01 mg/mL.

Results: Figure 6-9 (a) and **Figure 6-9 (b)**, respectively, show the zeta potential variation of *E. coliA* and *S. aureus* decorated with BSA. **Figure 6-9 (c)** shows the fluorescence intensity measurements and **Figure 6-9 (d)** portrays a pictorial view of decorating bacteria with the FITC-BSA compound. BSA is a large globular protein, containing 14% basic groups and 18% acidic groups, with reported PI of 4.7 [216] to 4.8 [217], which makes BSA negative at *p*H 7.4 [218]. The EDC/NHS process activated the free COOH groups of BSA which later bound to the free NH_2 groups of proteins, located on the bacteria outer-membrane. As it can be seen from **Figure 6-9 (a)**, exposing *E. coliA* to 0.01 mg/mL of BSA increased the negative zeta potential ~ 1.5-time, from -9.32 mV in 1X PBS and ~ 1.2-time, from -20.5 mV in 0.1X PBS. For *S. aureus*, **Figure 6-9 (b)**, the zeta potential values increased ~ 2-time, from - 7.1 mV in 1X PBS and ~ 1.5-time, from -17.7 mV in 0.1X PBS. According to this data, the zeta potential of Gram-positive bacteria, decorated with BSA, was improved somewhat more than that of Gram-negative bacteria. Fluorescence intensity measurements, shown in **Figure 6-9 (c)**, indicated that from the initial FITC-BSA concentration of 0.01 mg/mL, there were ~ 1.7 µg/mL BSA in the solution containing *E. coliA*, whereas 2 µg/mL was found in the solution containing *S. aureus*. This might explain the slightly better charge enhancement for *S. aureus*. Generally, Gram-positive bacteria have more exposed proteins on their membrane in comparison with the Gram-negative bacteria [219]. Therefore, the probability of interaction between EDC-NHS activated BSA and Gram-positive bacteria could have been higher compared to Gram-negative bacteria. Furthermore, BSA attaches to the surface functional groups, which are associated with the thick peptidoglycan layer of Gram-positive bacteria [186]. The BSA decoration of bacteria offered promising results, though it required adding some additional chemical steps into the bacteria detection procedure.

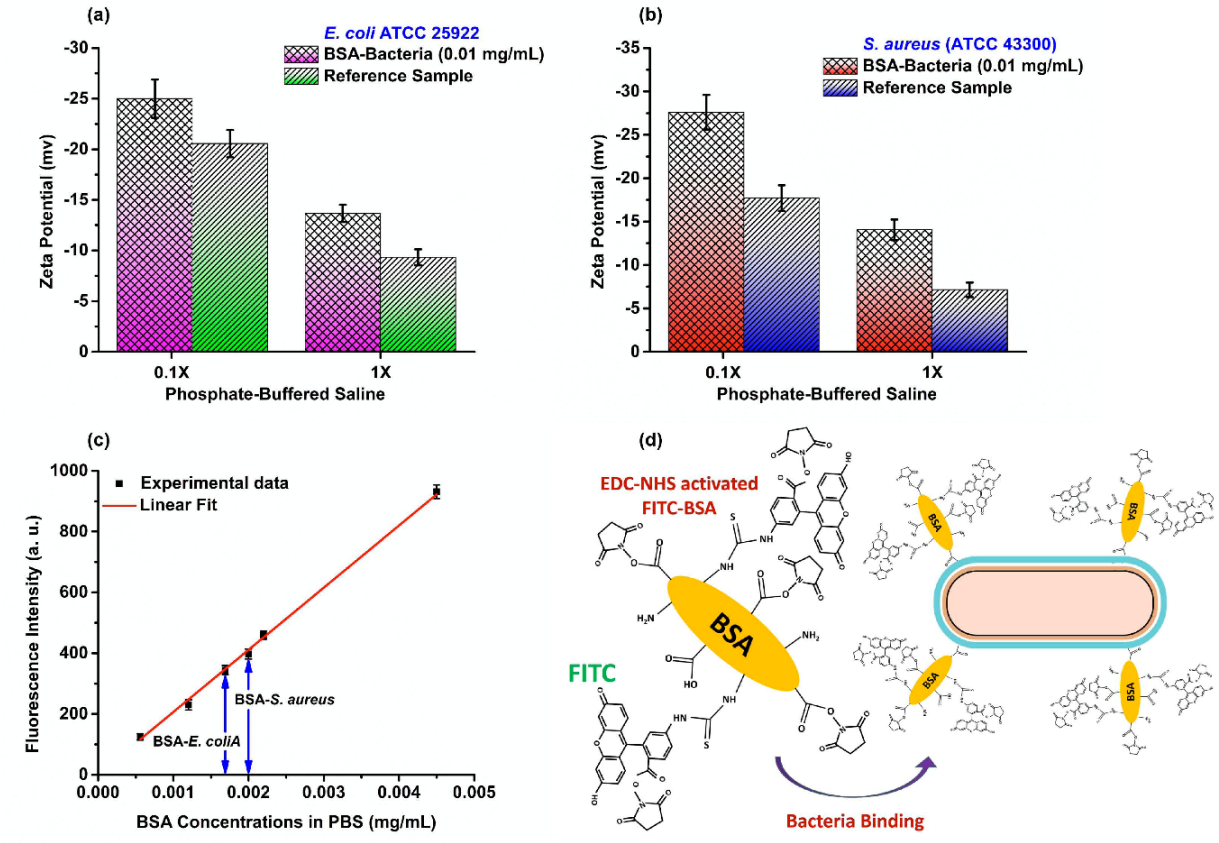

Figure 6-9. Bacterial cell zeta potential variation in PBS, *p*H 7.4, before and after being exposed to 0.01 mg/mL of BSA for *E. coliA* (a), and *S. aureus* (b). Efficiency of BSA conjugation was verified by fluorescence intensity measurement (c). Chemical structure of FITC-BSA, activated with EDC/NHS, and its binding to bacteria (not drawn to scale) presented in (d).

6.8.4. Conductivity measurements

Experimental procedure: A commercial TDS Meter (Model 4510, Jenway) was used for conductivity measurements. To achieve stable readouts, the results were recorded after 60-seconds delays. We first created a calibration curve for various concentration of SDS in DI H_2O, ranging from zero to 0.02 mg/mL. Heat-inactivated *L. pneumophila* (**10^9 CFU/mL**) was exposed to SDS at concentration of 0.02 mg/mL for 30 min in DI H_2O, and the bacteria were extracted using a PVDF membrane 0.22 μm filter (Millex-GV from Millipore, Canada). Conductivity of solution containing non-interacted SDS was compared to the SDS-DI H_2O calibration curve obtained formerly.

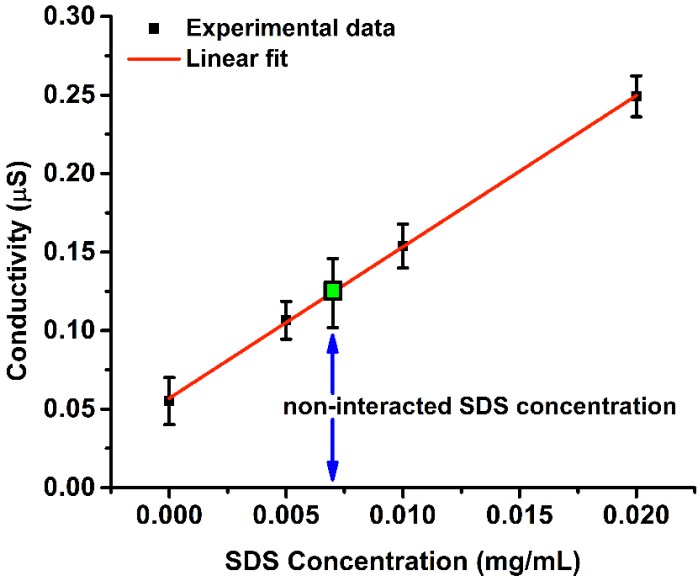

Figure 6-10. Quantification of SDS molecules using conductivity measurements in DI H_2O. The supernatant of SDS-bacteria solution is presented with bold (green) square.

Results: The conductometry experiments were carried out to complement the spectrophotometry data, however conductivity variations in PBS were not resolvable, hence we conducted these tests in DI H_2O. As shown in **Figure 6-10**, a linear conductivity variation between ~ 0.055 μS (DI H_2O) and 0.25 μS (SDS solution at 0.02 mg/mL) was observed, which was consistent with the literature [220, 221]. The conductivity of the supernatant solutions, contacting non-interacted SDS molecules, corresponded to 0.007 mg/mL of SDS in DI H_2O. This data is highlighted with a bold (green) square in Fig S4.

6.8.5. Live/dead assay

Sample preparation: We conducted live/dead assay using BacLight™ live/dead kit (ThermoFisher Scientific) comprising SYTO 9 dye (green) for live cells and propidium iodide dye (red) for dead cells as described previously [222]. Bacterial suspensions of *E. coliA* and *S. aureus* at a concentration of 10^9 CFU/mL in 1X PBS were exposed to 0.02 mg/mL of SDS for 30-min,

then rinsed twice with autoclaved 0.85% saline (NaCl) solution and diluted to 2×10^8 CFU/mL, *E. coliA,* and 2×10^7 CFU/mL, *S. aureus*, for staining purpose. The SYTO 9 and propidium iodide solutions were diluted to final concentrations of 1.25 μL/mL, in autoclaved 0.85% saline solution. Then, 500 μL of stain solution was added to the bacterial samples and incubated at room temperature for 15-min. The samples were then rinsed with autoclaved 0.85% saline solution, twice. Finally, imaging was carried out on the bacterial solutions at 10^6 CFU/mL, in 96-well white polystyrene microplates (Thermo Fisher Scientific, USA), using an AxioObserver Z1 inverted microscope (Zeiss, Germany). Images were analysed with ImageJ software.

Results: The reported effect of SDS on cell lysis and protein denaturation [223] was evaluated by investigating cell viability of bacteria exposed to 0.02 mg/mL of SDS. **Figure 6-11** displays the live/dead assay results, carried out on both unconjugated and SDS-decorated *E. coliA* and *S. aureus*. Because of safety precautions we were unable to perform live/dead assay on the live *L. pneumophila*. In **Figure 6-11**, the green color represents the live bacteria, while the red color shows the bacteria with damaged cell walls. The live/dead ratio, defined by number of green pixels per number of red pixels, indicates the effect of SDS (0.02 mg/mL) on cell viability. This ratio for *E. coliA* and SDS conjugated *E. coliA* was 1.27 and 1.19, respectively, and for *S. aureus* and SDS conjugated *S. aureus* live/dead ratio was 1.58 and 1.23, respectively. For the most part, the high intensity of the green fluorescence established that SDS at a concentration of 0.02 mg/mL did not cause severe cell damage for either bacteria. In the case of *E. coliA*, this was in agreement with findings of Woldringh *et al.*, who showed that 0.01% of SDS had no significant effect on bacteria, whereas 0.05% SDS dissolved the plasma membrane of 9×10^8 cell/mL of *E. coli* K12 [188]. Such a membrane acting agent, similar to antimicrobial peptides, can cause disruption of cell membrane integrity, and ultimately cell lysis, but only when their ratio to the quantity of lipid membrane has exceeded a threshold [224].

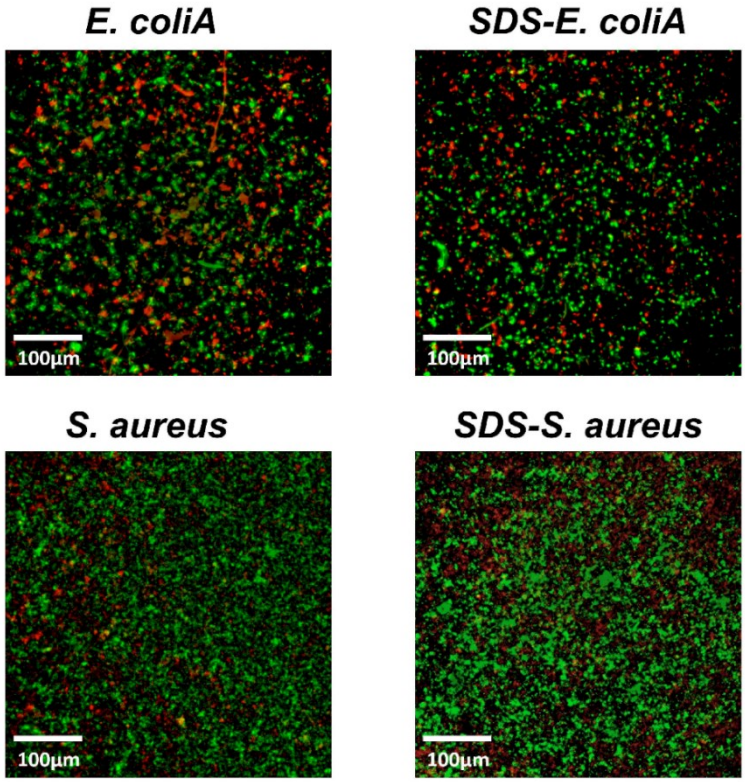

Figure 6-11. Representative florescence microscopic images of live/dead stained *E. coliA* and *S. aureus* cells before and after being exposed to 0.02 mg/mL of SDS. Green and red stains indicate live and dead bacteria, respectively.

6.8.6. The surface charge density of *L. pneumophila* in 1X PBS

Under many circumstances the shear plane of particles/bacteria may overlap with the surface, consequently the surface potential will be taken as the zeta potential [196]. Under low ionic concentration (1X PBS) and small zeta potential values (<25 mV), the Gouy-Chapman, 1-dimentional solution of the non-linear Poisson-Boltzmann equation, can provide an estimated surface charge density of bacteria based on zeta potential values. However, the actual surface charge density values could be higher than those estimated by Gouy-Chapman model [196, 197, 225, 226]. Above all, bacterial surface is not impenetrable against the ions, consequently calculating bacterial surface charge density is complicated [53, 196, 197]. Taking this into account, we employed Gouy-Chapman to estimate the charge density of *L. pneumophila* in 1X PBS. The surface charge, σ, of bacteria has been calculated as follows:

$$\sigma = \sqrt{8cN\varepsilon_r\varepsilon_0 k_B T}\, Sinh\left(\frac{e\xi}{2k_B T}\right) \qquad (6\text{-}1)$$

where c is the ionic concentration of solution, N is the Avogadro constant, ε_r and ε_0 are the vacuum and solution permittivity, respectively, k_B is the Boltzmann's constant, T is the temperature, e is the electronic charge and ζ is the zeta potential (overlapped with surface potential).

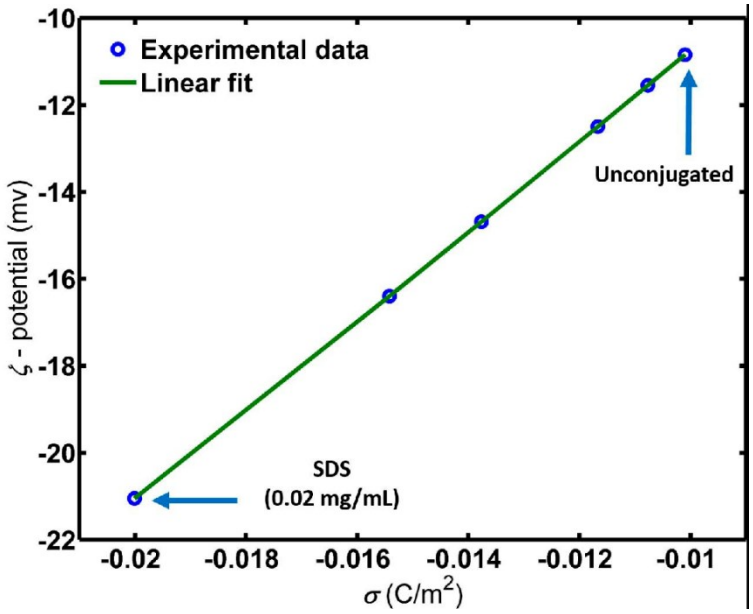

Figure 6-12. Estimation of surface charge density from zeta potential of *L. pneumophila* in 1X PBS, experimental data were extracted from Figure 6-2 (a).

Figure 6-12 depicts the estimation of surface charge density, based on zeta potential measurements carried out on *L. pneumophila* in 1X PBS, with and without SDS (**Figure 6-2 (a)**). Such a linear relation projected that the bacterial surface charge density was nearly doubled at SDS concentration of 0.02 mg/mL, compared to surface charge density of unconjugated bacteria (reference sample). As it can be seen in **Figure 6-12**, *L. pneumophila* initially carried ~ 0.01 C/m^2, i.e. ~ 1.3×10^5 electrons for a bacterial size of 1μm by 2μm. This simplified approach, based on Gouy-Chapman equation, showed a qualitatively reasonable relation between the surface charge density of *E. coli* and its zeta potential values, while it was considered that surface charge density of bacteria could have been underestimated [197]. Nonetheless, the ratio of surface charge density at 0.02 mg/mL SDS (indicated with arrow in **Figure 6-12**) over the surface charge density of unconjugated bacteria could be accurate, since Gouy-Champan predicted an appropriate trend of bacterial surface charge density variations [196, 197]. In view of that, we determined that 35.5 ×

10^6 SDS molecule (from spectrophotometric measurements) doubled the surface charge density of *L. pneumophila*, from ~ 0.01 C/m^2 in 1X PBS.

6.8.7. Assessing nonspecific binding of *E. coliK* and *L. pneumophila* to neutravidin

Experimental procedure: Bulk GaAs surfaces were coated with thiols and neutravidin as explained in the section 6.4.5 of this chapter, except antibody grafting step was not carried out. Then, these biochips, with neutravidin as the top layer, were exposed to *E. coliK* and *L. pneumophila* at concentration of 10^6 CFU/mL for 30 min. Next, biochips were rinsed with 1X PBS and DI H_2O. Images of surfaces were acquired using an Optical microscope (Zeiss, Axiotech) and processed with ImageJ software.

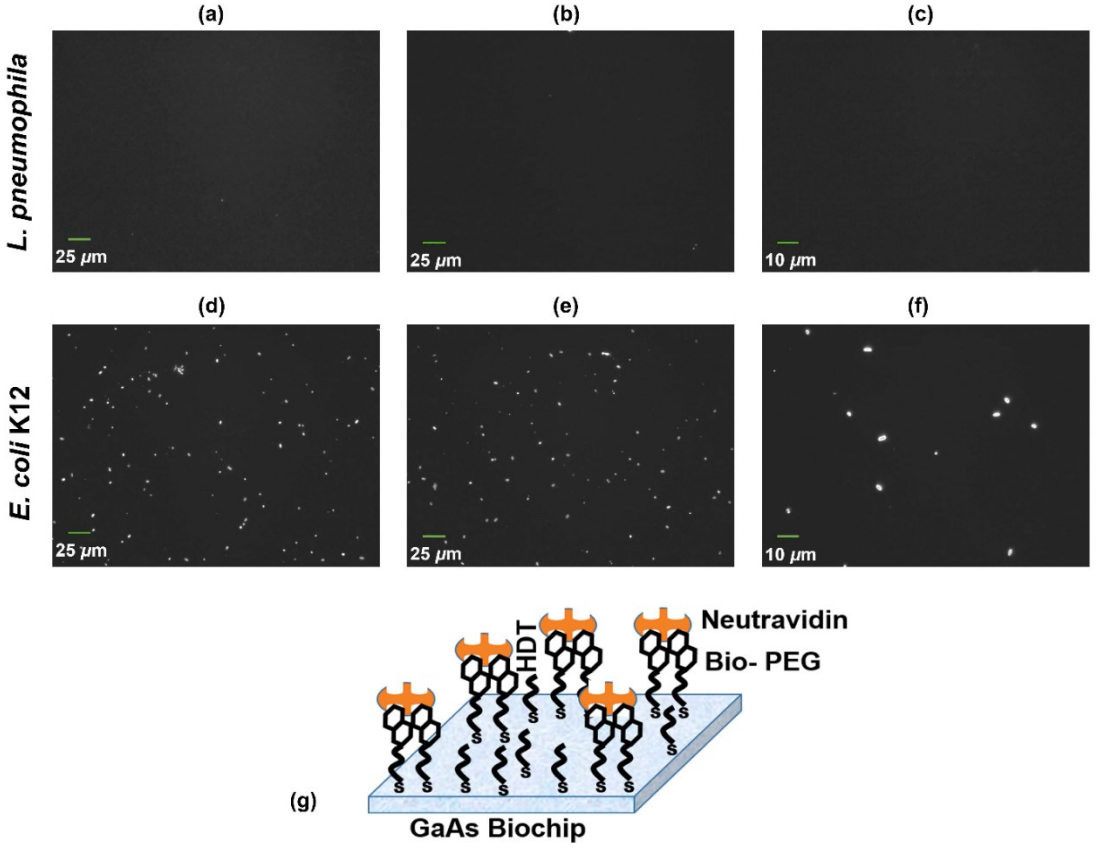

Figure 6-13. Optical microscopic images of GaAs surfaces exposed to *L. pneumophila* (a), (b), (c) and exposed to *E. coli* K12 (d), (e), (f). The employed bio-architecture consisted of self-assembled monolayer of thiols and neutravidin and it is depicted (not drawn to scale) in (g)

Results: Figure 6-13 shows the representative images with different magnification scales and schematic view of the bio-architecture, used for capturing bacteria. The top row images (**Figure 6-13 (a)**, **Figure 6-13 (b)** and **Figure 6-13 (c)**) belongs to the GaAs surfaces exposed to *L. pneumophila*. The fairly clean surface of these samples indicated that immobilization of *L. pneumophila* on GaAs/AlGaAs biosensor using bio-PEG/HDT/neutravidin/antibody architecture did not involve nonspecific binning of *L. pneumophila* to neutravidin. The bottom row images (**Figure 6-13 (d)**, **Figure 6-13 (e)** and **Figure 6-13 (f)**) corresponds to the GaAs surfaces exposed to *E. coli* K12. The rod shape of *E.coli* bacteria, typically of 2 μm in length and 0.5 μm in width [53], are clearly observed. This suggested that nonspecific binding of *E. coli* K12 to neutravidin must be taken into account when bio-PEG/HDT/neutravidin/antibody architecture is employed as bioreceptor.

6.9. Acknowledgments

This project was carried out in the frame of the Canada Research Chair in Quantum Semiconductors Program (JJD, Grant no. 950-220304). The support by the Natural Sciences and Engineering Research Council of Canada (NSERC Discovery Grant RGPIN-2015-04448) and Strategic Partnership Grant (NSERC SPG-2016-494057) is greatly appreciated. MRA acknowledges the support from NSERC-CREATE Training Program in Integrated Sensor Systems. NA acknowledges the support from the American Heart Association (AHA, 16DG31280010) and the National Institutes of Health (R01-EB023052; R01HL140618). The fabrication of GaAs/AlGaAs wafers was subsidized by the CMC Microsystems (Kingston, Canada). Technical assistance of Dr. Khalid Moumanis (Université de Sherbrooke) and Dr. Iman Noshadi (Northeastern University) is greatly appreciated. We also thank Prof. Thomas Webster (Northeastern University) for kindly supplying *E. coli* ATCC 25922 and *S. aureus* ATCC 43300 bacteria, Prof. Carmel Jolicoeur (Université de Sherbrooke) and Prof. Mansoor M. Amiji (Northeastern University) for making available to us their zeta potential measurement setup.

CHAPTER 7. Conclusions and Perspectives

Photo atomic layer etching of GaAs/AlGaAs nanoheterostructures, with significant implications for III-V semiconductors nano-structuring as well as biosensing in aqueous environment, has been investigated. To address the aforesaid objectives of this project, the fundamental aspects and mechanism of photo-induced material dissolution as well as formation of stoichiometric surfaces of GaAs/AlGaAs nanoheterostructures were studied. The response of photocorrosion based biosensor for detection of *L. pneumophila*, as the principal target of this research, was examined. Following successful detection of this pathogen, certain strategies for enhancing the performance of PL-based biosensors were proposed and enhanced detection of *L. pneumophila* was demonstrated. Here, the main outcomes of this thesis are summarized.

First, the mechanism of DIP of GaAs/$Al_{0.35}Ga_{0.65}As$ nanoheterostructures in both DI H_2O and NH_4OH environments was studied. A low power LED ($P \approx 16\text{-}20$ mW/cm^2 & $\lambda = 660$ nm) was employed to induce the photocorrosion process, and the photoluminescence of the investigated nanoheterostructures was monitored *in situ*. ICP-MS analysis provided the stoichiometry information of the surfaces that underwent the DIP process. It was shown that the concentration of As^{3+} ions released in DI H_2O was similar to the number of these ions expected to be released by the GaAs/AlGaAs nanoheterostructure DIP up to 60 nm deep. However, this was the case for Ga^{3+} ions only up to ~ 8 nm. The related discrepancy in the concentration of Ga^{3+} ions was investigated with XPS and FTIR and accumulation of, mainly Ga_2O_3 as well as Al_2O_3 and $Al(OH)_3$ was observed. On the other hand, NH_4OH solution provided attractive conditions for producing stoichiometric surfaces as an excellent agreement between the calculated and ICP-MS detected concentration of As^{3+} and Ga^{3+} has been observed for the photocorrosion depths slightly exceeding 100 nm. AFM was also utilized to examine the morphology of the DIP surfaces, and it was shown that photocorrosion in DI H_2O resulted in formation of a rough surface ($\sigma_{RMS} = 2.1$ nm) of a GaAs/AlGaAs nanoheterostructure photocorroded by 105.6 nm, whereas photocorrosion in NH_4OH created a relatively smooth surface ($\sigma_{RMS} = 0.93$ nm) for the same etch depth. It was further observed that neither DI H_2O nor NH_4OH could provide suitable conditions for dissolving Al_2O_3 and $Al(OH)_3$ that accumulated on the surface of processed nanoheterostructures. Consequently, DIP of significantly thicker nanoheterostructures will require an Al-oxide etching

environment, such as that based on hydrofluoric or phosphoric acids. Some major differences and potential advantages of the DIP process for nanostructuring of compound semiconductors and fabrication of advanced nanoscale devices, which distinguish DIP from conventional digital etching techniques, were pointed out. The most important, the DIP process allowed a sub-monolayer precision of material removal without the need of changing the hardware. In addition, the DIP process was monitored *in situ* with photoluminescence of the processed wafer, and it was shown that PL could be employed for exploring DIP for fabrication of stoichiometric surfaces. Thus, these results demonstrated the feasibility of a simple and relatively inexpensive method for fabrication of some III-V semiconductor nanodevices with *in situ* monitored atomic level etching rates.

In the next step, the PL transducer was employed for detection of *L. pneumophila* in aqueous solution. To monitor photocorrosion of GaAs/AlGaAs nanoheterostructures a quantum semiconductor photonic biosensor (QSPB) reader was used. Provided that the photocorrosion rate of GaAs/AlGaAs nanoheterostructure could be controlled and modified with the concentration of holes reaching the semiconductor/electrolyte interface, it was shown that the electrostatic interaction between *L. pneumophila* and the biofunctionalized GaAs/AlGaAs biochips affected the photo-etching rate and, consequently, the position of temporal PL maximum-intensity was changed. Detection of *L. pneumophila* in 0.1X PBS at concentrations of 10^4 to 10^6 bacteria/ml was achieved in the first step. It was achieved in a 100-fold diluted PBS (0.1X PBS) that allowed to compensate for the weaker interaction of the biosensor with *L. pneumophila* characterized by much lower negative charge compared to that of *E. coli* K12 that was previously detected by this technique.

In order to improve immobilization of *L. pneumophila* on the surface of the biosensor, GaAs/AlGaAs biochips were electrically biased. For such a purpose, an electrochemical cell with a 3-electrode configuration and an Ag/AgCl reference electrode was designed. The conventional bio-architecture consist of bio-PEG/HDT/Neutravidin/Antibody was employed to capture bacteria and FITC conjugated antibodies as well as fluoresce microscopy technique was used to study the impact of the applied bias on the bacteria immobilization process. Control of semiconductor band bending was achieved using a moderate applied voltage. Under increased band bending at applied E = 0.2 V, the repulsion force originating from semiconductor-bacteria double layers was reduced.

This allowed capturing almost 2 times more *L. pneumophila* at the surface of a biosensor, suggesting that an enhanced LOD could be expected using electrical biasing of the GaAs/AlGaAs biochip. However, this technique was limited in terms of bias amplitude and duration, as the electrical current degraded the transducer performance.

In order to enhance the LOD of the photocorrosion based biosensor, negatively charged molecules were bound to the bacterial surface with the aim of amplifying the bacterial surface charge. Zeta potential measurements were utilized to monitor the charge effect of bacteria. It was shown that SDS could increase significantly the zeta potential of *E. coli* as well as it reduced the nonspecific binding of *E. coli* to the employed bio-architecture. Consequently, the PL based detection of *L. pneumophila* at 10^3 CFU/ml was achieved by decorating these bacteria with SDS. Hence, an innovative method for improving the performance of biosensors detecting negatively charged bacteria was demonstrated. Such a chemical modification of the bacterial surface charge was neither complicated nor expensive.

Furthermore, some interesting directions for future studies could be defined. First, regarding the outstanding characteristics of the DIP process for nano-structuring, it would be interesting to investigate other types of III-V nanoheterostructures to provide an economically interesting counterpart to modern technologies of device nanofabrication. Moreover, digital dissolution of III-V nanoheterostructures should be investigated in solutions with different *p*H because, as pointed out by Sharma *et al.* [105], the resolution of PL-monitored interfaces in GaAs/AlGaAs quantum well microstructures depends strongly on an acidic strength of the photocorrosion solution.

Additionally, the performance of the investigated biosensor could be further improved by automating some essential parts. The employed QSPB reader excites samples and collects data only for a short fraction of time, followed by a relatively long idle condition. This means that the optical setup can be used for measuring PL of multiple biochips in quasi-parallel. Therefore, the throughput (number of tests per day) of a biosensor could be significantly increased by applying a servomotor-based stage for processing of several different biochips. Finally, the potential applications of the QSPB technology could be attractive for cell biology research, as some recent results have shown that the movement of ions across plasma membranes of cancer cells could

create a significant negative charge [227]. It is reasonable to expect that such a phenomenon could be detected with the QSPB platform.

Conclusions et Perspectives Français

La gravure de la couche photo-atomique des nano-hétérostructures GaAs/AlGaAs, avec des implications significatives pour la nano-structuration des semi-conducteurs III-V et la bio-sensibilité en milieu aqueux, a été étudiée. Pour aborder les objectifs cités dans ce projet, les aspects fondamentaux et le mécanisme de la dissolution photo-induite du matériau, ainsi que la formation des surfaces stœchiométriques des nano-hétérostructures GaAs/AlGaAs ont été étudiés. La réponse du biocapteur à base de photocorrosion pour la détection de *L. pneumophila*, en tant que cible principale de cette recherche, a été examinée. Suite à la détection réussie de ce pathogène, certaines stratégies visant à améliorer la performance du biocapteur à base de la photoluminescence (PL) ont été proposées et une détection améliorée de *L. pneumophila* a été démontrée. Ci-dessous, les principaux résultats de cette thèse sont résumés.

Tout d'abord, le mécanisme de DIP des nano-hétérostructures GaAs/$Al_{0.35}Ga_{0.65}As$ dans les environnements DI H_2O et NH_4OH a été étudié. Une LED de puissance assez faible (P ≈ 16-20 mW/cm^2 & λ = 660 nm) a été utilisée pour induire le processus de photocorrosion, et la PL des nano-hétérostructures étudiées a été contrôlée *in situ*. L'analyse ICP-MS a fourni les informations stœchiométriques des surfaces ayant subi un processus DIP. Il a été montré que la concentration des ions As^{3+} libérés dans DI H_2O était similaire au nombre de ces ions qui devraient être libérés par le DIP des nano-hétérostructure GaAs/AlGaAs jusqu'à 60 nm de profondeur. Cependant, c'était le cas pour les ions Ga^{3+} jusqu'à environ 8 nm. La divergence dans la concentration des ions Ga^{3+} a été étudiée avec XPS et FTIR et l'accumulation de, principalement Ga_2O_3, Al_2O_3 et $Al(OH)_3$, a été identifiée comme la source de cette incohérence. D'autre part, la solution de HN_4OH a fourni les conditions requises pour produire des surfaces stœchiométriques gravées car un excellent accord entre la concentration calculée et celle détectée par ICP-MS de As^{3+} et Ga^{3+} a été observé pour les profondeurs de photocorrosion dépassant légèrement 100 nm. L'AFM a également été utilisé pour examiner la morphologie des surfaces produites et il a été montré que la photocorrosion dans DI H_2O entraînait la formation d'une surface rugueuse (σ_{RMS} = 2.1 nm) d'une nano-hétérostructure GaAs/AlGaAs de 105.6 nm d'épaisseur, tandis que la photocorrosion dans NH_4OH a créé une surface relativement lisse (σ_{RMS} = 0.93 nm) pour la même profondeur de gravure. Il a ensuite été soutenu que ni DI H_2O ni NH_4OH ne pouvaient constituer une condition adéquate pour dissoudre Al_2O_3 et $Al(OH)_3$; ils pourraient donc s'accumuler à la surface des nano-

hétérostructures GaAs/AlGaAs. Par conséquent, la DIP des nano-hétérostructures beaucoup plus épaisses nécessitera un environnement de gravure à l'oxyde d'Al, tel que celui basé sur les acides fluorhydrique ou phosphorique. Certaines différences majeures et avantages potentiels du processus DIP pour la nano-structuration des semi-conducteurs composés et la fabrication de dispositifs nanométriques avancés, qui distinguent le DIP des techniques classiques de gravure digitale, ont été soulignés. Pour commencer, le processus DIP a permis une précision de de gravure de la sous-monocouche sans avoir à changer le système. En outre, le processus DIP a été monitoré *in situ* avec la photoluminescence de l'échantillon étudié. De plus, il a été montré que les données PL pourraient être remplacées par des données ICP-MS pour explorer la stœchiométrie de surface. Enfin, les résultats obtenus ont démontré la faisabilité d'un procédé simple et relativement peu coûteux pour la fabrication des nano-dispositifs à semi-conducteurs composés, avec les surfaces stœchiométriques s'étendant en profondeur dans des nano-hétérostructures gravées.

Dans l'étape suivante, le transducteur PL a été utilisé pour la détection de *L. pneumophila* en solution aqueuse. Pour le monitoring de la photocorrosion des nano-hétérostructures de GaAs/AlGaAs, un lecteur portable et miniaturisé de biocapteurs photoniques à semi-conducteur quantique (QSPB) a été utilisé. Pourvu que le taux de photocorrosion de la nano-hétérostructure GaAs/AlGaAs puisse être contrôlée et modifiée avec la concentration des trous atteignant l'interface semi-conducteur/électrolyte, il a été démontré que l'interaction électrostatique entre les bactéries *L. pneumophila* et les biopuces GaAs/AlGaAs bio-fonctionnalisées affectait le taux de photogravure et que, par conséquent, la position de l'intensité maximale de PL temporelle était modifiée. Ainsi, la détection de *L. pneumophila* dans du PBS 0.1 X à des concentrations de 10^4 à 10^6 bactéries/ml a été obtenue. C'était démontré que le PBS dilué 100 fois (PBS 0.1X) offrait la condition électrostatique nécessaire à la détection de *L. pneumophila*, qui présentait une charge négative inférieure à celle obtenue avec *E. coli* K12 qui précédemment a été détectée par cette technique. Il a été expliqué que la sensibilité plus faible du transducteur à base de PL contre *L. pneumophila* (10^4 bactéries/ml) par rapport à celle d'E. *coli* K12 (10^3 bactéries/ml) était due à l'effet de charge et la longueur de Debye ont joué un rôle crucial. Cependant, les propriétés du biorécepteur employé, principalement l'affinité des anticorps dans ces tests, peuvent avoir une influence sur la sensibilité du système de bio-détection.

Afin d'améliorer l'immobilisation de *L. pneumophila* à la surface du biocapteur, les biopuces GaAs/AlGaAs étaient polarisées électriquement. Dans ce but, une cellule électrochimique avec une configuration à trois électrodes et une électrode de référence Ag/AgCl a été conçue. La bio-architecture conventionnelle composée de bio-PEG/HDT/Neutravidin/Antibody a été utilisée pour capturer les bactéries et les anticorps conjugués par FITC ainsi que la technique de microscopie à fluorescence ont été utilisée pour étudier l'impact du champ appliqué sur le processus de l'immobilisation des bactéries. Le contrôle de la courbure des semi-conducteurs a été réalisé en utilisant une tension appliquée modérée. Sous l'augmentation de la flexion de bande à E = 0.2 V appliquée, la force de répulsion provenant des doubles couches des bactéries et de semi-conductrice a été réduite, ce qui a permis de capturer près de 2 fois plus de *L. pneumophila* à la surface du biocapteur. Cela suggère qu'une LOD améliorée peut être attendue en utilisant la polarisation électrique de la biopuce GaAs/AlGaAs. Cependant, cette technique était limitée en termes d'amplitude et de durée de polarisation, car le courant électrique pouvait dégrader les performances du transducteur.

Pour améliorer la LOD du biocapteur à base de la photocorrosion, la liaison de molécules chargées négativement à la surface bactérienne dans le but d'amplifier la charge bactérienne de surface a été étudiée. Les mesures du potentiel zêta ont été utilisées pour surveiller l'effet de charge des bactéries. Il a été montré que l'acide aspartique augmentait le potentiel zêta de *L. pneumophila* inactivé par la chaleur, environ 18-21%, la liaison chimique de la BSA à *E. coli* et *S. aureus* améliorait leur potentiel zêta négatif jusqu'à 46% et 96% respectivement, et le SDS a doublé le potentiel zêta bactérien. Compte tenu des résultats prometteurs obtenus à partir de bactéries décorées par du SDS, ce composé chimique a été étudié pour améliorer la détection de *L. pneumophila*. SDS à une concentration de 0.02 mg/ml n'a pas endommagé la membrane cellulaire ni pour les bactéries à Gram négatif ni pour les bactéries à Gram positif. Des traces IR de SDS ont confirmé une interaction hydrophobe du SDS avec la surface d'E. *coli*. De plus, le SDS a réduit la liaison non spécifique d'*E. coli* à la bio-architecture utilisée. Dans la dernière étape, une détection de *L. pneumophila* basée sur la PL avec une LOD améliorée de 10^3 UFC/ml a été rapportée. Ainsi, une méthode innovante pour améliorer les performances des biocapteurs détectant la charge négative des bactéries a été démontrée. Une telle modification chimique de la charge bactérienne de surface n'était ni compliquée ni coûteuse.

Dans le cadre de cette thèse, certaines questions fondamentales concernant le processus de photocorrosion digital (DIP) ont été étudié. En utilisant les mesures ICP MS et les techniques de caractérisation de surface les plus récentes, il a été démontré que le DIP peut fournir une condition pour la gravure sous-monocouche des semi-conducteurs composés tout en préservant la stœchiométrie de leurs surfaces. L'application de la DIP pour la détection de bactéries chargées électriquement a été étudiée, et il a été montré que *L. pneumophila* décorée par des biomolécules chargées négativement pouvait être détectée à 10^3 UFC/ml, ce qui est considéré comme l'un des meilleurs résultats rapportés à ce jour avec la technologie de biosensing basée sur DIP, tout en soulignant l'importance de la longueur de Debye pour la performance QSPB.

Par ailleurs, des pistes intéressantes pour des futures études pourraient être définies. Tout d'abord, en ce qui concerne les caractéristiques exceptionnelles du processus DIP pour la nano-structuration stœchiométrique, il serait intéressant d'étudier d'autres types de nano-hétérostructures III-V pour fournir un équivalent économiquement intéressant aux technologies modernes de nano-fabrication. De plus, la dissolution digitale des nano-hétérostructures III-V devrait être étudiée dans des solutions de *p*H différent car, comme l'ont souligné par Sharma *et al.* [105], la résolution des interfaces contrôlées par PL dans des microstructures GaAs/AlGaAs à puits quantiques dépend fortement de la résistance acide de la solution de photocorrosion.

En outre, les performances du biocapteur étudié pourraient être améliorées en automatisant certaines parties essentielles. Le lecteur de biocapteur utilisé (lecteur QSPB) excite les échantillons et ne collecte les données que pendant une courte fraction de temps, puis il reste inactif pendant une période relativement longue. Cela signifie que la configuration optique peut être utilisée pour mesurer le PL de plusieurs biopuces en parallèle. Par conséquent, le débit (nombre des tests par jour) du biocapteur pourrait être considérablement augmenté en créant un étage basé sur un servomoteur capable de repositionner les biopuces lors de la collection des données PL. Enfin, les applications potentielles de la technologie QSPB pourraient être intéressantes pour la recherche en biologie cellulaire, car certains résultats récents ont montré que le mouvement des ions à travers les membranes plasmiques des cellules cancéreuses pourrait créer une charge négative importante [227]. Il est raisonnable de s'attendre à ce qu'un tel phénomène puisse être détecté avec la plate-forme QSPB.

References

[1] G. López-Campos, J. V. Martínez-Suárez, M. Aguado-Urda, and V. López-Alonso, "Detection, Identifi cation, and Analysis of Foodborne Pathogens," *Microarray detection and characterization of bacterial foodborne pathogens*, pp. 13-32, New York: Springer, 2012.

[2] Y. Yamamoto, "PCR in Diagnosis of Infection: Detection of Bacteria in Cerebrospinal Fluids," *Clinical and Vaccine Immunology,* vol. 9, no. 3, pp. 508-514, 2002.

[3] "Cleaning up water," *Nature Materials* vol. 7, no. 5, pp. 341-341, 2008.

[4] M. A. Shannon, P. W. Bohn, M. Elimelech, J. G. Georgiadis, B. J. Marinas, and A. M. Mayes, "Science and technology for water purification in the coming decades," *Nature,* vol. 452, no. 7185, pp. 301-10, Mar 20, 2008.

[5] World Health Organization., *Emerging issues in water and infectious disease*, Geneva: World Health Organization, 2003.

[6] J. D. van Elsas, A. V. Semenov, R. Costa, and J. T. Trevors, "Survival of Escherichia coli in the environment: fundamental and public health aspects," *The Isme Journal,* vol. 5, pp. 173, 06/24/online, 2010.

[7] R. R. Isberg, T. J. O'Connor, and M. Heidtman, "The Legionella pneumophila replication vacuole: making a cosy niche inside host cells," *Nature Reviews Microbiology,* vol. 7, pp. 13, 11/17/online, 2008.

[8] S. Lévesque, P.-L. Plante, N. Mendis, P. Cantin, G. Marchand, H. Charest, F. Raymond, C. Huot, I. Goupil-Sormany, F. Desbiens, S. P. Faucher, J. Corbeil, and C. Tremblay, "Genomic Characterization of a Large Outbreak of Legionella pneumophila Serogroup 1 Strains in Quebec City, 2012," *PLOS ONE,* vol. 9, no. 8, pp. e103852, 2014.

[9] *Legionella and the prevention of legionellosis*: World Health Organization, 2007.

[10] I. Oren, T. Zuckerman, I. Avivi, R. Finkelstein, M. Yigla, and J. M. Rowe, "Nosocomial outbreak of Legionella pneumophila serogroup 3 pneumonia in a new bone marrow transplant unit: evaluation, treatment and control," *Bone Marrow Transplantation,* vol. 30, pp. 175, 08/15/online, 2002.

[11] P. Joly, P.-A. Falconnet, J. André, N. Weill, M. Reyrolle, F. Vandenesch, M. Maurin, J. Etienne, and S. Jarraud, "Quantitative Real-Time Legionella PCR for Environmental

Water Samples: Data Interpretation," *Applied and Environmental Microbiology,* vol. 72, no. 4, pp. 2801-2808, 10/31/received 02/06/accepted, 2006.

[12] A. P. F. Turner, "Biosensors: sense and sensibility," *Chemical Society Reviews,* vol. 42, no. 8, pp. 3184-3196, 2013.

[13] D. L. Enrico, M. G. Manera, G. Montagna, F. Cimaglia, M. Chiesa, P. Poltronieri, A. Santino, and R. Rella, "SPR based immunosensor for detection of Legionella pneumophila in water samples," *Optics Communications,* vol. 294, pp. 420-426, 2013/05/01/, 2013.

[14] E. Howe, and G. Harding, "A comparison of protocols for the optimisation of detection of bacteria using a surface acoustic wave (SAW) biosensor," *Biosensors and Bioelectronics,* vol. 15, no. 11–12, pp. 641-649, 2000.

[15] N. Li, A. Brahmendra, A. J. Veloso, A. Prashar, X. R. Cheng, V. W. Hung, C. Guyard, M. Terebiznik, and K. Kerman, "Disposable immunochips for the detection of Legionella pneumophila using electrochemical impedance spectroscopy," *Anal Chem,* vol. 84, no. 8, pp. 3485-8, Apr 17, 2012.

[16] F. Patolsky, G. Zheng, and C. M. Lieber, "Nanowire-based biosensors," *Anal Chem,* vol. 78, no. 13, pp. 4260-9, Jul 1, 2006.

[17] Y. Cui, Q. Wei, H. Park, and C. M. Lieber, "Nanowire nanosensors for highly sensitive and selective detection of biological and chemical species," *Science,* vol. 293, no. 5533, pp. 1289-92, Aug 17, 2001.

[18] E. Katz, and I. Willner, "Biomolecule-functionalized carbon nanotubes: applications in nanobioelectronics," *Chemphyschem,* vol. 5, no. 8, pp. 1084-104, Aug 20, 2004.

[19] P. Bergveld, "Thirty years of ISFETOLOGY: What happened in the past 30 years and what may happen in the next 30 years," *Sensors and Actuators B: Chemical,* vol. 88, no. 1, pp. 1-20, 1/1/, 2003.

[20] L. Bousse, N. F. De Rooij, and P. Bergveld, "Operation of chemically sensitive field-effect sensors as a function of the insulator-electrolyte interface," *Electron Devices, IEEE Transactions on,* vol. 30, no. 10, pp. 1263-1270, 1983.

[21] G. Steinhoff, M. Hermann, W. J. Schaff, L. F. Eastman, M. Stutzmann, and M. Eickhoff, "pH response of GaN surfaces and its application for pH-sensitive field-effect transistors," *Applied Physics Letters,* vol. 83, no. 1, pp. 177, 2003.

[22] B. Baur, J. Howgate, H. G. von Ribbeck, Y. Gawlina, V. Bandalo, G. Steinhoff, M. Stutzmann, and M. Eickhoff, “Catalytic activity of enzymes immobilized on AlGaN/GaN solution gate field-effect transistors,” *Applied Physics Letters,* vol. 89, no. 18, pp. 183901, 2006.

[23] J. A. Garrido, A. Härtl, S. Kuch, M. Stutzmann, O. A. Williams, and R. B. Jackmann, “pH sensors based on hydrogenated diamond surfaces,” *Applied Physics Letters,* vol. 86, no. 7, pp. 073504, 2005.

[24] A. Härtl, J. A. Garrido, S. Nowy, R. Zimmermann, C. Werner, D. Horinek, R. Netz, and M. Stutzmann, “The Ion Sensitivity of Surface Conductive Single Crystalline Diamond,” *Journal of the American Chemical Society,* vol. 129, no. 5, pp. 1287-1292, 2007/02/01, 2007.

[25] V. Duplan, E. Frost, and J. J. Dubowski, “A photoluminescence-based quantum semiconductor biosensor for rapid in situ detection of Escherichia coli,” *Sensors and Actuators B: Chemical,* vol. 160, no. 1, pp. 46-51, 2011.

[26] G. Ashkenasy, D. Cahen, R. Cohen, A. Shanzer, and A. Vilan, “Molecular Engineering of Semiconductor Surfaces and Devices,” *Accounts of Chemical Research,* vol. 35, no. 2, pp. 121-128, 2002/02/01, 2002.

[27] A. Vilan, and D. Cahen, “How organic molecules can control electronic devices,” *Trends in Biotechnology,* vol. 20, no. 1, pp. 22-29, 2002.

[28] C.-L. Tsai, J.-C. Chen , and W.-J. Wang, “Near-infrared Absorption Property of Biological Soft Tissue Constituents,” *Journal of Medical and Biological Engineering,* vol. 21, no. 1, pp. 7-14, 2001.

[29] J. J. Dubowski, "Novel Quantum Dot based Approach for Biosensing." in Photon-based Nanoscience and Nanobiotechnology, NATO Science Series, Eds., J.J. Dubowski and S. TAnev, Springer 2006, pp. 159–173.

[30] E. Nazemi, S. Aithal, W. M. Hassen, E. H. Frost, and J. J. Dubowski, “GaAs/AlGaAs heterostructure based photonic biosensor for rapid detection of *Escherichia coli* in phosphate buffered saline solution,” *Sensors and Actuators B: Chemical,* vol. 207, Part A, pp. 556-562, 2015.

[31] M. L. Y. Sin, K. E. Mach, P. K. Wong, and J. C. Liao, “Advances and challenges in biosensor-based diagnosis of infectious diseases,” *Expert review of molecular diagnostics,* vol. 14, no. 2, pp. 225-244, 02/13, 2014.

[32] J. Davis, D. Huw Vaughan, and M. F. Cardosi, “Elements of biosensor construction,” *Enzyme and Microbial Technology,* vol. 17, no. 12, pp. 1030-1035, 1995/12/01/, 1995.

[33] B. Byrne, E. Stack, N. Gilmartin, and R. O'Kennedy, “Antibody-based sensors: principles, problems and potential for detection of pathogens and associated toxins,” *Sensors (Basel),* vol. 9, no. 6, pp. 4407-45, 2009.

[34] T. Sano, C. L. Smith, and C. R. Cantor, “Immuno-PCR: very sensitive antigen detection by means of specific antibody-DNA conjugates,” *Science,* vol. 258, no. 5079, pp. 120, 1992.

[35] E. de Boer, and R. R. Beumer, “Methodology for detection and typing of foodborne microorganisms,” *International Journal of Food Microbiology,* vol. 50, no. 1, pp. 119-130, 1999/09/15/, 1999.

[36] M.-I. Rocha-Gaso, C. March-Iborra, Á. Montoya-Baides, and A. Arnau-Vives, “Surface Generated Acoustic Wave Biosensors for the Detection of Pathogens: A Review,” *Sensors,* vol. 9, no. 7, pp. 5740, 2009.

[37] K. Länge, B. E. Rapp, and M. Rapp, “Surface acoustic wave biosensors: a review,” *Analytical and Bioanalytical Chemistry,* vol. 391, no. 5, pp. 1509-1519, July 01, 2008.

[38] R. Fogel, J. Limson, and Ashwin A. Seshia, “Acoustic biosensors,” *Essays In Biochemistry,* vol. 60, no. 1, pp. 101, 2016.

[39] W. HASSEN MOHAMED, “Elaboration de biocapteurs basés sur différentes méthodes d’immobilisation de la couche de reconnaissance et différentes techniques de transduction,” Ecole Doctorale de Chimie, Génie Biologique, L’UNIVERSITE CLAUDE BERNARD – LYON 1, France, 2009.

[40] V. Ferrari, and R. Lucklum, "Overview of Acoustic-Wave Microsensors," *Piezoelectric Transducers and Applications*, A. Arnau Vives, ed., pp. 39-54, Berlin, Heidelberg: Springer Berlin Heidelberg, 2004.

[41] R. Bashir, “BioMEMS: state-of-the-art in detection, opportunities and prospects,” *Advanced Drug Delivery Reviews,* vol. 56, no. 11, pp. 1565-1586, 2004/09/22/, 2004.

[42] J. L. Arlett, E. B. Myers, and M. L. Roukes, "Comparative advantages of mechanical biosensors," *Nature Nanotechnology,* vol. 6, pp. 203, 03/27/online, 2011.

[43] L. D. Mello, and L. T. Kubota, "Review of the use of biosensors as analytical tools in the food and drink industries," *Food Chemistry,* vol. 77, no. 2, pp. 237-256, 2002.

[44] D. Grieshaber, R. MacKenzie, J. Vörös, and E. Reimhult, "Electrochemical Biosensors - Sensor Principles and Architectures," *Sensors (Basel, Switzerland),* vol. 8, no. 3, pp. 1400-1458, 2008.

[45] K. Habermüller, M. Mosbach, and W. Schuhmann, "Electron-transfer mechanisms in amperometric biosensors," *Fresenius' Journal of Analytical Chemistry,* vol. 366, no. 6, pp. 560-568, March 01, 2000.

[46] Z. Altintas, M. Akgun, G. Kokturk, and Y. Uludag, "A fully automated microfluidic-based electrochemical sensor for real-time bacteria detection," *Biosensors and Bioelectronics,* vol. 100, pp. 541-548, 2018/02/15/, 2018.

[47] A. Bard, and L. Faulkner, *Electrochemical Methods: Fundamentals and Applications*: John Wiley & Sons, Inc, 2001.

[48] Y. Naoki, T. Sato, and M. Akinori, "Liquid-phase chemical sensors using InP-based open-gate FETs." pp. 1305-1308.

[49] C.-S. Lee, S. Kim, and M. Kim, "Ion-Sensitive Field-Effect Transistor for Biological Sensing," *Sensors,* vol. 9, no. 9, pp. 7111, 2009.

[50] P. Singh, "SPR Biosensors: Historical Perspectives and Current Challenges," *Sensors and Actuators B: Chemical,* vol. 229, pp. 110-130, 2016/06/28/, 2016.

[51] C. Liu, T. Lei, K. Ino, T. Matsue, N. Tao, and C.-Z. Li, "Real-time monitoring biomarker expression of carcinoma cells by surface plasmon resonance biosensors," *Chemical Communications,* vol. 48, no. 84, pp. 10389-10391, 2012.

[52] Y. Tang, X. Zeng, and J. Liang, "Surface Plasmon Resonance: An Introduction to a Surface Spectroscopy Technique," *Journal of chemical education,* vol. 87, no. 7, pp. 742-746, 2010.

[53] A. T. Poortinga, R. Bos, W. Norde, and H. J. Busscher, "Electric double layer interactions in bacterial adhesion to surfaces," *Surface Science Reports,* vol. 47, no. 1, pp. 1-32, 2002.

[54] E. V. Usachev, O. V. Usacheva, and I. E. Agranovski, “Surface plasmon resonance-based bacterial aerosol detection,” *Journal of Applied Microbiology,* vol. 117, no. 6, pp. 1655-1662, 2014.

[55] T. H. Gfroerer, "Photoluminescence in Analysis of Surfaces and Interfaces," *Encyclopedia of Analytical Chemistry*, R. A. Meyers, ed., pp. 9209–9231, Chichester, UK: John Wiley & Sons Ltd., 2006.

[56] M. Enache, C. Negrila, M. Anastasescu, G. Dobrescu, M. F. Lazarescu, and V. Lazarescu, “Surface States- and Field-Effects at GaAs(100) Electrodes in Sodium Dodecyl Sulfate Acid Solution,” *Journal of The Electrochemical Society,* vol. 165, no. 4, pp. H3008-H3017, January 1, 2018, 2018.

[57] G. M. Marshall, G. P. Lopinski, F. Bensebaa, and J. J. Dubowski, “Electro-optic investigation of the surface trapping efficiency in n-alkanethiol SAM passivated GaAs(001),” *Nanotechnology,* vol. 22, no. 23, pp. 235704, 2011.

[58] T. Fink, and R. M. Osgood, “Photoelectrochemical Etching of GaAs / AlGaAS Multilayer Structures,” *Journal of The Electrochemical Society,* vol. 140, no. 9, pp. 2572-2581, September 1, 1993, 1993.

[59] B. A. Balko, E. A. Miller, and G. L. Richmond, “Picosecond Photoluminescence Studies of Photocorrosion and Passivation of n-GaAs in Na2S-Containing Solutions,” *The Journal of Physical Chemistry,* vol. 99, no. 12, pp. 4124-4131, 1995/03/01, 1995.

[60] E. A. Miller, and G. L. Richmond, “Photocorrosion of n-GaAs and passivation by Na{sub 2}S: A comparison of the (100), (110), and (111)B faces,” *Journal Name: Journal of Physical Chemistry B: Materials, Surfaces, Interfaces, amp Biophysical; Journal Volume: 101; Journal Issue: 14; Other Information: PBD: 3 Apr 1997*, pp. Medium: X; Size: pp. 2669-2677, 1997.

[61] K. Rajeshwar, "Fundamentals of Semiconductor Electrochemistry and Photoelectrochemistry," *Encyclopedia of Electrochemistry: Semiconductor Electrodes and Photoelectrochemistry* A. J. Bard, M. Stratmann and S. Licht, eds.: Wiley-VCH Verlag GmbH, 2002.

[62] J. F. Kauffman, C. S. Liu, and M. W. Karl, “Surface Recombination Kinetics at the GaAs/Electrolyte Interface via Photoluminescence Efficiency Measurements,” *The Journal of Physical Chemistry B,* vol. 102, no. 35, pp. 6766-6773, 1998.

[63] T. Fujimoto, and K. Awaga, "Electric-double-layer field-effect transistors with ionic liquids," *Physical Chemistry Chemical Physics,* vol. 15, no. 23, pp. 8983-9006, 2013.

[64] H. S. Mavi, S. S. Islam, S. Rath, B. S. Chauhan, and A. K. Shukla, "Laser-induced etching of Cr-O doped GaAs and wavelength dependent photoluminescence," *Materials Chemistry and Physics,* vol. 86, no. 2-3, pp. 414-419, 2004.

[65] B. Joshi, S. S. Islam, H. S. Mavi, V. Kumari, T. Islam, A. K. Shukla, and Harsh, "Size-selective laser-induced etching of semi-insulating GaAs: Photoluminescence studies," *Physica E: Low-dimensional Systems and Nanostructures,* vol. 41, no. 4, pp. 690-694, 2009.

[66] A. Sze, D. Erickson, L. Ren, and D. Li, "Zeta-potential measurement using the Smoluchowski equation and the slope of the current–time relationship in electroosmotic flow," *Journal of Colloid and Interface Science,* vol. 261, no. 2, pp. 402-410, 2003/05/15/, 2003.

[67] M. Kaszuba, J. Corbett, F. M. Watson, and A. Jones, "High-concentration zeta potential measurements using light-scattering techniques," *Philosophical Transactions of the Royal Society A: Mathematical, Physical and Engineering Sciences,* vol. 368, no. 1927, pp. 4439, 2010.

[68] E. Stern, R. Wagner, F. J. Sigworth, R. Breaker, T. M. Fahmy, and M. A. Reed, "Importance of the Debye Screening Length on Nanowire Field Effect Transistor Sensors," *Nano Letters,* vol. 7, no. 11, pp. 3405-3409, 2007.

[69] G.-J. Zhang, G. Zhang, J. H. Chua, R.-E. Chee, E. H. Wong, A. Agarwal, K. D. Buddharaju, N. Singh, Z. Gao, and N. Balasubramanian, "DNA Sensing by Silicon Nanowire: Charge Layer Distance Dependence," *Nano Letters,* vol. 8, no. 4, pp. 1066-1070, 2008/04/01, 2008.

[70] S. Sorgenfrei, C.-y. Chiu, M. Johnston, C. Nuckolls, and K. L. Shepard, "Debye Screening in Single-Molecule Carbon Nanotube Field-Effect Sensors," *Nano Letters,* vol. 11, no. 9, pp. 3739-3743, 2011/09/14, 2011.

[71] Y. H. An, R. B. Dickinson, and R. J. Doyle, "Mechanisms of Bacterial Adhesion and Pathogenesis of Implant and Tissue Infections," *Handbook of Bacterial Adhesion: Principles, Methods, and Applications*, Y. H. An and R. J. Friedman, eds., pp. 1-27, Totowa, NJ: Humana Press, 2000.

[72] K. C. Marshall, "Mechanisms of Bacterial Adhesion at Solid-Water Interfaces," *Bacterial Adhesion: Mechanisms and Physiological Significance*, D. C. Savage and M. Fletcher, eds., pp. 133-161, Boston, MA: Springer US, 1985.

[73] D. C. Mays, "Using the Quirk-Schofield Diagram to Explain Environmental Colloid Dispersion Phenomena," *JOURNAL OF NATURAL RESOURCES & LIFE SCIENCES EDUCATION* vol. 36, pp. 45-52, 2007.

[74] L. Li, P. A. Salvador, and G. S. Rohrer, "Photocatalysts with internal electric fields," *Nanoscale,* vol. 6, no. 1, pp. 24-42, 2014.

[75] N. Idil, M. Hedström, A. Denizli, and B. Mattiasson, "Whole cell based microcontact imprinted capacitive biosensor for the detection of Escherichia coli," *Biosensors and Bioelectronics,* vol. 87, pp. 807-815, 2017/01/15/, 2017.

[76] N. Nikkhoo, P. G. Gulak, and K. Maxwell, "Rapid Detection of E. coli Bacteria Using Potassium-Sensitive FETs in CMOS," *IEEE Transactions on Biomedical Circuits and Systems,* vol. 7, no. 5, pp. 621-630, 2013.

[77] E. Yilmaz, D. Majidi, E. Ozgur, and A. Denizli, "Whole cell imprinting based Escherichia coli sensors: A study for SPR and QCM," *Sensors and Actuators B: Chemical,* vol. 209, pp. 714-721, 2015/03/31/, 2015.

[78] M. Martín, P. Salazar, C. Jiménez, M. Lecuona, M. J. Ramos, J. Ode, J. Alcoba, R. Roche, R. Villalonga, S. Campuzano, J. M. Pingarrón, and J. L. González-Mora, "Rapid Legionella pneumophila determination based on a disposable core–shell Fe3O4@poly(dopamine) magnetic nanoparticles immunoplatform," *Analytica Chimica Acta,* vol. 887, pp. 51-58, 2015/08/05/, 2015.

[79] A. M. Foudeh, H. Trigui, N. Mendis, S. P. Faucher, T. Veres, and M. Tabrizian, "Rapid and specific SPRi detection of L. pneumophila in complex environmental water samples," *Analytical and Bioanalytical Chemistry,* vol. 407, no. 18, pp. 5541-5545, 2015/07/01, 2015.

[80] K. F. Lei, and P. H. M. Leung, "Microelectrode array biosensor for the detection of Legionellapneumophila," *Microelectronic Engineering,* vol. 91, pp. 174-177, 2012/03/01/, 2012.

[81] J. J. Rosenberg, M. Benlamri, P. D. Kirchner, J. M. Woodall, and G. D. Pettit, "An $In_{0.15}Ga_{0.85}$ As/GaAs pseudomorphic single quantum well HEMT," *IEEE Electron Device Letters,* vol. 6, no. 10, pp. 491-493, 1985.

[82] F. W. Smith, A. R. Calawa, C. L. Chen, M. J. Manfra, and L. J. Mahoney, "New MBE buffer used to eliminate backgating in GaAs MESFETs," *IEEE Electron Device Letters,* vol. 9, no. 2, pp. 77-80, 1988.

[83] S. Tsukamoto, Y. Nagamune, M. Nishioka, and Y. Arakawa, "Fabrication of GaAs quantum wires on epitaxially grown V grooves by metal-organic chemical-vapor deposition," *Journal of Applied Physics,* vol. 71, no. 1, pp. 533-535, 1992.

[84] G. C. Dyer, G. R. Aizin, S. J. Allen, A. D. Grine, D. Bethke, J. L. Reno, and E. A. Shaner, "Induced transparency by coupling of Tamm and defect states in tunable terahertz plasmonic crystals," *Nat Photon,* vol. 7, no. 11, pp. 925-930, 11//print, 2013.

[85] S. S. Chen, C. C. Lin, C. K. Peng, and Y. J. Chan, "Molecular beam epitaxy regrowth and device performance of GaAs-based pseudomorphic high electron mobility transistors using a thin indium passivation layer," *Journal of Materials Science-Materials in Electronics,* vol. 11, no. 6, pp. 483-487, Aug, 2000.

[86] D. Inoue, J. Lee, T. Hiratani, Y. Atsuji, T. Amemiya, N. Nishiyama, and S. Arai, "Sub-milliampere threshold operation of butt-jointed built-in membrane DFB laser bonded on Si substrate," *Opt Express,* vol. 23, no. 6, pp. 7771-8, Mar 23, 2015.

[87] T. Kosugi, H. Iwase, and K. Gamo, "Characteristics of ion beam assisted etching of GaAs: Surface stoichiometry," *Journal of Vacuum Science & Technology B: Microelectronics and Nanometer Structures Processing, Measurement, and Phenomena,* vol. 11, no. 6, pp. 2214-2218, 1993.

[88] S. Sugata, and K. Asakawa, "Investigation of GaAs Surface Morphology Induced by Cl_2 Gas Reactive Ion Beam Etching," *Japanese Journal of Applied Physics,* vol. 22, no. 12A, pp. L813, 1983.

[89] L. Xu, Z. Haiping, D. W. W. Chris, and G. T. Iain, "Optical Emission Spectrometry of Plasma in Low-Damage Sub-100 nm Tungsten Gate Reactive Ion Etching Process for Compound Semiconductor Transistors," *Japanese Journal of Applied Physics,* vol. 45, no. 10S, pp. 8364, 2006.

[90] S. Sugata, and K. Asakawa, "GaAs Radical Etching with a Cl_2 Plasma in a Reactive Ion Beam Etching System," *Japanese Journal of Applied Physics,* vol. 23, no. 8A, pp. L564, 1984.

[91] M. Takashi, I. Masashi, K. Hirokazu, H. Manabu, H. Tamio, Y. Yasuhiro, and A. Yoshinobu, "Layer-By-Layer Controlled Digital Etching by Means of an Electron-Beam-Excited Plasma System," *Japanese Journal of Applied Physics,* vol. 29, no. 10R, pp. 2216, 1990.

[92] P. A. Maki, and D. J. Ehrlich, "Laser bilayer etching of GaAs surfaces," *Applied Physics Letters,* vol. 55, no. 2, pp. 91-93, 1989/07/10, 1989.

[93] J. J. Dubowski, A. Compaan, and M. Prasad, "Laser-assisted dry etching ablation of InP," *Applied Surface Science,* vol. 86, no. 1, pp. 548-553, 1995/02/01/, 1995.

[94] K. J. Kanarik, T. Lill, E. A. Hudson, S. Sriraman, S. Tan, J. Marks, V. Vahedi, and R. A. Gottscho, "Overview of atomic layer etching in the semiconductor industry," *Journal of Vacuum Science & Technology A: Vacuum, Surfaces, and Films,* vol. 33, no. 2, pp. 020802, 2015.

[95] Y. Lee, J. W. DuMont, and S. M. George, "Trimethylaluminum as the Metal Precursor for the Atomic Layer Etching of Al2O3 Using Sequential, Self-Limiting Thermal Reactions," *Chemistry of Materials,* vol. 28, no. 9, pp. 2994-3003, 2016/05/10, 2016.

[96] Y. Lee, and S. M. George, "Thermal Atomic Layer Etching of Titanium Nitride Using Sequential, Self-Limiting Reactions: Oxidation to TiO2 and Fluorination to Volatile TiF4," *Chemistry of Materials,* vol. 29, no. 19, pp. 8202-8210, 2017/10/10, 2017.

[97] A. I. Abdulagatov, and S. M. George, "Thermal Atomic Layer Etching of Silicon Using O2, HF, and Al(CH3)3 as the Reactants," *Chemistry of Materials,* vol. 30, no. 23, pp. 8465-8475, 2018/12/11, 2018.

[98] G. C. DeSalvo, C. A. Bozada, J. L. Ebel, D. C. Look, J. P. Barrette, C. L. A. Cerny, R. W. Dettmer, J. K. Gillespie, C. K. Havasy, T. J. Jenkins, K. Nakano, C. I. Pettiford, T. K. Quach, J. S. Sewell, and G. D. Via, "Wet Chemical Digital Etching of GaAs at Room Temperature," *Journal of The Electrochemical Society,* vol. 143, no. 11, pp. 3652-3656, 1996.

[99] M. N. Ruberto, X. Zhang, R. Scarmozzino, A. E. Willner, D. V. Podlesnik, and R. M. Osgood, Jr., "The Laser-Controlled Micrometer-Scale Photoelectrochemical Etching of

III–V Semiconductors," *Journal of The Electrochemical Society,* vol. 138, no. 4, pp. 1174-1185, 1990.

[100] A. E. Willner, D. V. Podlesnik, H. H. Gilgen, and R. M. O. Jr., "Photobias effect in laser-controlled etching of InP," *Applied Physics Letters,* vol. 53, no. 13, pp. 1198-1200, 1988.

[101] P. A. Kohl, and F. W. J. Ostermayer, "Photoelectrochemical Methods for III-V Compound Semiconductor Device Processing," *Annual Review of Materials Science,* vol. 19, no. 1, pp. 379-399, 1989.

[102] C. K. Shang, V. Wang, R. Chen, S. Gupta, Y.-C. Huang, J. J. Pao, Y. Huo, E. Sanchez, Y. Kim, T. I. Kamins, and J. S. Harris, "Dry-wet digital etching of $Ge_{1-x}Sn_x$," *Applied Physics Letters,* vol. 108, no. 6, pp. 063110, 2016.

[103] K. Shinoda, N. Miyoshi, H. Kobayashi, M. Miura, M. Kurihara, K. Maeda, N. Negishi, Y. Sonoda, M. Tanaka, N. Yasui, M. Izawa, Y. Ishii, K. Okuma, T. Saldana, J. Manos, K. Ishikawa, and M. Hori, "Selective atomic-level etching using two heating procedures, infrared irradiation and ion bombardment, for next-generation semiconductor device manufacturing," *Journal of Physics D: Applied Physics,* vol. 50, no. 19, pp. 194001, 2017.

[104] M. R. Aziziyan, W. M. Hassen, D. Morris, E. H. Frost, and J. J. Dubowski, "Photonic biosensor based on photocorrosion of GaAs/AlGaAs quantum heterostructures for detection of Legionella pneumophila," *Biointerphases,* vol. 11, no. 1, pp. 019301, 2016.

[105] H. Sharma, K. Moumanis, and J. J. Dubowski, "pH-Dependent Photocorrosion of GaAs/AlGaAs Quantum Well Microstructures," *The Journal of Physical Chemistry C,* vol. 120, no. 45, pp. 26129-26137, 2016/11/17, 2016.

[106] M. R. Aziziyan, W. M. Hassen, and J. J. Dubowski, "Electrically biased GaAs/AlGaAs heterostructures for enhanced detection of bacteria," *Synthesis and Photonics of Nanoscale Materials XIII,* vol. 9737, pp. 97370E-97370E-6, 2016.

[107] E. Nazemi, W. M. Hassen, E. H. Frost, and J. J. Dubowski, "Monitoring growth and antibiotic susceptibility of *Escherichia coli* with photoluminescence of GaAs/AlGaAs quantum well microstructures," *Biosensors and Bioelectronics*, 2016.

[108] S. Aithal, N. Liu, and J. J. Dubowski, "Photocorrosion metrology of photoluminescence emitting GaAs/AlGaAs heterostructures," *Journal of Physics D: Applied Physics,* vol. 50, no. 3, pp. 035106, 2017.

[109] S. Aithal, and J. J. Dubowski, "Open circuit potential monitored digital photocorrosion of GaAs/AlGaAs quantum well microstructures," *Applied Physics Letters,* vol. 112, no. 15, pp. 153102, 2018.

[110] D. Pröfrock, and A. Prange, "Inductively Coupled Plasma–Mass Spectrometry (ICP-MS) for Quantitative Analysis in Environmental and Life Sciences: A Review of Challenges, Solutions, and Trends," *Applied Spectroscopy,* vol. 66, no. 8, pp. 843-868, 2012.

[111] J. Sabine Becker, R. S. Soman, T. Becker, V. K. Panday, and H.-j. Dietze, "Trace and ultratrace analysis of gallium arsenide by different mass spectrometric techniques," *Journal of Analytical Atomic Spectrometry,* vol. 13, no. 9, pp. 983-987, 1998.

[112] C. Kyoung Jin, M. Jae Kyoung, P. Min, K. Haechon, and L. Jong-Lam, "Effects of Photowashing Treatment on Gate Leakage Current of GaAs Metal-Semiconductor Field-Effect Transistors," *Japanese Journal of Applied Physics,* vol. 41, no. 5R, pp. 2894, 2002.

[113] M. Passlack, M. Hong, J. P. Mannaerts, J. R. Kwo, and L. W. Tu, "Recombination velocity at oxide–GaAs interfaces fabricated by in situ molecular beam epitaxy," *Applied Physics Letters,* vol. 68, no. 25, pp. 3605-3607, 1996.

[114] H. J. Joyce, C. J. Docherty, Q. Gao, H. H. Tan, C. Jagadish, J. Lloyd-Hughes, L. M. Herz, and M. B. Johnston, "Electronic properties of GaAs, InAs and InP nanowires studied by terahertz spectroscopy," *Nanotechnology,* vol. 24, no. 21, pp. 214006, May 31, 2013.

[115] H. Yoshikazu, O. Jiro, and I. Naohisa, "In Situ Observation of Monolayer Steps during Molecular Beam Epitaxy of Gallium Arsenide by Scanning Electron Microscopy," *Japanese Journal of Applied Physics,* vol. 33, no. 4B, pp. L563, 1994.

[116] H.-Y. Lee, "Growth of GaAs Oxide Layer Using Photoelectrochemical Method," *Journal of The Electrochemical Society,* vol. 155, no. 7, pp. G141, 2008.

[117] E. M. M. Sutter, M. Le Gall, and C. Debiemme-Chouvy, "Behavior of p-Type GaAs in an Aerated Boric Acid Solution at the Open-Circuit Potential. Influence of the Presence of Co(II) Ions," *The Journal of Physical Chemistry B,* vol. 105, no. 21, pp. 4840-4845, 2001/05/01, 2001.

[118] Y. Huang, J. Luo, and D. G. Ivey, "Comparative study of GaAs corrosion in H_2SO_4 and $NH_3 \cdot H_2O$ solutions by electrochemical methods and surface analysis," *Materials Chemistry and Physics,* vol. 93, no. 2, pp. 429-442, 2005/10/15/, 2005.

[119] M. Passlack, M. Hong, E. F. Schubert, J. R. Kwo, J. P. Mannaerts, S. N. G. Chu, N. Moriya, and F. A. Thiel, "In situ fabricated Ga_2O_3–GaAs structures with low interface recombination velocity," *Applied Physics Letters,* vol. 66, no. 5, pp. 625-627, 1995/01/30, 1995.

[120] Z. Liliental-Weber, C. W. Wilmsen, K. M. Geib, P. D. Kirchner, J. M. Baker, and J. M. Woodall, "Structure and chemical composition of water-grown oxides of GaAs," *Journal of Applied Physics,* vol. 67, no. 4, pp. 1863-1867, 1990/02/15, 1990.

[121] J. F. Kauffman, and G. L. Richmond, "Photoluminescence enhancement monitored in real time during photowashing of GaAs," *Applied Physics Letters,* vol. 59, no. 5, pp. 561-563, 1991/07/29, 1991.

[122] A. R. Clawson, "Guide to references on III–V semiconductor chemical etching," *Materials Science and Engineering: R: Reports,* vol. 31, no. 1, pp. 1-438, 2001/01/15/, 2001.

[123] K. Djebaili, Z. Mekhalif, A. Boumaza, and A. Djelloul, "XPS, FTIR, EDX, and XRD Analysis of Al_2O_3 Scales Grown on PM2000 Alloy," *Journal of Spectroscopy,* vol. 2015, pp. 1-16, 2015.

[124] Y. Cheng, J. Chen, K. Yang, Y. Wang, Y. Yin, H. Liang, and G. Du, "Structural, morphological, FTIR and photoluminescence properties of gallium oxide thin films," *Journal of Vacuum Science & Technology B, Nanotechnology and Microelectronics: Materials, Processing, Measurement, and Phenomena,* vol. 32, no. 3, pp. 03D119, 2014/05/01, 2014.

[125] G. Schön, "Auger and direct electron spectra in X-ray photoelectron studies of zinc, zinc oxide, gallium and gallium oxide," *Journal of Electron Spectroscopy and Related Phenomena,* vol. 2, no. 1, pp. 75-86, 1973/01/01/, 1973.

[126] I. Hiroaki, T. Chiei, and I. Shoji, "XPS and AES Studies on the Oxidation of Layered Semiconductor GaSe," *Japanese Journal of Applied Physics,* vol. 21, no. 1R, pp. 94, 1982.

[127] M. Procop, "XPS data for sputter-cleaned In0.53Ga0.47As, GaAs, and InAs surfaces," *Journal of Electron Spectroscopy and Related Phenomena,* vol. 59, no. 2, pp. R1-R10, 1992/07/01/, 1992.

[128] A. K. Dua, V. C. George, and R. P. Agarwala, "Characterization and microhardness measurement of electron-beam-evaporated alumina coatings," *Thin Solid Films,* vol. 165, no. 1, pp. 163-172, 1988/11/15/, 1988.

[129] C. D. Wagner, D. E. Passoja, H. F. Hillery, T. G. Kinisky, H. A. Six, W. T. Jansen, and J. A. Taylor, "Auger and photoelectron line energy relationships in aluminum–oxygen and silicon–oxygen compounds," *Journal of Vacuum Science and Technology,* vol. 21, no. 4, pp. 933-944, 1982/11/01, 1982.

[130] J. T. Kloprogge, L. V. Duong, B. J. Wood, and R. L. Frost, "XPS study of the major minerals in bauxite: Gibbsite, bayerite and (pseudo-)boehmite," *Journal of Colloid and Interface Science,* vol. 296, no. 2, pp. 572-576, 2006/04/15/, 2006.

[131] J. Takahashi, "Direct measurement of metallic impurities in 20% ammonium hydroxide by Agilent 7700s ICP-MS," *Application Note from Agilent Technologies,* vol. Publication Number 5990-7914EN, pp. 1-6, 2011.

[132] M. Pino, J. Chacón, E. Fatás, and P. Ocón, "Performance of commercial aluminium alloys as anodes in gelled electrolyte aluminium-air batteries," *Journal of Power Sources,* vol. 299, no. Supplement C, pp. 195-201, 2015/12/20/, 2015.

[133] R. J. Nelson, and R. G. Sobers, "Interfacial recombination velocity in GaAlAs/GaAs heterostructures," *Applied Physics Letters,* vol. 32, no. 11, pp. 761-763, 1978.

[134] A. J. Downs, *Chemistry of aluminium, gallium, indium and thallium*, 1st ed., London Blackie Academic & Professional, 1993.

[135] S. Karkare, and I. Bazarov, "Effect of nanoscale surface roughness on transverse energy spread from GaAs photocathodes," *Applied Physics Letters,* vol. 98, no. 9, pp. 094104, 2011/02/28, 2011.

[136] I. O. Akhundov, D. M. Kazantsev, A. S. Kozhuhov, and V. L. Alperovich, "Optimization of conditions for thermal smoothing GaAs surfaces," *Journal of Physics: Conference Series,* vol. 993, no. 1, pp. 012010, 2018.

[137] E.-A. Moon, J.-L. Lee, and H. M. Yoo, "Selective wet etching of GaAs on $Al_xGa_{1-x}As$ for AlGaAs/InGaAs/AlGaAs pseudomorphic high electron mobility transistor," *Journal of Applied Physics,* vol. 84, no. 7, pp. 3933-3938, 1998.

[138] C. Edwards, A. Arbabi, G. Popescu, and L. L. Goddard, "Optically monitoring and controlling nanoscale topography during semiconductor etching," *Light: Science & Applications,* vol. 1, pp. e30, 09/28/online, 2012.

[139] C. K. Kim, G. M. Marshall, M. Martin, M. Bisson-Viens, Z. Wasilewski, and J. J. Dubowski, "Formation dynamics of hexadecanethiol self-assembled monolayers on (001)

GaAs observed with photoluminescence and Fourier transform infrared spectroscopies," *Journal of Applied Physics,* vol. 106, no. 8, pp. 083518, 2009.

[140] S. M. Sze, *Semiconductor Devices Physics and Technology*, 2nd ed., New York: J. Wiley, 1985.

[141] S. Ariponnammal, and S. Chandrasekaran, "Theoretical Study on The Electrical Properties of Some III-V and IV-IV Compounds," *Chalcogenide Letters,* vol. 8, no. 1, pp. 45-51, 2011.

[142] R. R. Isberg, T. J. O'Connor, and M. Heidtman, "The Legionella pneumophila replication vacuole: making a cosy niche inside host cells," *Nat Rev Microbiol,* vol. 7, no. 1, pp. 13-24, Jan, 2009.

[143] J. W. Mercante, and J. M. Winchell, "Current and Emerging Legionella Diagnostics for Laboratory and Outbreak Investigations," *Clinical Microbiology Reviews,* vol. 28, no. 1, pp. 95-133, January 1, 2015, 2015.

[144] B. A. Cunha, A. Burillo, and E. Bouza, "Legionnaires' disease," *The Lancet,* vol. 387, no. 10016, pp. 376–385, 2015.

[145] I. Oren, T. Zuckerman, I. Avivi, R. Finkelstein, M. Yigla, and J. M. Rowe, "Nosocomial outbreak of Legionella pneumophila serogroup 3 pneumonia in a new bone marrow transplant unit: evaluation, treatment and control," *Bone Marrow Transplant,* vol. 30, no. 3, pp. 175-9, Aug, 2002.

[146] F. Lagarde, and N. Jaffrezic-Renault, "Cell-based electrochemical biosensors for water quality assessment," *Analytical and Bioanalytical Chemistry,* vol. 400, no. 4, pp. 947-964, 2011/05/01, 2011.

[147] C. D. Chin, V. Linder, and S. K. Sia, "Commercialization of microfluidic point-of-care diagnostic devices," *Lab on a Chip,* vol. 12, no. 12, pp. 2118-2134, 2012.

[148] A. Singh, S. Poshtiban, and S. Evoy, "Recent advances in bacteriophage based biosensors for food-borne pathogen detection," *Sensors (Basel),* vol. 13, no. 2, pp. 1763-86, 2013.

[149] L. M. d. Costa Silva, V. P. S. dos Santos, A. Medeiros, and K. Signori, "Biosensors for Contaminants Monitoring in Food and Environment for Human and Environmental Health," *State of the Art in Biosensors - Environmental and Medical Applications*, T. Rinken, ed., pp. 151-168, Croatia InTech, 2013.

[150] Fazila Seker, Kathleen Meeker, Thomas F. Kuech, and A. B. Ellis, “Surface Chemistry of Prototypical Bulk II-VI and III-V Semiconductors and Implications for Chemical Sensing,” *Chem. Rev.,* vol. 100, pp. 2505-2536, 2000.

[151] T. Fink, and R. M. Osgood, Jr., “Photoelectrochemical Etching of GaAs / AlGaAS Multilayer Structures ” *Journal of the Electrochemical Society,* vol. 140, no. 9, pp. 2572-2581, 1993.

[152] J. E. Stout, M. G. Best, and V. L. Yu, “Susceptibility of members of the family Legionellaceae to thermal stress: implications for heat eradication methods in water distribution systems,” *Applied and Environmental Microbiology,* vol. 52, no. 2, pp. 396-399, 1986.

[153] R. van de Krol, "Principles of Photoelectrochemical Cells," *Photoelectrochemical Hydrogen Production*, 102, R. van de Krol and M. Grätzel, eds., pp. 13-67, Boston, MA: Springer US, 2012.

[154] P. Schmukia, J. Frasera, C. M. Vitusb, G. M. J., and I. H. S., “Initiation and Formation of Porous GaAs,” *Journal of The Electrochemical Society,* vol. 143, no. 10, pp. 3316-3322, 1996.

[155] H. Gerischer, “Electrolytic decomposition and photodecomposition of compound semiconductors in contact with electrolytes,” *Journal of Vacuum Science and Technology,* vol. 15 no. 4, pp. 1422-1428, 1978.

[156] Z. Zhang, and J. T. Yates, Jr., “Band bending in semiconductors: chemical and physical consequences at surfaces and interfaces,” *Chem Rev,* vol. 112, no. 10, pp. 5520-51, Oct 10, 2012.

[157] J. S. Blakemore, “Semiconducting and other major properties of gallium arsenide,” *Journal of Applied Physics,* vol. 53, no. 10, pp. R123-R181, 1982.

[158] C. W. Wilmsen, P. D. Kirchner, and J. M. Woodall, “Effects of N_2, O_2, and H_2O on GaAs passivated by photowashing or coating with $Na_2S{\cdot}9H_2O$,” *Journal of Applied Physics,* vol. 64, no. 6, pp. 3287-3289, 1988/09/15, 1988.

[159] S. D. Offsey, J. M. Woodall, A. C. Warren, P. D. Kirchner, T. I. Chappell, and G. D. Pettit, “Unpinned (100) GaAs surfaces in air using photochemistry,” *Applied Physics Letters,* vol. 48, no. 7, pp. 475-477, 1986.

[160] W. Wang, G. Lee, M. Huang, R. M. Wallace, and K. Cho, "First-principles study of GaAs(001)-β2(2×4) surface oxidation and passivation with H, Cl, S, F, and GaO," *Journal of Applied Physics,* vol. 107, no. 10, pp. 103720, 2010.

[161] M. Passlack, E. F. Schubert, W. S. Hobson, M. Hong, N. Moriya, S. N. G. Chu, K. Konstadinidis, J. P. Mannaerts, M. L. Schnoes, and G. J. Zydzik, "Ga2O3 films for electronic and optoelectronic applications," *Journal of Applied Physics,* vol. 77, no. 2, pp. 686-693, 1995.

[162] J. Guo-Ping, and H. E. Ruda, "The origin of Ga_2O_3 passivation for reconstructed GaAs(001) surfaces," *Journal of Applied Physics,* vol. 83, no. 11, pp. 5880-5884, 1998.

[163] S. Aithal, N. Liu, and J. Dubowski, "Photocorrosion of unfunctionalized GaAs/AlGaAs quantum heterostructures," *in preparation*.

[164] B. Li, and B. E. Logan, "Bacterial adhesion to glass and metal-oxide surfaces," *Colloids and Surfaces B: Biointerfaces,* vol. 36, no. 2, pp. 81-90, 2004.

[165] J. D. Cirillo, S. Falkow, and L. S. Tompkins, "Growth of Legionella pneumophila in Acanthamoeba castellanii enhances invasion," *Infection and Immunity,* vol. 62, no. 8, pp. 3254-3261, 1994.

[166] J. T. Kindt, and R. C. Bailey, "Chaperone Probes and Bead-Based Enhancement To Improve the Direct Detection of mRNA Using Silicon Photonic Sensor Arrays," *Analytical Chemistry,* vol. 84, no. 18, pp. 8067-8074, 2012/09/18, 2012.

[167] D. F. Yaradou, S. Hallier-Soulier, S. Moreau, F. Poty, Y. Hillion, M. Reyrolle, J. Andre, G. Festoc, K. Delabre, F. Vandenesch, J. Etienne, and S. Jarraud, "Integrated real-time PCR for detection and monitoring of Legionella pneumophila in water systems," *Applied Environmental Microbiology,* vol. 73, no. 5, pp. 1452-1456, March, 2007.

[168] J. J. Dubowski, "Novel Quantum Dot based Approach for Biosensing," in Lasers and Electro-Optics Society, 2006. LEOS 2006. 19th Annual Meeting of the IEEE, 2006, pp. 302-303.

[169] M. Katsikogianni, and Y. F. Missirlis, "Concise review of mechanisms of bacterial adhesion to biomaterials and of techniques used in estimating bacteria-material interactions," *European cells & materials,* vol. 8, pp. 37-57, 2004.

[170] M. V. Lebedev, T. Masuda, and K. Uosaki, "Charge transport at the interface of n-GaAs (100) with an aqueous HCl solution: Electrochemical impedance spectroscopy study," *Semiconductors,* vol. 46, no. 4, pp. 471-477, 2012.

[171] L. Neng, H. Xiaohuan, and J. J. Dubowski, "Selective area in situ conversion of Si (001) hydrophobic to hydrophilic surface by excimer laser irradiation in hydrogen peroxide," *Journal of Physics D: Applied Physics,* vol. 47, no. 38, pp. 385106, 2014.

[172] A. Katsiaflaka, S. Pournaras, I. Kristo, V. A. Mouchtouri, M. Kyritsi, E. Velonakis, A. C. Vatopoulos, and C. Hadjichristodoulou, "Epidemiological Investigation of Legionella pneumophila Serogroup 2 to 14 Isolates from Water Samples by Amplified Fragment Length Polymorphism and Sequence-Based Typing and Detection of Virulence Traits," *Applied and Environmental Microbiology,* vol. 82, no. 20, pp. 6102-6108, October 15, 2016, 2016.

[173] O. Lazcka, F. J. D. Campo, and F. X. Muñoz, "Pathogen detection: A perspective of traditional methods and biosensors," *Biosensors and Bioelectronics,* vol. 22, no. 7, pp. 1205-1217, 2007/02/15/, 2007.

[174] F. Lisdat, and D. Schäfer, "The use of electrochemical impedance spectroscopy for biosensing," *Analytical and Bioanalytical Chemistry,* vol. 391, no. 5, pp. 1555, 2008/04/16, 2008.

[175] J. Choi, T. W. Seong, M. Jeun, and K. H. Lee, "Field-Effect Biosensors for On-Site Detection: Recent Advances and Promising Targets," *Advanced Healthcare Materials,* vol. 6, no. 20, 2017.

[176] F. Seker, K. Meeker, T. F. Kuech, and A. B. Ellis, "Surface Chemistry of Prototypical Bulk II−VI and III−V Semiconductors and Implications for Chemical Sensing," *Chemical Reviews,* vol. 100, no. 7, pp. 2505-2536, 2000/07/01, 2000.

[177] S. Chen, L. Liu, J. Zhou, and S. Jiang, "Controlling Antibody Orientation on Charged Self-Assembled Monolayers," *Langmuir,* vol. 19, no. 7, pp. 2859-2864, 2003/04/01, 2003.

[178] W. M. Hassen, H. Sanyal, M. Hammood, K. Moumanis, E. H. Frost, and J. J. Dubowski, "Chemotaxis for enhanced immobilization of Escherichia coli and Legionella pneumophila on biofunctionalized surfaces of GaAs," *Biointerphases,* vol. 11, no. 2, pp. 021004, 2016/06/01, 2016.

[179] Q. Zhang, X.-D. Wang, T. Tian, and L.-Q. Chu, "Incorporation of multilayered silver nanoparticles into polymer brushes as 3-dimensional SERS substrates and their application for bacteria detection," *Applied Surface Science,* vol. 407, pp. 185-191, 2017/06/15/, 2017.

[180] S. Choinière, E. H. Frost, and J. J. Dubowski, "Binding strategies for capturing and growing Escherichia coli on surfaces of biosensing devices," *Talanta,* vol. 192, pp. 270-277, 2019/01/15/, 2019.

[181] J. G. Hurdle, A. J. O'Neill, I. Chopra, and R. E. Lee, "Targeting bacterial membrane function: an underexploited mechanism for treating persistent infections," *Nature Reviews Microbiology,* vol. 9, pp. 62, 12/16/online, 2010.

[182] H. Yan, C. Catania, and G. C. Bazan, "Membrane-Intercalating Conjugated Oligoelectrolytes: Impact on Bioelectrochemical Systems," *Advanced Materials,* vol. 27, no. 19, pp. 2958-2973, 2015.

[183] S. Hideshima, K. Fujita, Y. Harada, M. Tsuna, Y. Seto, S. Sekiguchi, S. Kuroiwa, T. Nakanishi, and T. Osaka, "Signal amplification in electrochemical detection of buckwheat allergenic protein using field effect transistor biosensor by introduction of anionic surfactant," *Sensing and Bio-Sensing Research,* vol. 7, pp. 90-94, 2016/03/01/, 2016.

[184] K. R. Rupprecht, E. Z. Lang, S. D. Gregory, J. M. Bergsma, T. D. Rae, and J. R. Fishpaugh, "A precise spectrophotometric method for measuring sodium dodecyl sulfate concentration," *Analytical Biochemistry,* vol. 486, pp. 78-80, 2015/10/01/, 2015.

[185] D. Lepage, and J. J. Dubowski, "Miniaturized quantum semiconductor surface plasmon resonance platform for detection of biological molecules," *Biosensors,* vol. 3, no. 2, pp. 201-210, 2013.

[186] S. Halder, K. K. Yadav, R. Sarkar, S. Mukherjee, P. Saha, S. Haldar, S. Karmakar, and T. Sen, "Alteration of Zeta potential and membrane permeability in bacteria: a study with cationic agents," *SpringerPlus,* vol. 4, pp. 672, 11/04

07/29/received

10/27/accepted, 2015.

[187] N. Lloret, R. S. Frederiksen, T. C. Møller, N. I. Rieben, S. Upadhyay, L. D. Vico, J. H. Jensen, J. Nygård, and K. L. Martinez, "Effects of buffer composition and dilution on nanowire field-effect biosensors," *Nanotechnology,* vol. 24, no. 3, pp. 035501, 2013.

[188] C. L. Woldringh, and W. Van Iterson, “Effects of Treatment with Sodium Dodecyl Sulfate on the Ultrastructure of Escherichia coli,” *Journal of Bacteriology,* vol. 111, no. 3, pp. 801-813, September 1, 1972, 1972.

[189] M. Arakha, M. Saleem, B. C. Mallick, and S. Jha, “The effects of interfacial potential on antimicrobial propensity of ZnO nanoparticle,” *Scientific Reports,* vol. 5, pp. 9578, 04/15/online, 2015.

[190] M. M. Domingues, P. M. Silva, H. G. Franquelim, F. A. Carvalho, M. A. R. B. Castanho, and N. C. Santos, “Antimicrobial protein rBPI21-induced surface changes on Gram-negative and Gram-positive bacteria,” *Nanomedicine: Nanotechnology, Biology and Medicine,* vol. 10, no. 3, pp. 543-551, 2014/04/01/, 2014.

[191] J. S. Hansen, A. Vararattanavech, I. Plasencia, P. Greisen, Jr., J. Bomholt, J. Torres, J. Emnéus, and C. Hélix-Nielsen, “Interaction between sodium dodecyl sulfate and membrane reconstituted aquaporins: A comparative study of spinach SoPIP2;1 and E. coli AqpZ,” *Biochimica et Biophysica Acta (BBA) - Biomembranes,* vol. 1808, no. 10, pp. 2600-2607, 2011/10/01/, 2011.

[192] A. K. Bhuyan, “On the mechanism of SDS-induced protein denaturation,” *Biopolymers,* vol. 93, no. 2, pp. 186-199, 2010.

[193] U. Zähringer, Y. A. Knirel, B. Lindner, J. H. Helbig, A. Sonesson, R. Marre, and E. T. Rietschel, “The lipopolysaccharide of Legionella pneumophila serogroup 1 (strain Philadelphia 1): chemical structure and biological significance,” *Progress in clinical and biological research,* vol. 392, pp. 113-139, 1995, 1995.

[194] Y. A. Knirel, A. S. Shashkov, Y. E. Tsvetkov, P.-E. Jansson, and U. Zähringer, "5,7-DIAMINO-3,5,7,9-TETRADEOXYNON-2-ULOSONIC ACIDS IN BACTERIAL GLYCOPOLYMERS: CHEMISTRY AND BIOCHEMISTRY," *Advances in Carbohydrate Chemistry and Biochemistry*, pp. 371-417: Academic Press, 2003.

[195] F. Chellat, Y. Merhi, A. Moreau, and L. H. Yahia, “Therapeutic potential of nanoparticulate systems for macrophage targeting,” *Biomaterials,* vol. 26, no. 35, pp. 7260-7275, 2005/12/01/, 2005.

[196] D. A. Haydon, “The surface charge of cells and some other small particles as indicated by electrophoresis: I. The zeta potential-surface charge relationships,” *Biochimica et Biophysica Acta,* vol. 50, no. 3, pp. 450-457, 1961/07/08/, 1961.

[197] D. A. Haydon, “The surface charge of cells and some other small particles as indicated by electrophoresis: II. The interpretation of the electrophoretic charge,” *Biochimica et Biophysica Acta,* vol. 50, no. 3, pp. 457-462, 1961/07/08/, 1961.

[198] M. Pisárčik, F. Devínsky, and M. Pupák, "Determination of micelle aggregation numbers of alkyltrimethylammonium bromide and sodium dodecyl sulfate surfactants using time-resolved fluorescence quenching," *Open Chemistry*, 1, 2015.

[199] D. Naumann, D. Helm, and H. Labischinski, “Microbiological characterizations by FT-IR spectroscopy,” *Nature,* vol. 351, pp. 81, 05/02/online, 1991.

[200] J. Schmitt, and H.-C. Flemming, “FTIR-spectroscopy in microbial and material analysis,” *International Biodeterioration & Biodegradation,* vol. 41, no. 1, pp. 1-11, 1998/01/01/, 1998.

[201] S. R. Ede, U. Nithiyanantham, R. S. Gill, and S. Kundu, “Electrically conducting osmium nano-chain networks with superior catalytic and SERS performance,” *RSC Advances,* vol. 4, no. 105, pp. 60762-60775, 2014.

[202] G. F. Schneider, B. F. Shaw, A. Lee, E. Carillho, and G. M. Whitesides, “Pathway for Unfolding of Ubiquitin in Sodium Dodecyl Sulfate, Studied by Capillary Electrophoresis,” *Journal of the American Chemical Society,* vol. 130, no. 51, pp. 17384-17393, 2008/12/24, 2008.

[203] F. SHAFA, and M. R. J. SALTON, “Disaggregation of Bacterial Cell Walls by Anionic Detergents,” *Microbiology,* vol. 23, no. 1, pp. 137-141, 1960.

[204] R. H. Wilson, “A model for the current-voltage curve of photoexcited semiconductor electrodes,” *Journal of Applied Physics,* vol. 48, no. 10, pp. 4292-4297, 1977.

[205] H. S. Hilal, and J. A. Turner, “Controlling charge-transfer processes at semiconductor/liquid junctions,” *Electrochimica Acta,* vol. 51, no. 28, pp. 6487-6497, 2006/09/15/, 2006.

[206] Z. Zhang, and J. T. Yates, “Effect of Adsorbed Donor and Acceptor Molecules on Electron Stimulated Desorption: O2/TiO2(110),” *The Journal of Physical Chemistry Letters,* vol. 1, no. 14, pp. 2185-2188, 2010/07/15, 2010.

[207] L. Boulangé-Petermann, M.-N. Bellon-Fontaine, and B. Baroux, “An electrochemical method for assessing biodeposition on stainless steel,” *Journal of Microbiological Methods,* vol. 21, no. 1, pp. 83-96, 1995/01/01/, 1995.

[208] A. T. Poortinga, R. Bos, and H. J. Busscher, "Measurement of charge transfer during bacterial adhesion to an indium tin oxide surface in a parallel plate flow chamber," *Journal of Microbiological Methods,* vol. 38, no. 3, pp. 183-189, 11//, 1999.

[209] L. Frolov, Y. Rosenwaks, S. Richter, C. Carmeli, and I. Carmeli, "Photoelectric Junctions Between GaAs and Photosynthetic Reaction Center Protein," *The Journal of Physical Chemistry C,* vol. 112, no. 35, pp. 13426-13430, 2008/09/04, 2008.

[210] T.-W. Kim, G. Wang, H. Song, N.-J. Choi, H. Lee, and T. Lee, "Charge Transport of Alkanethiol Self-Assembled Monolayers in Micro-Via Hole Devices," *Journal of Nanoscience and Nanotechnology,* vol. 6, no. 11, pp. 3487-3490, //, 2006.

[211] J. J. Dubowski, O. Voznyy, and G. M. Marshall, "Molecular self-assembly and passivation of GaAs (001) with alkanethiol monolayers: A view towards bio-functionalization," *Applied Surface Science,* vol. 256, no. 19, pp. 5714-5721, 2010.

[212] M. R. Aziziyan, H. Sharma, and J. J. Dubowski, "Photo-Atomic-Layer-Etching for Stoichiometric Nanostructuring of GaAs/AlGaAs Quantum Semiconductors," *In Preparation* 2018.

[213] A. Sigel, H. Sigel, and R. K. O. Sigel, *The Alkali Metal Ions: Their Role for Life*, Switzerland: Springer International Publishing, 2016.

[214] A. Camara-Artigas, D. Brune, and J. P. Allen, "Interactions between lipids and bacterial reaction centers determined by protein crystallography," *Proceedings of the National Academy of Sciences,* vol. 99, no. 17, pp. 11055-11060, 2002.

[215] G. Hungerford, J. Benesch, J. F. Mano, and R. L. Reis, "Effect of the labelling ratio on the photophysics of fluorescein isothiocyanate (FITC) conjugated to bovine serum albumin," *Photochemical & Photobiological Sciences,* vol. 6, no. 2, pp. 152-158, 2007.

[216] Z. G. Peng, K. Hidajat, and M. S. Uddin, "Selective and sequential adsorption of bovine serum albumin and lysozyme from a binary mixture on nanosized magnetic particles," *Journal of Colloid and Interface Science,* vol. 281, no. 1, pp. 11-17, 2005/01/01/, 2005.

[217] T. Coradin, A. Coupé, and J. Livage, "Interactions of bovine serum albumin and lysozyme with sodium silicate solutions," *Colloids and Surfaces B: Biointerfaces,* vol. 29, no. 2, pp. 189-196, 2003/06/01/, 2003.

[218] L. Medda, B. Barse, F. Cugia, M. Boström, D. F. Parsons, B. W. Ninham, M. Monduzzi, and A. Salis, "Hofmeister Challenges: Ion Binding and Charge of the BSA Protein as Explicit Examples," *Langmuir,* vol. 28, no. 47, pp. 16355-16363, 2012/11/27, 2012.

[219] O. Schneewind, and D. M. Missiakas, "Protein secretion and surface display in Gram-positive bacteria," *Philosophical Transactions of the Royal Society B: Biological Sciences,* vol. 367, no. 1592, pp. 1123-1139, 2012.

[220] G. D. Parfitt, and A. L. Smith, "CONDUCTIVITY OF SODIUM DODECYL SULFATE SOLUTIONS BELOW THE CRITICAL MICELLE CONCENTRATION," *The Journal of Physical Chemistry,* vol. 66, no. 5, pp. 942-943, 1962/05/01, 1962.

[221] S. M. Bystryak, M. A. Winnik, and J. Siddiqui, "Unusual Conductivity Changes for Sodium Dodecyl Sulfate Solutions in the Presence of Polyethyleneimine and Polyvinylamine," *Langmuir,* vol. 15, no. 11, pp. 3748-3751, 1999/05/01, 1999.

[222] E. Shirzaei Sani, R. Portillo-Lara, A. Spencer, W. Yu, B. M. Geilich, I. Noshadi, T. J. Webster, and N. Annabi, "Engineering Adhesive and Antimicrobial Hyaluronic Acid/Elastin-like Polypeptide Hybrid Hydrogels for Tissue Engineering Applications," *ACS Biomaterials Science & Engineering,* vol. 4, no. 7, pp. 2528-2540, 2018/07/09, 2018.

[223] M. Arand, T. Friedberg, and F. Oesch, "Colorimetric quantitation of trace amounts of sodium lauryl sulfate in the presence of nucleic acids and proteins," *Analytical Biochemistry,* vol. 207, no. 1, pp. 73-75, 1992/11/15/, 1992.

[224] S. B. Nielsen, and D. E. Otzen, "Impact of the antimicrobial peptide Novicidin on membrane structure and integrity," *Journal of Colloid and Interface Science,* vol. 345, no. 2, pp. 248-256, 2010/05/15/, 2010.

[225] R. M. Venable, Y. Luo, K. Gawrisch, B. Roux, and R. W. Pastor, "Simulations of Anionic Lipid Membranes: Development of Interaction-Specific Ion Parameters and Validation Using NMR Data," *The Journal of Physical Chemistry B,* vol. 117, no. 35, pp. 10183-10192, 2013/09/05, 2013.

[226] Z. Ge, and Y. Wang, "Estimation of Nanodiamond Surface Charge Density from Zeta Potential and Molecular Dynamics Simulations," *The Journal of Physical Chemistry B,* vol. 121, no. 15, pp. 3394-3402, 2017/04/20, 2017.

[227] B. Chen, W. Le, Y. Wang, Z. Li, D. Wang, L. Ren, L. Lin, S. Cui, J. J. Hu, Y. Hu, P. Yang, R. C. Ewing, D. Shi, and Z. Cui, "Targeting Negative Surface Charges of Cancer Cells by Multifunctional Nanoprobes," *Theranostics,* vol. 6, no. 11, pp. 1887-1898, 2016.